

# Observations of Two Complete Substorm Cycles During the Cassini Earth Swing–By: Cassini Magnetometer Data in a Global Context

H. Khan<sup>1</sup>, S.W.H. Cowley<sup>1</sup>, E. Kolesnikova<sup>1</sup>, M. Lester<sup>1</sup>, M.J. Brittnacher<sup>2</sup>, T.J. Hughes<sup>3</sup>, W.J. Hughes<sup>4</sup>, W.S. Kurth<sup>5</sup>, D.J. McComas<sup>6</sup>, L. Newitt<sup>7</sup>, C.J. Owen<sup>8</sup>, G.D. Reeves<sup>9</sup>, H.J. Singer<sup>10</sup>, C.W. Smith<sup>11</sup>, D.J. Southwood<sup>12</sup>, and J.F. Watermann<sup>13</sup>

<sup>1</sup> Department of Physics & Astronomy, University of Leicester, Leicester LE1 7RH, UK

<sup>2</sup> Geophysics Programme, University of Washington, Seattle, Washington 98195, USA

<sup>3</sup> Canadian Space Agency, PO Box 7275, Vanier, Ontario K1L 8E3, Canada

<sup>4</sup> Center for Space Physics, Boston University, Boston, Massachusetts 02215, USA

<sup>5</sup> Department of Physics & Astronomy, The University of Iowa, Iowa City, Iowa 52242, USA

<sup>6</sup> Southwest Research Institute, San Antonio, Texas 78238-51666, USA

<sup>7</sup> Geological Survey of Canada, 7 Observatory Crescent, Ottawa, Ontario K1A 0Y3, Canada

<sup>8</sup> Mullard Space Science Laboratory, Holmbury St. Mary, Dorking, Surrey RH5 6NT, UK

<sup>9</sup> Los Alamos National Laboratory, Los Alamos, New Mexico 87545, USA

<sup>10</sup> NOAA Space Environment Center, 325 Broadway, Boulder, Colorado 80303, USA

<sup>11</sup> Bartol Research Institute, University of Delaware, Newark, Delaware 19716-4793, USA

<sup>12</sup> Blackett Laboratory, Imperial College, London SW7 2BZ, UK

<sup>13</sup> Danish Meteorological Institute, Lyngbyvej 100, 2100 Copenhagen, Denmark

Proofs and reprints to:

H. Khan

Radio and Space Plasma Physics Group  
Department of Physics & Astronomy  
University of Leicester  
University Road  
Leicester LE1 7RH  
UK

Email: [hina.khan@ion.le.ac.uk](mailto:hina.khan@ion.le.ac.uk)

Draft B: Incorporating responses to referee comments

Submitted to *Journal of Geophysical Research* (Cassini ESB Special Section)

**Abstract.** During the Earth swing-by of the Cassini spacecraft, a world-wide programme of data-gathering was undertaken to define the prevailing interplanetary and geophysical conditions. This included observations of the interplanetary medium, outer magnetosphere, geostationary orbit, UV aurora, geomagnetic disturbance, and ionospheric flow. These data show that during the Cassini outbound passage through the geomagnetic tail the magnetosphere underwent two complete ‘classic’ substorm cycles. The global data are used to set the Cassini data into a context which allows a much fuller interpretation. The pass took place through the dawn tail, where previous Geotail observations indicate that the plasma sheet usually remains ‘stationary’ at expansion phase onset. Reconnection and plasmoid formation are typically dusk and midnight phenomena. The Cassini observations nevertheless show a marked response of the plasma sheet both to the growth phase (thinning), and expansion phase onset (expansion without heating). Subsequent impulsive expansion of the substorm into the Cassini sector, however, resulted in the prompt appearance of reconnection-related phenomena (earthward flowing plasma and strongly disturbed fields), though the spacecraft footprint remained poleward of the intense UV auroras. Due to continuing strong southward-directed IMF during the expansion phases, a quasi-equilibrium appears to have formed between dayside and near-Earth nightside reconnection for  $\sim 30$  min after onset. Auroral zone recovery began about  $\sim 10$  min after a northward turn of the IMF to nearer-zero values in each case. A net closure of open flux then ensued, leading to deflation of the tail lobe field, ‘dipolarisation’ of the near-Earth tail plasma sheet field, simultaneous reduction in the earthward plasma sheet flow and the flow in the nightside ionosphere, and displacement of the ground-based disturbance to high latitudes.

## 1. Introduction.

The Cassini Earth swing-by (ESB) manoeuvre on 18 August 1999 provided an excellent opportunity to undertake an investigation of the Earth's magnetosphere by a spacecraft having an unusual and rapid trajectory through the system. Such flybys are relatively rare, previous opportunities having been afforded by those of the Giotto and Galileo spacecraft [e.g. *Glassmeier et al.*, 1991; *Kivelson et al.*, 1993; *Reeves et al.*, 1993]. Cassini entered the magnetosphere near the subsolar point, and after a close planetary approach in the dusk local time sector flew down the geomagnetic tail, exiting on the northern dawn side at a geocentric distance of  $\sim 67 R_E$ . Such a trajectory provides an opportunity to investigate a range of phenomena, but in particular provides an almost unique cut through the geomagnetic tail. During the swing-by, a programme of ground-based observations by magnetometers and radars was put in place in order to form a broad-based geophysical context for the Cassini observations. In addition, the auroral imagers on the Polar spacecraft were requested to operate in support of the Cassini interval. Data were also requested from a host of other spacecraft, as well as from ground-based instruments which were running routinely. This paper describes the supporting instrumentation that provided data during the Cassini ESB, before discussing in detail the ground-based and space-based observations, including Cassini data, during the tail pass.

The ESB interval was particularly interesting as two complete magnetospheric substorm cycles occurred in the  $\sim 6$  h period during which the spacecraft traversed the tail. Magnetospheric substorms remain a topic of considerable debate despite over 40 years of continued study. Much of the debate at present centres on the cause of the onset of the expansion phase, with particular reference to the timing of magnetic reconnection in the geomagnetic tail in comparison with signatures of expansion phase onset in the ionosphere and near-Earth magnetosphere. The advocates of the near-earth neutral line model propose that reconnection of magnetic flux at a site in the near earth tail is the cause of expansion phase onset [*Hones*, 1979; *Baker et al.*, 1996]. This view has been strongly supported by recent field and flow results from Geotail, which indicate that reconnection typically begins in the dusk sector plasma sheet at down-tail distances of  $\sim 20\text{--}30 R_E$  a few minutes before the onset of expansion phase signatures on the ground [*Nagai et al.*, 1998; *Nagai and Machida*, 1998; *Petrukovich et al.*, 1998; *Machida et al.*, 1999]. In this case the near-Earth signatures such as dipolarisation of the magnetic field and particle injections at geosynchronous orbit, auroral break up, and the onset of enhanced electrojets in the high latitude ionosphere, are a direct result of reconnection at the near-Earth neutral line, via plasma inflow followed by braking and flux 'pile-up' at the interface between quasi-dipolar and 'tail-like' field

lines [e.g. *Birn and Hesse*, 1996; *Shiokawa et al.*, 1997, 1998; *Birn et al.*, 1999]. Recovery then takes place in association with a movement of the neutral line into the more distant tail. An alternative view [*Lui*, 1991, 1996] is that the near-geostationary signatures described above are a result of some other near-Earth mechanism, often termed ‘current disruption’, and that reconnection further down the tail may then follow.

The present data set does not allow us to contribute directly to this debate, specifically because the outbound Cassini trajectory took place in the post-midnight and dawn sector which is usually not strongly responsive to substorm onset. As indicated above, Geotail observations have shown that reconnection and plasmoid formation are generally dusk and midnight near-Earth phenomena [*Nagai et al.*, 1998; *Nagai and Machida*, 1998; *Machida et al.*, 1999]. The Cassini data thus provide an opportunity to study the behaviour of the dawn plasma sheet over a range of distances during two substorms. We find that this does indeed show marked substorm responses, which are the primary focus of this paper. Observations during ‘substorm 1’, which spanned the interval 0345-0645 UT on 18 August 1999, are discussed in Section 3, while observations during ‘substorm 2’, which spanned 0645-0945 UT, are discussed in Section 4. Before this, however, we provide in the next section an overview of the data set that was obtained during the Cassini ESB interval.

## **2. Instrumentation**

The database acquired during the Cassini ESB contains information on the solar wind and IMF from ACE, IMP-8, and Geotail, as well as data from the magnetosheath and outer magnetosphere obtained by Interball-Tail and Wind. Field and particle monitoring data from geostationary orbit were obtained from two GOES spacecraft and three LANL instruments on geosynchronous spacecraft. Ground-based data on geomagnetic disturbance are available from a large network of magnetic observatories, spanning the Japanese, Canadian/American, and European sectors. Ionospheric flows were measured by the SuperDARN network of HF radars, as well as by the Søndrestrøm incoherent-scatter radar in Greenland. Finally, ultra violet (UV) auroral images at high-time resolution were obtained over much of the flyby interval by the Polar spacecraft. Not all of the instruments have been used here because we are mainly interested in the tail and substorms, and hence nightside data. Below we give further details of those instruments used in the present study.

### *2.1 Space-based instrumentation*

A central focus of this paper is the magnetic field data obtained by the fluxgate magnetometer on the Cassini spacecraft [Dougherty *et al.*, 2001]. The magnetic field investigation provided magnetic measurements at 32 samples per second throughout the terrestrial encounter, though they are employed here in averaged form. Observations of auroral kilometric radiation (AKR) from the Cassini Radio and Plasma Wave Science (RPWS) investigation [Gurnett *et al.*, 2001] are also used to help identify the timing of major substorm features [Kurth *et al.*, 2001]. Plasma and energetic particle data from Cassini are described in other papers in this special issue [Rymer *et al.*, 2001; Abel *et al.*, 2001; Lagg *et al.*, 2001], and will be cross-referenced in our discussion. Upon approach to Earth, Cassini was travelling almost directly along the Earth-Sun line, intersecting the bow shock at 0151 UT with GSM coordinates  $(X,Y,Z)$   $(+14.9,+3.2,-0.1) R_E$ , and the magnetopause at 0226 UT at  $(+9.5,+2.5,-0.2) R_E$ . After its passage by the Earth, the spacecraft made a rapid 6-hour transit of the tail in the dawn sector, finally exiting the northern tail lobe into the magnetosheath at  $\sim 1047$  UT, at a geocentric radial distance of  $67 R_E$ . Figure 1 shows the projection of the Cassini trajectory in GSM coordinates, in the  $X$ - $Z$  (top panel) and  $X$ - $Y$  (bottom panel) planes. Open circles give hour markers (in UT on 18 August 1999) along the trajectory. A model bow shock and magnetopause are shown using the models of Peredo *et al.* [1995] and Roelof and Sibeck [1993], determined for typical solar wind conditions during this interval (i.e. solar wind velocity  $\sim 600 \text{ km s}^{-1}$ , upstream dynamic pressure  $\sim 2 \text{ nPa}$ , number density  $\sim 3 \text{ cm}^{-3}$ , IMF  $B_z$  field  $\sim -2 \text{ nT}$ , and total field strength,  $B_T \sim +7.5 \text{ nT}$ ). It is clear from Figure 1 that between  $\sim 0400$  and  $\sim 1000$  UT Cassini was in the tail of the magnetosphere, placing it in an appropriate position to observe conditions during substorm activity. As indicated above, two complete substorm cycles took place, during the contiguous intervals 0345-0645 UT and 0645-0945 UT, respectively. During the first interval the Cassini spacecraft moved outbound from a position within the nightside plasmasphere at GSM coordinates  $(X,Y,Z) \sim (-2.9,+0.1,-0.1) R_E$  (the plasmopause was crossed at  $\sim 0350$  UT at a radial distance of  $3.7 R_E$ ), to the dawn-side near-Earth tail at  $(-27.7,-11.4,+4.3) R_E$ . During the second interval it moved from the latter position to the mid-tail at  $(-52.3,-21.6,+10.8) R_E$ , prior to final exit from the northern tail magnetopause at  $\sim 1047$  UT.

During the pass the upstream solar wind and IMF were measured using the SWEPAM and MAG instruments, respectively, on the ACE spacecraft [McComas *et al.*, 1998; Smith *et al.*, 1998; Stone *et al.*, 1998]. ACE was located in the solar wind near the Earth-Sun L1 libration point, and for the purposes of this study we use magnetic field and plasma data at 16 s and 64 s resolution, respectively. All magnetic field and spacecraft position data presented in this paper are in GSM coordinates. At the time of these observations, ACE was located at GSM coordinates  $(X,Y,Z)$   $(+248.3,+6.3,+23.9) R_E$ . The calculation of the delay between the observations recorded at the spacecraft and the incidence of these conditions at the subsolar magnetopause was determined using the technique described by Khan and Cowley [1999]. In this instance, since the spacecraft was located relatively close to the Earth-Sun line, the  $X_{GSM}$  position of the spacecraft and the observed solar wind speed have been used to calculate the transit time of field changes between the spacecraft and the subsolar bow shock. Thereafter the technique employs a fourfold decrease of the

solar wind speed at the shock, and a subsequent deceleration through the magnetosheath to an inflow speed of  $\sim 20 \text{ km s}^{-1}$  at the subsolar magnetopause. This procedure gives an average delay of  $\sim 47.5 \text{ min}$ , which has been included here in our analysis.

In addition to the ACE spacecraft, magnetic field measurements at 3 s resolution from the Wind spacecraft [Lepping *et al.*, 1995] are also used, as it passed through the magnetosheath into the magnetosphere on the dusk flank. The Wind spacecraft entered the magnetosphere at  $\sim 0320 \text{ UT}$  at a GSM position  $(-6.5, +20.5, -3.0) R_E$ . The projection of the Wind track is also indicated in Figure 1, showing that the spacecraft is in the southern dusk flank as Cassini travelled down-tail.

Also shown in Figure 1 is the track of the geostationary GOES-10 satellite, positioned at  $135^\circ \text{ W}$  geographic longitude near the western coast of the USA. Magnetic field measurements are used here with a resolution of 90 s. Magnetic data from the eastern satellite, GOES-8, positioned at  $75^\circ \text{ W}$  geographic longitude, are also used in this study. Geostationary orbit electron and proton fluxes (50 keV–1.6 MeV and 50 keV–50 MeV, respectively) were obtained from the Los Alamos National Laboratory (LANL) Synchronous Orbit Particle Analyzers (SOPA) on satellites 1989-046, 1994-084, and LANL-97A. However, only data from the first of these satellites is employed here, since the other two were located on the dayside, away from the particle injection region.

## 2.2 Ground magnetometer stations

A major feature of this paper is that we relate features observed in space to those on the ground. To this end, a large network of ground magnetometer stations have been used to set the Cassini tail data into a global context. During the flyby, data from four nightside magnetometer arrays have been investigated. From west to east these are the Canadian CANOPUS array [Rostoker *et al.*, 1995], the stations operated by the Geological Survey of Canada, the western high-latitude stations of the MACCS array [Engebretson *et al.*, 1995], and the Greenland west-coast magnetometer chain [Wilhjelm and Friis-Christensen, 1976]. Data from a selection of these stations are presented in the following section. All the magnetic observations have been made using fluxgate magnetometers with sampling intervals between 5 s and 20 s, and data are presented in a common geographic coordinate system where  $X$  is northward,  $Y$  eastward, and  $Z$  vertically down. Other northern hemisphere magnetometer arrays, such as the IMAGE [Lühr, 1994], SAMNET [Yeoman *et al.*, 1990], and CPMN [Yumoto *et al.*, 1996] arrays, also collected data. However they are not employed in this study because they were mainly located on the dayside during the interval of interest.

Figure 2 shows the position in magnetic local time (MLT) and magnetic latitude of the magnetometer stations we have employed at two particular key times, 0511 UT (Figure 2a, upper plot) and 0733 UT (Figure 2b, lower plot), which correspond to the expansion phase onsets of the

two substorms studied here. Also plotted in Figure 2 are the footprint tracks and positions at the specified times (solid triangles) of the Cassini (post-perigee only), Wind, and geostationary spacecraft, mapped using the Tsyganenko (T89) model with  $K_p = 5$  in Figure 2a and  $K_p = 4$  in Figure 2b [Tsyganenko, 1989]. The motivations for use of these particular Tsyganenko models will be described below.

### 2.3 SuperDARN radar measurements

Ionospheric convection velocities in this study were provided by the three pairs of northern hemisphere HF coherent radars, forming part of the international Super Dual Auroral Radar Network (SuperDARN) [Greenwald *et al.*, 1995]. Figure 3 presents the fields of view (f-o-v) of the radars plotted on a magnetic grid system in the same format as Figure 2, to allow comparison with the magnetometer positions. Each radar is frequency agile within the range 8-20 MHz, measuring ionospheric backscatter from field-aligned irregularities which move with the background plasma at F-region altitudes, thus providing information on the large-scale convection pattern. During standard operations, the radar experiment comprises of a full scan of 16 beam positions separated by  $3.24^\circ$ , where each beam is gated into 75 range gates of 45 km length along the line of sight (l-o-s) of the radar, with a dwell time for each beam of 3 s or 7 s. This configuration provides coverage of  $52^\circ$  in azimuth and over 3000 km in range (an area of over  $4 \times 10^6 \text{ km}^2$ ) every 1 or 2 min. For each of the beams and ranges an 18-lag complex autocorrelation function is determined, from which the l-o-s Doppler velocity, spectral width, and backscatter power of the irregularities are calculated.

The data presentation in the subsequent sections uses the ‘map-potential’ technique developed by Ruohoniemi and Baker [1998], where the l-o-s velocities from each of the radars are combined and then fitted to an expansion of the electrostatic potential in spherical harmonic functions [e.g. Bristow *et al.*, 1998]. From this the overall ionospheric convection pattern is generated, the solution being constrained by a statistical model keyed to the IMF conditions, in this case as measured by the ACE spacecraft. The order of the expansion can be specified in the procedure; in the absence of complete data coverage, higher orders generally require increased contributions from the statistical model to constrain the fitted solution. It is generally accepted that unless the data coverage is exceptionally high, a relatively low order of expansion is appropriate, which provides a good indication of the overall global convection pattern, if not the details [Ruohoniemi and Baker, 1998]. In this analysis an expansion of order 4 has been used, such that the derived electrostatic contours principally follow the character of the observed data in the region of coverage, rather than being strongly influenced by the statistical model. The map-potential technique also outputs several different types of velocity flow vectors, some of which are derived directly from the model, while others use information which are closer to the original observations. In this study, the ‘true vectors’ are presented, which are produced by combining the transverse component of the fitted velocity

vectors (that is, the transverse velocity components obtained from the fitted convection pattern) with the measured l-o-s velocity, thus allowing small-scale variations of the l-o-s velocity to be recovered.

#### 2.4 Polar UVI data

Finally, to complete the ancillary data set, observations from the Ultraviolet Imager (UVI) instrument on the Polar spacecraft [Torr *et al.*, 1995] were used to provide images of the aurora during the fly-by. UVI measures auroral emissions in the Lyman-Birge-Hopfield (LBH) system of bands, the result of electron impact excitation of N<sub>2</sub>, with filters LBH1 and LBHs, which are centred on 170 and 150 nm, respectively. During the ESB only the LBH1 filter was employed, to maximise the time resolution. The integration period was 36 s. In the time frame of this study, ~03-10 UT, the Polar spacecraft was increasing in altitude on the dawn side towards its apogee of 9 R<sub>E</sub> (~8 UT), such that UVI was able to image the entire northern auroral oval throughout the interval.

### 3. Substorm interval 1: 0345-0645 UT

#### 3.1 Geophysical conditions

We now employ the data obtained from the various ground and space-based instrumentation introduced above to describe the geophysical conditions prevailing during the Cassini tail passage, and begin with substorm interval 1 corresponding to 0345-0645 UT. Prior to this interval the magnetosphere had been moderately disturbed, with  $Kp = 4+$  for the interval 0000–0300 UT, but examination of the ground magnetic records indicates that this disturbance had largely died away by the start of the interval considered here. We note for future reference that the  $Kp$  index for 0300-0600 UT was 5-.

#### 0345-0511 UT: Substorm 1 – Growth phase

Examination of Figures 4-8 shows that the period 0345–0511 UT was an interval of magnetic quiet, corresponding to the growth phase of the first substorm. In each of these plots the vertical dashed lines mark key times during the substorm, as will be elucidated in the following sections. These times correspond to substorm expansion phase onset, indicated by ‘S1’, impulsive intensification, ‘I1’, onset of auroral zone recovery, ‘R1’, and the end of the recovery phase, ‘E1’.

Interplanetary parameters measured upstream of the magnetosphere by the ACE spacecraft are shown in Figure 4. These data are plotted lagged in time by 47.5 min to the subsolar magnetopause, as discussed above. The data show the presence of a relatively fast ( $\sim 600 \text{ km s}^{-1}$ ), moderate-density ( $\sim 3 \text{ cm}^{-3}$ ) solar wind throughout the growth phase, and a relatively steady interplanetary magnetic field (IMF). IMF  $B_x$  was consistently negative at  $\sim -6 \text{ nT}$ , while IMF  $B_y$  was predominantly positive at  $\sim +4 \text{ nT}$ , with some  $\sim 10 \text{ min}$  excursions towards near-zero and negative values. IMF  $B_z$  was mainly negative at  $\sim -2$  to  $-5 \text{ nT}$ , but with some  $\sim 10 \text{ min}$  excursions to positive after  $\sim 0400 \text{ UT}$  and  $\sim 0500 \text{ UT}$ . The predominantly negative values indicate that reconnection and open flux production was active at the dayside magnetopause during the interval, leading to enhancement of the flux in the tail lobes and growth of the tail current system.

Confirmation of flux transport into the tail can be found in the SuperDARN velocities, which are consistent with the presence of a well-developed twin-vortex flow throughout the interval, with a transpolar voltage of  $\sim 50\text{-}60 \text{ kV}$ . In Figure 9a we show data for the 2-min interval starting at 0454 UT, which is representative of the radar data for the  $\sim 20 \text{ min}$  interval prior to substorm expansion phase onset (at 0511 UT). The solid lines show superposed equipotential streamlines, derived from the ‘map-potential’ algorithm discussed above. Well-developed flows were present on both the day and night sides, consistent with a twin-vortex flow of  $\sim 60 \text{ kV}$  transpolar voltage, which we infer was driven predominantly by dayside reconnection at this time.

The lack of substantial nightside driving is indicated by the lack of significant magnetic disturbance during the interval, the lack of AKR emission, and the lack of nightside auroral features. Ground magnetic data are shown in Figures 5-7. Figure 5a shows data from a latitudinal chain spanning  $62.3^\circ\text{-}77.5^\circ$  with a longitude such that  $\text{MLT} \sim \text{UT} + 15.6 \text{ h}$  (stations MEA to CBB, see Figure 2a). Figure 6 then illustrates the longitudinal variation of magnetic features at a typical ‘auroral zone’ magnetic latitude of  $\sim 67^\circ$ , the data spanning a  $\sim 9\text{-hour}$  interval of local time from  $\sim 2$  hours earlier than the latitude chain to  $\sim 7$  hours after (stations DAW to NAQ). Figure 7 similarly presents magnetic data from a higher-latitude longitudinal chain at  $\sim 74^\circ$ , which extends in local time  $\sim 7 \text{ h}$  of MLT to the east of the latitudinal chain (stations CON to ATU). None of these stations indicate the presence of significant electrojet activity during the growth phase interval.

The upper panel of Figure 5b similarly shows a logarithmic plot of the integrated AKR power flux measured by the Cassini RPWS instrument during ‘substorm 1’ (taken from a longer data set discussed by *Kurth et al.* [2001]), while the lower panel shows X component data from station MCM (as in Figure 5a) for ease of comparison with the ground magnetic data. During this interval

(and that of ‘substorm 2’), Cassini was sufficiently close to the midnight meridian that it was well situated to observe AKR from the nightside auroral region. The correlation of AKR with discrete auroral arcs [Gurnett, 1974] and subsequent demonstrations of the correlation between AKR intensity and the auroral electrojet ( $A_E$ ) index [Voots *et al.*, 1977], has led to the development of AKR indices as proxies for  $A_E$  [Murata *et al.*, 1997; Kurth and Gurnett, 1998; Kurth *et al.*, 1998]. This index has the advantage of being obtainable by a single suitably-positioned spacecraft because of the global nature of the detection of AKR. The index itself is obtained by integrating the power flux from 50 to 800 kHz, and scaling to some convenient radial distance, since the received power falls as  $R^{-2}$ . To be consistent with Kurth *et al.* [1998], we choose the scaling distance to be  $9 R_E$ , and have calculated the integrated power flux once per minute. AKR sometimes violates both of these spectral limits, but the power outside of the chosen band is a small fraction of the total, and the potential for contamination from other radio sources is minimized. Some solar type III radio bursts do occur during the interval and contribute to the power in the band, but we do not believe they substantially affect the integrated power flux. These data also confirm that the power flux in the AKR band was low and essentially unvarying during the growth phase interval (the low-amplitude ‘spikes’ at the beginning of the interval appear to be due to magnetospheric emissions observed at and just outside the plasmopause, see Kurth *et al.* [2001]).

UVI images for the interval indicate the presence of weak auroras in the midnight and morning sectors, centred near  $\sim 63^\circ$  latitude, which tended to weaken as the growth phase progressed. A grey-scaled UVI image obtained simultaneously with the radar data (for the 36 s interval beginning at 0454:12 UT) is superposed on the SuperDARN plot in Figure 9a. It shows only the presence of very weak nightside UV emission, in the post-midnight sector. As in Figure 2a, the Cassini footprint at this time has been mapped into the ionosphere using the T89  $Kp = 5$  model. The choice of this model was motivated by two factors. First, the prevailing  $Kp$  value for the interval was indeed 5-, as noted above. Second, the model field was found to fit the Cassini data during this interval tolerably well (better than other related models), as will be shown below. The footprint is shown in the dawn sector of the figure by the solid triangle (as are the footprints of the three geostationary spacecraft to its west). We note that this mapping places Cassini essentially within the auroral oval at this time, a little poleward of geostationary orbit in the region of closed-field line sunward return flow in the dawn cell. The spacecraft was located at GSM co-ordinates  $(-12.7, -4.6, +1.2) R_E$  at that time.

Evidence for the presence of tail-like fields at geostationary orbit during the growth phase can be seen in the GOES-8 and GOES-10 magnetic data shown in Figure 8. Here the lighter lines

represent the magnetic data obtained from GOES–10 at MLT  $\sim$  UT + 15.0 h, whilst the heavier lines indicate GOES–8 data at MLT  $\sim$  UT + 19.1 h. The latter data show that the geostationary field near midnight was already tail-like at the beginning of the interval, with a latitude angle of  $\sim 25^\circ$ . This then decreased to  $\sim 20^\circ$  by the end of the growth phase, due mainly to an increasing  $B_x$  component, while  $B_z$  remained relatively constant. The GOES–10 data, nearer to dusk, also show a decreasing latitude angle during the growth phase, from  $\sim 55^\circ$  to  $\sim 35^\circ$ . In this case, however, the effect was mainly due to falling  $B_z$  in the presence of relatively steady  $B_x$  and  $B_y$  components. Comparison with the T89  $K_p = 5$  model (shown by the dashed lines) indicates that a significant part of this effect was due to spacecraft motion towards midnight.

#### *0511-0532 UT: Substorm 1 – Expansion phase onset and initial development*

The UVI data show that the expansion phase onset of ‘substorm 1’ took place at 0511 UT, when a localised patch of UV emission appeared at  $\sim 63^\circ$  in the pre-midnight sector, spanning  $\sim 2030$ – $2230$  MLT, with the brightest emission occurring at the westward end. This onset time is shown by the vertical dashed line marked S1 in Figures 4-8. The nearest magnetometer stations, MCM and MEA, recorded the onset of a weak magnetic disturbance at that time (Figure 5a), while weak Pi2-band activity also began at these and at a number of other low-latitude stations (data not shown). The Cassini AKR index data shown in Figure 5b confirm the onset of AKR emissions at that time, concurrent with the onset at MCM, which then grew in intensity by three orders of magnitude over the next  $\sim 10$  min. At geostationary orbit, a modest ‘dipolarisation’ of the field occurred at GOES–10 over the same interval, located just to the west of the auroral onset region, due mainly to a rapid increase in the  $B_z$  component at the spacecraft (lighter lines in Figure 8). Correspondingly, a weak undispersed energetic ion injection was observed shortly afterwards at spacecraft 1989–046 at  $\sim 1830$  MLT. Energetic electrons at the latter spacecraft were initially unaffected, indicating a location just beyond the westward end of the geostationary injection region. The field at GOES–8 at  $\sim 0030$  MLT, well to the east of the initial region of disturbance, showed less marked behaviour, though the  $B_x$  component started to decline (together with the total field strength), and the  $B_z$  component to modestly increase, after  $\sim 0518$  UT (heavier lines in Figure 8).

Over the next  $\sim 20$  min the disturbed region expanded both in latitude and local time, with the auroras reaching eastward to midnight (near the GOES–8 meridian) by  $\sim 0520$  UT, and westward to  $\sim 2000$  MLT by  $\sim 0530$  UT. Correspondingly, magnetometer stations on the  $\sim 67^\circ$  latitude chain (Figure 6) observed gradual bay development from DAW at  $\sim 1900$  MLT to GIL at  $\sim 2300$  MLT, but

not beyond to PBQ at  $\sim 0100$  MLT or NAQ at  $\sim 0400$  MLT. The disturbed region did not, therefore, extend to the local time of Cassini ( $\sim 0200$  MLT) during this interval. On the latitude chain (Figure 5a), which passed through the western end of the onset region at  $\sim 2100$  MLT, bay development was confined to stations at latitudes of  $\sim 68^\circ$  or lower, while the Z component indicates that the initial westward electrojet was centred near  $\sim 65^\circ$ . Correspondingly, stations on the higher-latitude  $\sim 74^\circ$  chain (Figure 7), observed no significant disturbances during this interval.

After expansion phase onset the velocities observed by the SuperDARN radars remained consistent with twin-vortex flow, with a similar transpolar voltage to that which prevailed during the late growth phase,  $\sim 55$  kV. We note from Figure 4 that while the (time-shifted) IMF  $B_z$  component was positive in the interval just before onset, it became negative again at about the time of onset, and throughout much of the expansion phase. We thus infer that the magnetosphere remained strongly driven by dayside reconnection during much of the  $\sim 45$  min substorm expansion phase interval. In Figure 9b we show the SuperDARN flows for the 2-min interval starting at 0518 UT in the same format as Figure 9a, together with a superposed UVI auroral image (for the 36 s interval beginning at 0518:07 UT). Comparison with the pre-onset flows in Figure 9a shows that although the inferred transpolar voltage was essentially the same in the two cases, the form of the nightside flow was altered. In particular, the flow mapping to the vicinity of the disturbed auroral region had become very small, and the flow out of the polar cap towards the nightside auroral zone was also reduced. In effect, the foci of the flow cells are shown as having been displaced towards the dayside. In common with some previous studies, therefore, we find that the flow within the high-conductivity bulge region became semi-stagnant, with the surrounding flow being diverted around it [e.g. *Kirkwood et al.*, 1988; *Morelli et al.*, 1995; *Yeoman et al.*, 2000]. We note, however, that the flow in the vicinity of the Cassini footprint, which lay well to the east of the disturbed region, had also become small in this interval, a fact which will be commented upon in the next section below. However, this occurrence was only a temporary phenomenon, lasting from just after onset until  $\sim 0520$  UT. After this, a more rapid eastward flow was resumed in the Cassini sector.

#### *0532-0555 UT: Substorm 1 – Substorm intensification*

At 0532 UT an intensification of the substorm was suddenly initiated, resulting in an enhancement of the disturbance in the region already effected, together with a further expansion in latitude and local time. This time is shown by the vertical dashed line marked I1 in Figures 4-8.

The intensification was marked not only in the ground magnetic records in Figures 5-7, but also in an enhancement of Pi2-band signals at a large number of stations at low and medium latitudes, and in the AKR emissions, which reached their peak intensity shortly thereafter, at  $\sim 0539$  UT (Figure 5b). A further undispersed energetic ion injection was observed in the dusk sector at spacecraft 1989-046, which was much stronger than the first, while the energetic electrons at the spacecraft show the onset of a more gradual increase after this time (Figure 8). The GOES-10 spacecraft also observed the onset of further ‘dipolarisation’ of the dusk-side geostationary field shortly after this time, while the GOES-8 spacecraft, just past midnight, observed its first major increase in  $B_z$ .

As indicated by the GOES-8 data, the intensification caused an immediate expansion of the disturbance into the morning sector, resulting in onset at station PBQ at  $\sim 66^\circ$  and  $\sim 0100$  MLT (Figure 6), lying just to the west of the Cassini footprint at  $\sim 65^\circ$  and  $\sim 0200$  MLT (Figure 2a). No significant disturbance was observed at NAQ at the same latitude at  $\sim 0330$  MLT, however, lying to the east of the Cassini footprint. We thus infer that Cassini was located near the eastward-most edge of the disturbed region at this time (at GSM coordinates  $(-17.9, -7.0, +2.2) R_E$ ). The progress of the aurora during the intensification cannot be followed due to lack of imager coverage of the nightside sector during the interval 0529–0537 UT. However, the first image obtained after coverage was resumed shows that the substorm aurora now extended at lower latitudes (at  $\sim 65^\circ$  and below) to  $\sim 0230$  MLT, just past the mapped Cassini meridian. This image (for the 36 s interval beginning at 0537:45 UT) is shown together with simultaneous SuperDARN radar data (for the 2-min interval beginning 0538 UT) in Figure 9c. The radar data is typical of that observed over the  $\sim 15$  min interval following the intensification. The limited scatter observed from within the substorm-disturbed region on the nightside again indicates the presence of semi-stagnant flows in this region, such that the plasma streamlines are diverted around it. Elsewhere, vigorous sunward flows are observed in the early morning hours in the region of the mapped Cassini footprint, lying just poleward of the brightest auroras, as well as on the dayside, at  $\sim 0900$  MLT. A relative minimum in flow speed occurred at similar latitudes near dawn. This is interpreted as indicating multi-celled dawn-side flow by the ‘map potential’ algorithm. Physically, we interpret the strong nightside flows as being driven principally by the substorm-induced transport of tail flux, distorted by the effects of high conductivity within the disturbed region itself [e.g. Cowley *et al.*, 1998]. The dayside flows are correspondingly driven principally by continued magnetopause reconnection, it being recalled that (time-shifted) IMF  $B_z$  was strongly negative (around  $-6$  nT) at this time (Figure 4).

The UVI image in Figure 9c also shows a poleward expansion of the aurora in the pre-midnight sector compared with that in Figure 9b, an expansion which is reflected in the onset of magnetic disturbance at stations up to  $\sim 70^\circ$  in this sector (Figure 5a). The westward end of the main auroral emission had not progressed much farther, beyond  $\sim 2000$  MLT. However, after this time the westward end of the aurora began to extend beyond the limit established during the first expansion interval, reaching its maximum extent at  $\sim 0555$  UT. A UVI image obtained during the 36 s beginning at 0554:19 UT, together with superposed SuperDARN vectors for the 2-min interval beginning at 0554 UT, is shown in Figure 9d. Compared with Figure 9c, it shows the presence of a new region of auroral disturbance extending in local time from  $\sim 2100$  MLT westward to  $\sim 1700$  MLT, and in latitude up to  $\sim 78^\circ$ . The poleward progress of this expansion is marked in the magnetometer data from station CON at  $\sim 73^\circ$  (Figure 5a), which lay at the eastward end of the newly disturbed region at  $\sim 2100$  MLT. These data show the onset of a negative bay at  $\sim 0543$  UT, with weaker disturbances being observed at BLC and RAN at almost the same time further eastward at the same latitude (Figure 7). The westward progress of the auroral intensification at lower latitudes is also marked at station DAW at  $\sim 66^\circ$  (Figure 6) and  $\sim 1900$  MLT, which was newly engulfed by the active auroral region at  $\sim 0545$  UT. These magnetometer data show a distinctive rotating pattern of horizontal field perturbation over the following  $\sim 5$  min interval, together with a strong negative  $Z$  component perturbation. We take this to be indicative of the westward propagation of the upward field-aligned current region of the westward-travelling surge poleward of the station at that time [e.g. *Opgenoorth et al.*, 1983]. Similar field perturbations were also observed at earlier times on the more eastward stations of the  $\sim 67^\circ$  chain (Figure 6), starting at station FSM at  $\sim 2030$  MLT at the onset of the intensification at 0532 UT, and then progressing to stations FSI and DAW to its west. This suggests that a steady duskward development had been in progress since the start of the intensification, marked by a westward-travelling surge formed initially near  $\sim 2100$  MLT.

The SuperDARN flows in Figure 9d, for the 2-min interval starting at 0554 UT at the end of the main expansion phase, contain no information (other than statistical input) on the dusk cell flow in the region of main auroral development (see the SuperDARN radar coverage in Figure 3). In the dawn sector, they indicate the maintenance of rapid flows on the nightside, which continue to avoid the semi-stagnant main auroral region. The dayside flows, however, had diminished significantly compared with Figure 9c, consistent with the IMF  $B_z$  data (Figure 4) which indicate a shift to near-zero and positive values after  $\sim 0545$  UT.

Overall, we interpret the expansion of the substorm aurora to very high latitudes in the dusk sector during this interval as being the signature of rapid reconnection in the dusk sector of the tail, during which a significant amount of open flux was closed. The lack of such poleward progress during the prior interval then suggests a relative lack of net open flux closure during that period. This does not mean that significant open flux reconnection did not take place in the tail prior to this time, however. It must be remembered that IMF  $B_z$  was strongly negative during much of the expansion phase until  $\sim 0550$  UT, such that dayside reconnection will have caused simultaneous inflation of the polar cap, offsetting any closure of open flux on the nightside during that interval.

#### *0555-0635 UT: Substorm 1 – Recovery*

Although the period after 0555 UT is described here as the ‘recovery phase’ of the first substorm, with an onset shown by the vertical dashed line marked R1 in Figures 4-8, significant magnetic activity in fact remained present until  $\sim 0635$  UT (marked as end time E1 in these figures). However, during this time the magnetic disturbance was mainly confined to high magnetic latitudes, such that the ‘recovery’ to which we refer is related to usual auroral zone latitudes. If we consider data from the latitude chain in Figure 5a, for example, now located at  $\sim 2200$  MLT, it can be seen that the peak disturbance for the lower latitude stations generally occurred near  $\sim 0555$  UT and declined thereafter, reaching small values by  $\sim 0635$  UT. Examination of the magnetograms from the high-latitude chain at  $\sim 74^\circ$  in Figure 7 show instead that disturbance onset occurred shortly after 0555 UT at station CBB at  $\sim 77^\circ$ , with similar onsets or intensifications at BLC and RAN at  $\sim 2300$  MLT, and later at  $\sim 0605$  UT at IQA at  $\sim 0230$  MLT. This station lay just poleward of the mapped Cassini footprint at this time (Figure 2a). No significant disturbances intruded to the Greenland west meridian at  $\sim 0400$  MLT, however, as indicated by the data from station ATU in Figure 7. Similarly, data from the high-latitude MACCS stations RBX and PBX at  $\sim 77^\circ$  and  $\sim 2400$  MLT (not shown) indicate the onset of brief bay disturbances at  $\sim 0615$  UT, which peaked at  $\sim 0620$  UT and recovered by  $\sim 0635$  UT. The Cassini AKR index data in Figure 5b correspondingly show the presence of weaker sporadic emissions during the ‘recovery’ interval, which decreased to the background level after  $\sim 0630$  UT.

The magnetic data thus indicate an eastward and poleward propagation of the high-latitude disturbance during the ‘recovery’ interval starting at 0555 UT, with magnetic (and AKR) quiet conditions being restored after  $\sim 0635$  UT. The UVI data show that this development was initiated from the eastward end of the high-latitude dusk auroral ‘bulge’ region which was formed during the

interval of substorm intensification described above, and shown in Figure 9d. This is illustrated by the UVI image obtained during the 36 s interval beginning at 0608:25 UT shown in Figure 9e, where significant high-latitude ( $\sim 75^\circ$ ) emission now extended eastward from the main dusk bulge to  $\sim 2300$  MLT. The lower-latitude emission had faded somewhat at this time, as can be seen by comparison with the image shown in Figure 9d. Following the discussion given above, the implication seems to be that net closure of open flux in the tail proceeded downward across the tail during this interval, such that magnetic disturbance and auroras reached to higher latitudes than previously, moving into the morning sector (station IQA and the Cassini longitude) after  $\sim 0605$  UT. The corresponding SuperDARN flow map for the 2-min interval starting at 0608 UT in Figure 9e indicates the continued presence of a relatively vigorous ( $\sim 40$  kV) nightside flow, despite the concurrent weak and northward-directed (time-shifted) IMF. We thus infer that the flow was driven principally by the inferred tail reconnection at this time. We also note that the flow in the low-latitude midnight sector had now become enhanced compared with the near-stagnant flows observed in this region since the beginning of the expansion phase.

After this time, the auroral emissions began to fade rapidly, first principally in the midnight sector, and then also in the dusk ‘bulge’ region. By  $\sim 0635$  UT only weak emissions remained throughout the previously disturbed region, together with weak magnetic disturbances. AKR-band emission observed by Cassini also reached background at about that time, as noted above. Similarly, significant nightside dawn cell flows remained until  $\sim 0620$  UT, before falling to small values over the whole field-of-view by  $\sim 0635$  UT.

### 3.2 Magnetic observations in the tail during substorm 1 - Cassini and Wind data

In this section we now present the nightside magnetic field data observed during the first substorm by the Cassini and Wind spacecraft, and will interpret them in the light of the data outlined above. We will also refer to the Cassini particle observations reported in this issue, specifically to the plasma ion (1 eV-15 keV) and electron (0.6 eV-27 keV) data presented by *Rymer et al.* [2001] and *Abel et al.* [2001], and the energetic ion (30 keV-4.5 MeV) and electron (15 keV-9.5 MeV) observations reported by *Lagg et al.* [2001]. The principal features of the ground-based data as far as the Cassini footprint is concerned may be summarised as follows. First, the SuperDARN data shown in Figure 9 indicate that the spacecraft was located centrally in a region of sunward ‘return’ flow throughout the entire substorm. It is thus anticipated that Cassini was consistently located on closed field lines in the earthward-flowing plasma sheet during this interval,

and hence earthward of any tail reconnection region. Second, the spacecraft, located at  $\sim 0200$  MLT, was positioned eastward of the substorm-disturbed region at expansion phase onset at 0511 UT, and remained eastward of this region during the initial expansion, up to 0532 UT. The substorm intensification at the latter time resulted in the auroral and magnetic disturbance propagating eastward past the Cassini meridian, though the footprint remained just poleward of the bright UV auroras. Finally, the magnetic disturbance reached to higher latitudes at the Cassini meridian during the recovery phase after 0555 UT, reaching  $\sim 73^\circ$ , poleward of the spacecraft footprint at  $\sim 68^\circ$ , after  $\sim 0605$  UT.

In Figure 10a we show the Cassini magnetometer data for the interval 0345-0645 UT, which corresponds to these events. The dashed lines show the values of the T89  $Kp = 5$  field model at the spacecraft location. This model gave the best overall fit during the interval of any of the Tsyganenko models investigated, thus providing a motivation (together with the actual  $Kp$  value) for its use in mapping spacecraft positions to the ionosphere. The observed  $B_y$  field, however, was generally larger than that predicted by the model, probably reflecting positive  $B_y$  conditions in the IMF (Figure 4). At the beginning of the interval, Cassini was located in the dipolar field of the plasmasphere, dominated by the  $B_z$  component, at a radial distance of  $2.9 R_E$ , near the midnight meridian and on the equator. The plasmopause was crossed at  $\sim 0350$  UT at a radial distance of  $3.7 R_E$  [Kurth *et al.*, 2001]. The spacecraft then rapidly left the quasi-dipolar region due to its unusually high radial speed, and by  $\sim 0430$  UT was located in a tail-like region at a down-tail distance ( $|X_{GSM}|$ ) of  $\sim 9.3 R_E$ , dominated by a relatively steady  $B_x$  component with a smaller and still-falling  $B_z$ . The Cassini data thus provide a relatively rapid ‘snapshot’ of the growth-phase field structure in the near-Earth transition region between dipolar and tail-like fields.

Figure 10b shows field vectors projected onto the GSM  $X$ - $Z$  plane during the interval 0400-0700 UT, encompassing the whole of the first substorm interval. Small arrows indicate the spacecraft position at the same key substorm times as shown in Figure 10a and previous figures. It can be seen that the transition between approximately northward-pointing fields and approximately sunward-pointing fields took place at Cassini between  $\sim 0415$  and  $\sim 0425$  UT at down-tail distances between  $\sim 7.2$  and  $\sim 8.6 R_E$ , just outside geostationary orbit. However, this change in field direction appears to have been associated not so much with the radial motion of the spacecraft, but more with its northward motion to distances  $\sim 1 R_E$  above the GSM equatorial plane. This is indicated directly by the GOES-8 geostationary magnetic field data in Figure 8 (heavy line), which shows the simultaneous presence of tail-like fields closer to the Earth at  $\sim 6.6 R_E$  near midnight, at distances  $\sim 1.5 R_E$  above the GSM equatorial plane. Specifically, Cassini and GOES-8 were at the same

radial distance of  $6.61 R_E$  at 0409 UT. At that time Cassini was located at GSM co-ordinates  $(-6.4, -1.6, +0.3) R_E$  and observed a magnetic field with GSM components  $(+3, +15, +47)$  nT, i.e. essentially northward-pointing. Simultaneously, GOES-8 was located at  $(-6.3, +1.5, +1.5) R_E$  and observed a field with components  $(+98, -8, +44)$  nT, i.e. mainly sunward-pointing. The  $B_z$  components at the two spacecraft were thus very similar at about  $\sim 45$  nT, while the  $B_x$  component was  $+3$  nT at Cassini at  $Z_{GSM} \sim 0.3 R_E$ , compared with  $+98$  nT at GOES-8 at  $Z_{GSM} \sim 1.5 R_E$ . About 20 min after this, however, at  $\sim 0430$  UT, Cassini, located at GSM co-ordinates  $(-9.3, -3.0, +0.7) R_E$ , also became immersed in a dominant steady  $B_x$  field, of amplitude  $\sim 30$  nT. These data thus indicate the presence of a well-developed tail-like field and thin ( $\sim 1 R_E$  thickness) equatorial current sheet extending close to the Earth early during the growth phase. The observed field structure is in approximate conformity with that indicated by the T89  $Kp = 5$  field model, shown for the noon-midnight meridian by the dashed lines in Figure 10b. In particular the model confirms the expectation of tail-like fields at modest  $Z_{GSM}$  at and near geostationary orbit, as observed by GOES-8.

Although the transition to a tail-like field at Cassini was thus complete by  $\sim 0430$  UT at a down-tail distance of  $\sim 9.3 R_E$ , the rather variable nature of the field during the remainder of the interval, to  $\sim 0645$  UT at down-tail distances of  $\sim 27.8 R_E$ , suggests the continuous presence of plasma currents. In conformity with the above inference based on the footprint mapping, therefore, the field data thus suggest that the spacecraft was continuously immersed within the plasma sheet during the first substorm. The essentially continuous positive values of  $B_z$  also indicate the presence of closed field lines. This inference is confirmed by examination of the plasma data, which show that the spacecraft did not exit from the plasma sheet into the tail lobe until  $\sim 0730$  UT, shortly before the onset of the expansion phase of the second substorm [Rymer *et al.*, 2001; Abel *et al.*, 2001; Lagg *et al.*, 2001]. The Cassini data during this first interval thus allow an examination of the behaviour of the near-equatorial near-Earth dawn plasma sheet, at  $\sim 0130$ - $0200$  MLT, over a complete substorm cycle.

During the growth phase, the  $X$  component of the field at Cassini showed an overall increasing trend between  $\sim 0440$  UT and the onset of the expansion phase at  $0511$  UT, while the expectation based on the T89 model is for modestly decreasing values. The energetic particle data indicate steadily declining fluxes during this interval, with near-isotropic ions and bi-directional ('cigar' anisotropy) electrons [Lagg *et al.*, 2001]. The decrease in particle flux was no doubt mainly related to the rapidly increasing radial distance of the spacecraft. However, at  $\sim 0500$  UT the energetic ion fluxes started to decline much more precipitately, the rapidly declining fluxes of

energetic electrons also became isotropic, and the field strength increased more rapidly. These phenomena are all indicative of growth phase thinning of the plasma sheet, though the spacecraft (then located  $\sim 1.5 R_E$  above the GSM equatorial plane) did not exit from the layer before the expansion phase onset.

At onset at 0511 UT (S1), Cassini was located at GSM coordinates  $(-14.8, -5.6, +1.6) R_E$ , i.e. in the dawn sector of the near-Earth tail. Comparison with the prior results from Geotail in this vicinity leads to the expectation that the spacecraft lay at the eastward extremity of the region principally effected by the onset of near-Earth reconnection [Nagai and Machida, 1998; Nagai *et al.*, 1998; Machida *et al.*, 1999]. Specifically, the Geotail data indicate that after onset, the plasma sheet at this location generally remains either stationary, or exhibits earthward ‘non-convective’ (field-aligned) flows, due to reconnection tailward of that location. In the present case, the T89 footprint of the spacecraft was located well to the east of the initial break-up bulge, the latter extending eastward only to  $\sim 2230$  MLT initially, and only reaching near to the midnight meridian by  $\sim 0520$  UT (Figure 9b). In conformity with these observations, it is the former ‘stationary’ plasma sheet scenario which is found to apply in this case, with only weak earthward-directed anisotropies being observed in the ion data after onset [Lagg *et al.*, 2001]. However, the plasma sheet was not completely unresponsive. While the ion fluxes remained relatively steady, the field strength at Cassini underwent a major decline, from  $\sim 35$  nT at  $\sim 0510$  UT to  $\sim 25$  nT at  $\sim 0524$  UT, after which it remained relatively constant once more until  $\sim 0530$  UT. The field direction, however, remained essentially unchanged during this process.

It is clear from the T89 model field plotted in Figure 10a that only a minor part of the field decline can be ascribed to the outward motion of the spacecraft. We also note that a related decline in the  $B_x$  component was observed near midnight by the GOES-8 spacecraft after 0517 UT, as mentioned above (Figure 8). In addition, there was no reduction in solar wind dynamic pressure during this time which could provide an external explanation (Figure 4). Further, since the particle fluxes did not increase during the interval, but tended to remain relatively constant [Rymer *et al.*, 2001; Abel *et al.*, 2001; Lagg *et al.*, 2001], the decrease in strength was not due to the spacecraft penetrating more deeply into the plasma sheet. Rather, the indications are that the overall pressure underwent a rapid decrease, with the field pressure decreasing by a factor of  $\sim 2$ . As will be discussed further in Section 5, we envisage that this effect was the response of the dawn plasma sheet to the onset of rapid reconnection and flux removal from the tail at the onset of the expansion phase in the sector immediately to the west of the spacecraft. We propose that the loss of flux in the adjacent region resulted in an expansion of the otherwise unperturbed dawn plasma sheet and tail

lobe field lines across the tail towards dusk. We note that it was precisely during this interval that the dawn cell ionospheric flow in the vicinity of the Cassini footprint changed from its usual consistently eastward direction to small values and irregular directions, as was noted above in relation to Figure 9b. This transient change in the flow was temporally coincident with, and seems likely to be related to, this field effect.

At 0532 UT an intensification of the substorm took place (I1), resulting in a rapid expansion of the disturbance past midnight into the morning sector, to  $\sim 0230$  MLT. The T89 mapping then places Cassini, now positioned at  $(-17.9, -7.0, +2.2)$   $R_E$  in the tail, within the local time sector of the disturbance, near to its eastward edge and just poleward of the bright UV auroras (Figure 9c). Simultaneously, within about a minute, the Cassini field data underwent a radical change, exhibiting an onset of large-amplitude variations, together with a significant (but temporary) decrease in magnitude. Both signatures indicate the presence of hot flowing plasma, the onset of high-amplitude field variability, in particular, often accompanying the onset of intervals of rapid plasma flow initiated by reconnection bursts [e.g. *Petrukovich et al.*, 1998; *Shiokawa et al.*, 1999]. The energetic ion data indeed indicate the presence of bursty earthward-directed anisotropies along the field during this interval, which became particularly intense (and interspersed with brief intervals of tailward-directed anisotropies) after  $\sim 0540$  UT as the field strength increased again [*Lagg et al.*, 2001]. These characteristics suggest that the spacecraft made a brief entry into the plasma sheet boundary layer during this interval, lying downstream from a reconnection region located tailward of the spacecraft [e.g. *Cowley*, 1980]. We suggest that it was this earthward-directed flow which resulted in the field ‘dipolarisation’ in both the dusk and midnight sectors at geostationary orbit, as noted above (Figure 8), and powered the expansion phase features observed at latitudes just lower than the Cassini footprint over the  $\sim 23$  min interval between the onset of the impulsive intensification (0532 UT) and the onset of recovery (0555 UT). It is notable, however, that the field at Cassini at a down-tail distance of  $\sim 20 R_E$  remained tail-like throughout this interval, and showed little tendency to become ‘dipolarised’ locally, as often happens during similar earthward-directed flows observed closer to Earth [e.g. *Machida et al.*, 1999]. We suggest that after the initial dipolarisation had taken place in the nearer-Earth system, a quasi-equilibrium was reached between dayside and nightside reconnection, in which plasma and flux injected from the tail was removed by outflow towards the dayside magnetopause. It will be recalled that the IMF remained strongly negative at the subsolar magnetopause until  $\sim 0545$  UT (Figure 4), indicative of rapid dayside reconnection, as also indicated by the dayside flows measured by the SuperDARN radars (Figure 9).

Recovery of this substorm appears to have been linked to the northward turn of the IMF at  $\sim 0545$  UT, after which IMF  $B_z$  remained small and predominantly northward-pointing at the subsolar magnetopause, until  $\sim 0630$  UT (Figure 4). Given a  $\sim 10$  min interval in which the dayside flows died away, associated with the outward motion of the dayside magnetopause [Cowley and Lockwood, 1992], an effect on the nightside behaviour after  $\sim 0555$  UT seems plausible. Specifically, tail reconnection will then lead to a clear net closure of open magnetic flux after this time, such that magnetic disturbance and auroras will move poleward. As indicated in the previous subsections, such behaviour is indeed seen in the ground magnetic and UVI data during the recovery phase, spreading eastward from the dusk sector, and arriving at the Cassini meridian at  $\sim 0605$  UT. The consequence for the tail field structure will be an outward spreading of a ‘dipolarisation’ effect associated with closed flux pile-up and increasing  $B_z$ , a reduction in the earthward flow in the plasma sheet and in the sunward auroral zone flow in the ionosphere, and a tailward retreat of the reconnection region. Correspondingly, the Cassini field data in Figure 10a show that  $B_z$  started to increase at about  $\sim 0605$  UT, such that the latitude angle of the field increased from  $\sim 5^\circ$  at this time to  $\sim 30^\circ$  at and after  $\sim 0615$  UT. This change in field direction is also evident in the vector plot in Figure 10b. The energetic ion data indicate the presence of continuing variable earthward-directed anisotropies in the plasma sheet in the early recovery phase while the field remained tail-like, and we recall the continuing vigorous nightside dawn cells flows observed near the foot of the Cassini field line during this interval by the SuperDARN radars (see Figure 9e at 0608 UT). However, the Cassini ion distributions became near-isotropic after  $\sim 0615$  UT in association with the rotation of the field direction [Lagg *et al.*, 2001], and the near-conjugate SuperDARN flows also dropped to small values at about that time, as indicated above. The fluxes of energetic particles were also strongly enhanced and the field strength weakened as this process took place, indicative of the enhanced presence of hot diamagnetic plasma sheet plasma. The spacecraft was located at  $(-23.7, -9.6, +3.4) R_E$  at this time (0615 UT).

We finally briefly discuss the Wind magnetic data, shown in Figure 11 in the same format as the Cassini data in Figure 10a. In this case the spacecraft was moving much more slowly into the southern region of the near-Earth tail from the dusk magnetosheath. The GSM  $X$  and  $Z$  coordinates of the spacecraft were relatively unchanging at  $\sim -8 R_E$  and  $\sim -4 R_E$ , respectively, while  $Y$  declined from  $\sim 19 R_E$  to  $\sim 16 R_E$  during the interval. Wind thus provided information on conditions in the southern dusk plasma sheet which are complementary to the dawn side data from Cassini. However, previous results from Geotail indicate that in this case the spacecraft lay westward of the usual region of reconnection onset and plasmoid formation, the plasma sheet again usually

remaining ‘stationary’ at and after expansion phase onset at this location [Nagai and Machida, 1998; Nagai *et al.*, 1998].

Examination of the Wind field data in Figure 11 and plasma data (not shown) indicate that a magnetopause transition from the dusk flank magnetosheath to the tail boundary layer took place at  $\sim 0320$  UT, just prior to the interval shown here. After this, the spacecraft was located intermittently in the tail and its boundary layer up until after substorm onset, and it was only after  $\sim 0530$  UT that it was located consistently either in the tail lobe or the plasma sheet. Observations after this time show that the spacecraft was initially located in the southern tail lobe, where the  $\sim 35$  nT field was flared away from the tail axis such that  $B_z$  was small or negative. However, starting at  $\sim 0545$  UT, and continuing until  $\sim 0555$  UT, the field direction at Wind rotated northward, such that  $B_z$  became consistently positive ( $\sim 5$  nT) thereafter. This behaviour mirrors the ‘dipolarisation’ observed at GOES–10 at geostationary orbit in the dusk sector which occurred at approximately the same time (Figure 8). The timing is coincident with the strong development of the substorm intensification in the dusk sector discussed above (see Figures 9c and 9d). We suggest that the  $B_z$  increase observed by Wind represents the response to an expansion of the reconnection region into the dusk sector following the ‘intensification’, which caused the expansion of the ground-based disturbance at dusk to earlier local times and to higher latitudes.

#### **4. Substorm interval 2: 0645-0945 UT**

##### *4.1 Geophysical conditions*

In this section we now discuss the second interval of disturbance which occurred during the interval 0645-0945 UT, beginning by noting that the  $K_p$  value for the period 0600-0900 remained reasonably large at 4+. During this interval Cassini traversed the mid-tail at moderately high  $Z_{GSM}$  values from the central dawn region to the dawn flank. For this interval the T89 model was used with  $K_p = 4$ , placing the ionospheric footprint of the spacecraft in the early morning sector, from  $\sim 0230$  to  $\sim 0530$  MLT and at latitudes  $70^\circ$ - $74^\circ$  (Figure 2b), near the flow reversal boundary between the auroral zone and polar cap. As will be shown below, this indicates that the spacecraft was located well poleward and eastward of the disturbed region until very late in the substorm. For this reason our discussion of the ground-based data will be relatively brief.

### *0645-0733 UT: Substorm 2 – Growth phase*

Examination of the interplanetary data in Figures 4 and 12 show that the recovery phase of the first substorm coincided with a shift in the predominant sense of IMF  $B_z$  from negative to small and positive values at  $\sim 0545$  UT, as indicated above. The magnetic records displayed in Figures 5-7 and 13-15 then show that the ground magnetic disturbance died away by  $\sim 0635$  UT, such that the period 0645-0733 UT discussed here was again an interval of relative magnetic quiet. The Cassini AKR index data shown in Figure 13b was also close to background throughout the interval (the small peak centred near 0655 UT was due to a type III solar radio burst). However, at  $\sim 0630$  UT IMF  $B_z$  became negative once more, peaking at values  $\sim -7$  nT, and remained predominantly negative for the next hour, prior to the second expansion phase onset at 0733 UT. Positive IMF  $B_z$  occurred for  $\sim 10$  min intervals starting at  $\sim 0645$  UT and  $\sim 0715$  UT, such that, as in the first substorm, the IMF was briefly northward in the interval leading up to onset, then turned south again near onset (and, also as before, remained south through much of the following expansion phase). The IMF  $B_x$  and  $B_y$  components remained consistently negative and positive, respectively, at  $\pm 5$  nT, the wind speed was high at  $\sim 600$  km s<sup>-1</sup>, and the density gradually declined from  $\sim 3$  to  $\sim 2.5$  cm<sup>-3</sup>.

Negative IMF  $B_z$  again suggests dayside reconnection and tail growth during this interval, and indeed the UVI data (not displayed) show that significant auroral emissions were present on the dayside, being strongest in the post-noon sector. However, no significant emissions were observed on the nightside during this period. In Figure 16, GOES-10 data (light line) from the pre-midnight sector ( $\sim 2200$  MLT) confirm the strong development of a tail-like field in the near-Earth system, which was mainly associated with a decrease in the  $B_z$  field component following the strong dipolarisation which occurred in the first substorm. A similar but less marked development was observed by GOES-8 (heavy line) in the morning sector at  $\sim 0200$  MLT, mainly confined to the interval after  $\sim 0655$  UT.

### *0733-0748 UT: Substorm 2 – Expansion phase onset and initial development*

UVI data show that the expansion phase onset of the second substorm occurred at 0733 UT, with an epicentre at  $\sim 2200$  MLT and  $\sim 64^\circ$ , mapping to near geostationary orbit. The Cassini AKR index rose above background at essentially the same time, the power flux then increasing by two orders of magnitude in  $\sim 5$  min (Figure 13b). The nearest ground stations, MCM and MEA, lying just to the east of the UVI onset region, observed negative bay onset at the same time (lines S2 in

Figures 13a and 13b), while an enhancement of Pi2 band signals was observed at a number of stations in this sector, up to  $\sim 68^\circ$  latitude (not shown). The patch of auroral emission, which was confined to relatively low latitudes, initially extended between  $\sim 2130$  and  $\sim 2300$  MLT. It subsequently expanded, more in longitude than in latitude, reaching  $\sim 2030$  and  $\sim 0100$  MLT by  $\sim 0740$  UT, before fading over the next  $\sim 10$  min. This behaviour is reflected in the observations of ground magnetic disturbance. Negative bay onset was observed on the latitude chain (which was again close to the meridian of onset) at stations at and below  $\sim 68^\circ$  (Figure 13a). No significant disturbances were thus recorded during this initial interval by the  $\sim 74^\circ$  longitude chain (Figure 15). On the  $\sim 67^\circ$  longitude chain (Figure 14), onset was observed only in the  $\sim 2100$ - $0000$  MLT sector (and thus at stations DAW to RAB, but not at GIL to NAQ). Correspondingly, a pronounced and immediate dipolarisation was observed at GOES-10, which was located at the local time of onset, but little reaction was seen at GOES-8 at  $\sim 0300$  MLT (Figure 16). A prompt undispersed ion injection was also observed by spacecraft 1989-046 located at  $\sim 2045$  MLT, just to the west of the onset region, with little response in the electrons.

All these measures thus confirm that Cassini, located at onset at  $(-34.3, -14.2, +6.0) R_E$  in the tail, mapping to  $\sim 72^\circ$  and  $\sim 0315$  MLT in the ionosphere (Figure 2b), was located well to the east of the region initially effected by the substorm, and at much higher latitudes. This is illustrated in Figure 17a, where we show a UVI image obtained towards the end of the initial phase of expansion, for the 36 s interval beginning at 0740:25 UT, together with a superposed SuperDARN flow plot (for the 2-min interval beginning at 0740 UT). Patchy ‘bulge’ auroras extended at relatively low-latitudes from  $\sim 2030$  to  $\sim 0100$  MLT as indicated above. Semi-stagnant flows were again observed in the low-latitude morning sector mapping to the vicinity of the substorm-disturbed region, while faster dawn-cell flows were observed at higher latitudes in this sector, and at later local times. The Cassini footprint is thus inferred to have been located in a region of eastward and poleward flow near to but equatorward of the flow reversal boundary, well away from the substorm-disturbed region. A well-developed flow was also observed on the dayside at this time, consistent with the IMF  $B_y$  positive,  $B_z$  negative conditions which prevailed (Figure 12).

#### *0748-0810 UT: Substorm 2 –Substorm intensification*

The UVI data show that a distinct intensification of the substorm took place at 0748 UT (line 12). A new patch of intense emission appeared at lower latitudes at  $\sim 2200$  MLT, within the previously-disturbed region, and rapidly expanded poleward to  $\sim 70^\circ$  in that meridian by  $\sim 0755$  UT,

as well as duskward to  $\sim 2100$  MLT and dawnward to  $\sim 0200$  MLT (to  $\sim 0300$  MLT at lower latitudes). Corresponding behaviour was observed in the ground magnetic disturbance and Pi2-band signals, where intensification was observed at the lower latitude stations on the latitude chain (Figure 13a), at  $\sim 68^\circ$  and below (stations FSM to MEA), and onset was observed at  $\sim 70^\circ$  (station YKC), but not at higher latitudes (CBB and CON; see also Figure 15). On the  $\sim 67^\circ$  longitude chain (Figure 14), intensification was observed at local times from  $\sim 2100$  MLT just to the west of the longitude of onset, to  $\sim 0000$  MLT (stations DAW to RAB). Onset was simultaneously observed at  $\sim 0100$  MLT (GIL), while a weaker more gradual disturbance was recorded at  $\sim 0300$  MLT (PBQ). The disturbance did not reach station NAQ at  $\sim 0600$  MLT. The Cassini AKR index data also show that a sharp rise in the AKR power flux began at  $\sim 0748$  UT, increasing by about an order of magnitude in a few minutes, before falling again to the original post-onset level by  $\sim 0800$  UT (Figure 13b). Similarly, Figure 16 shows that a further increase of the geostationary Bz field was observed during this interval by GOES-10 at  $\sim 2300$  MLT, while GOES-8 in the morning sector at  $\sim 0300$  MLT now also observed a gradual but pronounced dipolarisation, with Bz increasing and Bx decreasing during the interval. A further undispersed ion injection (without electrons) was also observed by spacecraft 1989-046 located at  $\sim 2100$  MLT. After  $\sim 0800$  UT the expanded auroras again started to fade, and with them the lower latitude magnetic disturbance also started to recover. These data again show that although the intensification resulted in the disturbance expanding into the morning sector, to  $\sim 0200$  MLT at  $\sim 70^\circ$  and to  $\sim 0300$  MLT at geostationary latitudes, it still did not reach to Cassini field lines at  $\sim 73^\circ$  and  $\sim 0400$  MLT.

#### *0810-0900 UT: Substorm 2 – Recovery*

As in the first interval studied here, after initial expansion phase onset, development, and intensification, this substorm also exhibited a well-defined ‘recovery’ period in which intense disturbances were observed at higher latitudes, up to  $\sim 78^\circ$  (Figures 13-15). However, the sharpness of the onset of these disturbances at  $\sim 0810$  UT might qualify them to be better described as the onset of a new intensification leading to recovery, rather than ‘recovery’ of the overall disturbance itself. Indeed, the AKR index data in Figure 13b show a short-lived intense spike of radio emission centred near  $\sim 0810$  UT, though the power flux subsequently declined by more than an order of magnitude over the next  $\sim 5$  min to values similar to those observed in the recovery phase of the first substorm. In order to keep our nomenclature simple, however, we have not explicitly marked this short-lived intensification, centred near ‘R2’, in our plots. Our use of the term ‘recovery’ in this context thus again refers principally to usual auroral zone latitudes.

The choice of the ‘end’ time E2 of this substorm is also a little problematic, since variable modest magnetic disturbances continued at most stations for at least the following 90 min. However, the integrated AKR power flux returned to slowly-varying background values at 0900 UT (Figure 13b), which we have therefore taken as E2. The magnetic field at a majority of magnetometer stations was, albeit briefly, close to baseline values at that time. Sporadic AKR-band emissions then began again shortly before 0930 UT, in association with new lower-latitude geomagnetic disturbance which will not be discussed here.

Looking in more detail at the ‘recovery-phase’ data, we note again that high-latitude disturbances began at ~0810 UT, shortly after recovery began at geostationary latitudes. In conformity with the latter recovery, no substorm-related effects were observed at either of the GOES spacecraft, or at 1989–046, after this time (Figure 16). Bay (and Pi2-band signal) onsets were observed at ~0810 UT at stations CON (73°) and CBB (77°) on the latitude chain (Figure 13a) at ~2330 MLT, with the initial disturbance extending eastward to station RAN (73°) at ~0200 MLT (Figure 15). However, the initial disturbance did not reach to station IQA located at 73° and ~0430 MLT, and thus not to the location of the Cassini footprint. No corresponding features in the auroral emission could be discerned in the UVI data. In line with the discussion in Section 3, we suggest that the progress of the disturbance to high latitudes corresponded to an interval of substantial net closure of open flux in the tail. Initially this involved the midnight sector of the tail, but did not extend to the dawn flank where Cassini was located.

Sporadic magnetic disturbances were then observed over the next ~50 min, extending down from ~78° to ~65°, before (temporarily) reducing to small values at all stations at ~0900 UT (E2). Of particular interest here, however, is the fact that an onset at station IQA, near the Cassini footprint, was finally observed at ~0840 UT at ~0500 MLT, though still not extending to station ATU at this latitude at ~0630 MLT. The disturbance at IQA had two ~200 nT peaks, the first at ~0850, the second at ~0910 UT (after E2), before recovering to smaller values after ~0920 UT (Figure 15). We thus infer that the substorm disturbance finally reached the dawn flank tail very late in the substorm, after ~0840 UT. In Figure 17b we show UVI and SuperDARN data corresponding to this period, specifically the UVI data for the 36 s interval beginning at 0854:01 UT, and the SuperDARN data for the 2–min interval beginning at 0854 UT. No emissions can be seen in the UVI data at high latitudes in the morning sector which might correspond with the disturbances recorded by the ground magnetometers in this region. Rather, the main emissions were observed on the dayside in the post-noon hours (IMF Bz was once more negative during this

interval), together with some weaker lower latitude emissions near midnight. The SuperDARN data are indicative of a well-developed dawn-cell flow in the morning hours, with dayside flows near noon consistent with the pattern expected for IMF  $B_y$  positive and  $B_z$  negative. The Cassini footprint mapped to a region of inferred poleward flow in the vicinity of the flow reversal boundary.

#### 4.2 Magnetic observations in the tail during substorm 2 - Cassini and Wind data

We now consider the Cassini and Wind magnetic field data, shown in Figures 18 and 19 respectively, in the light of the above discussion, and begin with the Cassini data. At the beginning of the interval at 0645 UT, the spacecraft was located at GSM coordinates  $(-27.8, -11.4, +4.3) R_E$  in the mid-dawn sector of the tail, while at the end of the interval at 0945 UT Cassini had moved outwards towards the northern dawn flank at  $(-52.3, -21.6, +10.8) R_E$ . The final magnetopause crossing took place  $\sim 1$  hour later at a radial distance of  $\sim 67 R_E$ .

The Cassini data during the initial interval 0645-0733 UT are consistent with the growth phase development of the tail field (Figure 18). The  $B_x$  component at the spacecraft increased from  $\sim 10$  nT to  $\sim 20$  nT over the interval, despite the outward radial motion of the spacecraft, while  $B_z$  modestly declined while remaining positive. Consequently, the field latitude angle, which had increased to  $\sim 30^\circ$  during the recovery phase of the previous substorm (Figure 10a), now declined again to  $\sim 10^\circ$ . The increase in the field strength in the tail is indicative of a growth phase increase in open flux in the tail lobes. Such an increase could also be due to an increase in the solar wind dynamic pressure and tail compression. However, the dynamic pressure did not increase during the interval, but instead showed a modest decline (Figure 12). The Wind spacecraft, located at  $(-9.5, +16.0, -5.3) R_E$ , similarly observed a growth phase increase in the field strength in the outer plasma sheet, from  $\sim 30$  to  $\sim 35$  nT, mainly involving an increase in the  $B_x$  and  $B_y$  components. The  $B_z$  component at Wind also declined from small positive to small negative values during the interval, suggestive of increased flaring of the dusk tail field away from the equatorial plane.

Although the overall trend of the field at Cassini was towards increasing strengths during this interval, the field also exhibited moderate variability, indicative of the presence of plasma currents. The particle data confirm that the spacecraft remained within the dawn plasma sheet for almost the whole growth phase interval, though with strongly declining flux levels following the recovery phase enhancement at the end of the first substorm [Rymer *et al.*, 2001; Abel *et al.*, 2001; Lagg *et al.*, 2001]. However, in the final  $\sim 10$  min of the growth phase the energetic ion fluxes dropped

even more precipitately than before, culminating in a first transition into the tail lobe by Cassini about 5 min before expansion phase onset (at 0733 UT). This transition was accompanied by a few-minute interval of high steady fields in the Cassini magnetometer data which can be seen around  $\sim 0730$  UT (Figure 18). These data are thus again consistent with rapid late growth phase thinning of the plasma sheet. The spacecraft was thus located in the tail lobe at  $(-34.3, -14.2, +6.0)$   $R_E$  at expansion onset, a location consistent with the T89 mapping to near the flow reversal boundary in the early morning sector ( $\sim 71^\circ$  at  $\sim 0300$  MLT).

Almost immediately after the onset of substorm expansion, however, the field and plasma data show that Cassini was engulfed by the plasma sheet once more, and remained within it for a further  $\sim 25$  min interval during the initial expansion phase and after the subsequent intensification. The field strength declined sharply over  $\sim 10$  min after entry from  $\sim 20$  nT to  $\sim 16$  nT (a decrease in magnetic pressure of  $\sim 40\%$ ) while the direction was variable but remained tail-like throughout. No pronounced anisotropies were observed in the particle fluxes during this interval, and there were no indications of substantial plasma acceleration and heating, compared with growth phase values, that might be indicative of local reconnection processes [Rymer *et al.*, 2001; Abel *et al.*, 2001; Lagg *et al.*, 2001]. These observations are in conformity with previous Geotail results, which indicate that the plasma sheet generally remains ‘stationary’ in this vicinity at substorm onset [Nagai and Machida, 1998]. However, as in the previous substorm, the Cassini data thus show that the plasma sheet at  $\sim 35 R_E$  in the dawn sector does indeed react promptly to substorm onset, in this case showing a sudden outward expansion following the rapid thinning in the late growth phase.

Shortly after  $\sim 0800$  UT the field and plasma data show that Cassini underwent a final transition from the plasma sheet to the lobe, where it stayed throughout the recovery phase until encountering the lobe boundary layer and magnetopause just after 0900 UT. The magnetic field data thus provide an indication of the decay in the lobe field during the recovery process. It is first evident, however, that the lobe field strength observed at 0800 UT after expansion phase onset and intensification ( $\sim 19$  nT) differed only marginally from that observed nearer the Earth at 0730 UT at the end of the growth phase ( $\sim 20$  nT). Thus while the onset of the substorm appears to have halted the growth phase increase in the lobe field, the field strength had not changed significantly 30 min after the onset of expansion. This is presumably due to the strong negative IMF  $B_z$  that was present during the interval, and consequent dayside reconnection, which only moderated at the subsolar magnetopause after  $\sim 0800$  UT (Figure 12). The essentially unchanged strength of the lobe field thus suggests an approximate balance between flux removal from the tail via substorm-associated transport, and flux addition to the tail by magnetopause reconnection, over this 30-min interval.

The field at the Wind spacecraft in the near-Earth dusk sector similarly showed little response to the substorm expansion phase (Figure 19), except for a modest increase in the  $B_z$  component towards near-zero values, which prevailed until the end of the interval studied here. We note that in this case the spacecraft, whose T89 mapping was to  $\sim 73^\circ$  latitude near the dusk meridian, was again well-separated from the main region of substorm disturbance, which was generally confined to local times later than  $\sim 2000$  MLT as indicated above.

After  $\sim 0810$  UT Cassini remained within the lobe during the following  $\sim 50$  min ‘recovery’ interval. During this time a near-monotonic decline in the field strength was observed, which is significantly greater than can be accounted for by the outward motion of the spacecraft, as indicated by the superposed T89 model field (for  $K_p = 4$ ). We thus infer that a substantial net amount of open flux was reconnected during this interval and transported towards the Earth. As in the first substorm, this behaviour appears to have been triggered by a reduction in the magnitude of negative IMF  $B_z$ , though in this case the field remained typically negative during the recovery interval but with a lesser magnitude than during the expansion phase. It also again coincided with the onset of high-latitude disturbances observed in the ground-based magnetometer data. As the  $B_x$  field at Cassini declined, the  $B_z$  field increased from initially small negative values, becoming positive once more after  $\sim 0830$  UT, and then more strongly positive after  $\sim 0850$  UT, such that the field latitude had increased once more to  $\sim 15^\circ$  by 0900 UT. We note that this increase in field latitude coincided approximately with the first appearance of substorm-related magnetic disturbances near the footprint of the Cassini field line in the high-latitude morning sector. These first appeared at  $\sim 0840$  UT, and were present until  $\sim 0900$  UT (the first ‘bay’ at station IQA observed in Figure 15). The changing field direction at the spacecraft may then relate to flux pile-up in the underlying plasma sheet and tailward retreat of the dawn reconnection region, as suggested for the first substorm studied here.

Shortly after the onset of these field changes, however, the spacecraft made a transition through the magnetopause into the magnetosheath at  $\sim 0905$  UT, returning to the tail once more at  $\sim 0914$  UT. It is therefore difficult to be sure which changes in the field were due to substorm dynamics, and which to boundary layer dynamics. It seems likely, however, that the magnetopause crossing itself was substorm-related. The Cassini data show that the entry into the magnetosheath immediately followed a continuous  $\sim 50$  min interval of tail field deflation during the recovery phase, while the ground-based data suggest the onset of reconnection in this sector of the tail  $\sim 15$  min prior to the crossing. It thus seems reasonable to suggest that the magnetopause crossing (at a down-tail distance of  $\sim 47 R_E$ ) was caused by a decreasing tail radius caused by the

reconnection of lobe flux. After re-entry into the tail, the field strength remained relatively steady in the lobe, and even increased again before the final magnetopause encounter at  $\sim 1047$  UT (not shown). The temporary nature of the magnetosheath encounter may then have been due to the cessation of rapid tail reconnection at the end of ‘substorm 2’, combined with further episodes of open flux production at the magnetopause and build-up of the tail lobe flux (noting the sporadic appearance of strong negative IMF  $B_z$  at around this time).

## 5. Discussion

The extensive range of monitoring data presented above show that during the tail passage by the Cassini spacecraft, two complete substorm cycles occurred which were rather similar ‘classic’ events, consisting of well defined growth, onset, intensification, and recovery phases. The Cassini trajectory lay in the near-equatorial dawn-side tail, in the region where previous results from Geotail indicate that the plasma sheet generally remains ‘stationary’ or flows earthward after substorm expansion phase onset. The Cassini data thus allow an examination of the behaviour of the tail in the interface region between the relatively ‘inactive’ dawn sector of the plasma sheet, and the ‘active’ dusk and midnight sector where reconnection and plasmoid formation usually occur at expansion phase onset.

In the present substorms, the growth phases lasted 1-2 hours and were characterised by generally southward fields in the IMF, twin-cell ionospheric flow with a transpolar voltage of  $\sim 50$ - $60$  kV, growth of the tail current system, and low nightside auroral and magnetic activity. The presence of the tail currents was evidenced both by the tail-like fields observed at geostationary orbit on the nightside, and the increasing tail field strengths and tail-like field directions observed by Cassini and Wind. Cassini was immersed in relatively steady dominant sunward-directed fields only beyond down-tail distances of  $\sim 9.3 R_E$ , due to its near-equatorial location at smaller radial distances. The overall suite of growth phase observations is consistent with a system driven principally by reconnection at the dayside magnetopause, characterised by net accumulation of open flux in the tail lobes [see e.g. *Siscoe and Huang, 1985; Cowley and Lockwood, 1992*]. Despite representing the ‘inactive’ sector in terms of expansion phase phenomena, we find that the dawn tail still exhibited usual growth phase features, namely enhancement of the tail lobe field strength (as required by cross-lobe pressure balance), and thinning of the plasma sheet. In fact, evidence of rapid thinning of the dawn plasma sheet was observed  $\sim 10$  min prior to expansion phase onset in

both substorms, a process that was arrested rapidly after expansion onset to the west of the spacecraft in the pre-midnight sector.

Substorm expansion phase onset thus took place in each case in the pre-midnight sector well westward of the Cassini meridian, centred on  $\sim 2100$  MLT and  $\sim 2230$  MLT in the two substorms. Onset was signalled by the sudden brightening of UV aurora in an initially small patch  $\sim 1$  hour MLT wide centred near the latitude of geostationary orbit ( $\sim 63^\circ$ ), simultaneous co-located magnetic bay disturbance and enhancement of signals in the Pi2-band over a broader area, AKR emission onset, and near-simultaneous energetic particle injection and field dipolarisation at geostationary orbit in the local time sector of onset. The region of auroral and magnetic disturbance then expanded over the following  $\sim 15$ - $20$  min, before tending to fade towards the end of the initial onset phase. The principal expansion was in local time rather than latitude, extending over a  $\sim 4$  hour interval of MLT from post-dusk towards the midnight sector. The latitudinal extent of the substorm electrojet current within this region was from  $\sim 62^\circ$  to  $\sim 68^\circ$ , with the electrojet centred near  $\sim 65^\circ$ .

These data are consistent with an impulsive dipolarisation and plasma heating event in the near-geostationary environment which was initially localised in longitude in the pre-midnight sector, but then spread towards both dusk and midnight. In conformity with recent results obtained from Geotail observations, we infer that these effects originated from the onset of reconnection in the dusk-side plasma sheet at down-tail distances of  $20$ - $30 R_E$  [Nagai *et al.*, 1998; Nagai and Machida, 1998; Petrukovich *et al.*, 1998; Machida *et al.*, 1999], followed in the near-Earth tail by earthward flow, flux pile-up, and plasma compression at the interface between tail-like and quasi-dipolar fields [e.g. Birn and Hesse, 1996; Shiokawa *et al.*, 1997; Birn *et al.*, 1999]. The dawn side plasma sheet where Cassini was located did not participate initially in these ‘active’ processes, but nevertheless exhibited a prompt (1-2 minute) response to expansion onset. Specifically, immediately after the onset of the first expansion, Cassini, then located within the plasma sheet at a down-tail distance of  $\sim 16 R_E$ , observed a prompt reduction in the field strength, while the plasma sheet ion fluxes remained approximately constant. After the onset of the second substorm, when the spacecraft, then at  $\sim 35 R_E$ , had just emerged into the tail lobe at the end of the growth phase, the plasma sheet promptly expanded back across the spacecraft, though without evidence of enhanced particle fluxes that might indicate local heating of the plasma.

We suggest that these effects occurred in response to the onset of rapid reconnection on the dusk side of the tail, leading to a drop in total (field plus plasma) pressure in that sector of the tail. The drop in pressure should occur because first plasma sheet and then tail lobe field lines in that

sector move into the reconnection region, and then flow away towards the Earth on one side, and back into the solar wind on the other. The tail lobe and total plasma sheet pressure will consequently drop in that region, causing an inflow into that region of the surrounding field and plasma. This scenario is sketched in Figure 20, where we show the expansion of lobe field lines into the dusk reconnection region (at down-tail distances of  $\sim 20\text{-}30 R_E$ ) from both the dusk and dawn flanks. Such an expansion seems inescapable given the fact that pressure balance must be approximately maintained across the tail, implying in particular an approximately uniform field in the tail lobes. Consequently, the magnetic pressure must drop throughout the lobe, and hence the ‘inactive’ plasma sheet on the flanks will expand outward as shown. If a spacecraft lies within the ‘inactive’ plasma sheet at onset, therefore, a decrease in the pressure will be observed, as was the case during the first substorm studied here. If on the other hand the spacecraft lies just outside the dawn plasma sheet, as in the second substorm, then it will observe a plasma sheet expansion across it, as in the second substorm, though one which is not associated with local heating of the plasma.

After the first  $\sim 15\text{-}20$  min of the expansion phase, when the initial auroral disturbance had started to fade somewhat, an impulsive intensification took place in both substorms. Imager data of the auroral intensification are not available during the first substorm, but during the second the intensification was initiated locally and centrally within the already-disturbed region, at  $\sim 2200$  MLT and at near-geostationary latitudes. An expansion then took place, which rapidly (over  $\sim 5$  min) extended the intensified auroral region modestly in latitude, up to  $\sim 70^\circ$ , but principally in longitude, now to cover an expanded  $\sim 6$  hour MLT region from post-dusk to post-midnight. Corresponding intensifications or onsets were observed in the ground magnetometer data, with regard both to magnetic bays and Pi2-band signals. Further energetic particle injection and field dipolarisation were also observed at geostationary orbit, now also extending into the morning sector. After the initial expansion had taken place into the early morning sector, a major but slower expansion also occurred towards the dusk sector. This was much more fully developed in the first substorm than in the second, and in the former case resulted in the dusk auroras reaching to  $\sim 1700$  MLT and  $\sim 78^\circ$  over a further  $\sim 20$  min interval. Towards the end of this interval (i.e. about  $\sim 20$  min after the onset of the intensification) the auroras in the midnight sector began to fade (while those at dusk remained active during the first substorm). This signalled the onset of ‘recovery’ in the midnight sector in both auroral and magnetic disturbance at conventional ‘auroral zone’ latitudes (roughly  $62^\circ\text{-}70^\circ$ ).

Physically, the processes at work during the intensification appear to represent a re-run of those occurring at onset, but now involving an expanded region in local time. In particular, the

region of auroral and magnetic disturbance expanded quickly into the post-midnight sector, at least on near-geostationary field lines. We thus infer a corresponding eastward expansion in the reconnection region across the tail. During the first substorm, but not in the second, this expansion was sufficient to bring the disturbance into the Cassini local time sector, though the spacecraft footprint remained just poleward of the region of bright UV auroras. Correspondingly, in the first substorm Cassini promptly observed the signatures of hot earthward-flowing plasma in the plasma sheet together with highly variable fields, which we infer were related to the onset of reconnection tailward of the spacecraft (then located  $\sim 18 R_E$  down-tail). We further infer that it was this inflow that powered the substorm expansion phase phenomena which were present closer to the Earth (i.e. at lower latitudes). In the second substorm, the intensified disturbance still did not reach to the local time of Cassini, and no related features were observed within the plasma sheet where the spacecraft was located.

A particular feature of the nightside SuperDARN radar data during both ‘onset’ and ‘intensification’ expansion phases of both substorms, was the appearance of flow suppression to low values within the substorm-disturbed region, as outlined previously by *Kirkwood et al.* [1988], *Morelli et al.* [1995], and *Yeoman et al.* [2000]. The flow in the surrounding region of the nightside ionosphere generally remained vigorous, but was diverted around the disturbed region, as also discussed by *Cowley et al.* [1998] and *Opgenoorth and Pellinen* [1998]. This effect was presumably caused by the very high electrical conductivity of the auroral bulge ionosphere compared with its surroundings. The surrounding nightside flow itself was presumably driven principally by the substorm-related flux transport in the tail. It does not seem, for example, to be dependent on the prevailing direction of the IMF. The latter was found to continue to materially effect the dayside flow during these intervals, however. When the IMF pointed strongly southward, for example, strong dawn cell flows were observed in both the post-midnight and pre-noon sectors, with a relative minimum between at dawn, thus suggesting the temporary existence of two separate cells of anticlockwise flow driven by tail and dayside processes respectively.

At the end of the expansion phases discussed above, the substorm UV auroras extended from higher latitudes at dusk to lower latitudes post-midnight, and the latter had started to fade in concert with a recovery of the lower-latitude bays near midnight. This therefore represented the onset of the conventional auroral zone ‘recovery’ phase, and in the substorms studied here it approximately coincided with a turn in the IMF direction from strongly southward, to  $B_z$  values nearer to zero. However, this was merely the prelude to an extended  $\sim 40$ - $50$  min interval of significant nightside activity at higher latitudes, between  $\sim 70^\circ$  and  $\sim 80^\circ$ , as seems often to be the case [e.g. *Cogger and*

*Elphinstone, 1992*]. In the first substorm this activity appeared to develop eastward from the high-latitude intrusion of the substorm bulge into the dusk sector, reaching the Cassini footprint in the dawn sector at  $\sim 0200$  MLT about 10 min after the start of the recovery phase. In the second substorm a delay of  $\sim 30$  min occurred between the onset of high-latitude disturbances in the midnight sector at the start of ‘recovery’, and their appearance at the Cassini footprint at  $\sim 0430$  MLT. In these cases the timings have been determined from ground magnetic data, because there are no consistently corresponding high latitude auroral features present in the UVI data. This suggests that the disturbances were associated with less intense precipitation of electrons of overall lower energy than in the earlier phases of the substorm.

These observations thus emphasise the importance of the continuing direction of the IMF to the course of the substorm expansion phase. In both these substorms IMF  $B_z$  was strongly negative for a  $\sim 30$  min interval following expansion onset, suggesting continuing magnetospheric ‘driving’ by open flux production at the magnetopause, as also seen in the strong dayside flows present in the SuperDARN radar data. In both cases there is evidence that a quasi-equilibrium was formed during these intervals between reconnection on the dayside transferring open flux to the tail lobes, and near-Earth tail reconnection transferring closed flux back to the dayside. During the first substorm, for example, the earthward flow of the plasma sheet observed after the intensification persisted for an interval of  $\sim 40$  min, well into the start of the recovery phase, without producing any evidence for local ‘dipolarisation’ of the field. In the second substorm, the lobe field strength observed after  $\sim 30$  min of expansion phase had hardly changed from that observed at the end of the growth phase. The auroral zone ‘recovery’ phase described above then began about  $\sim 10$  min after a turn towards smaller and positive IMF  $B_z$  values. With this reduction in negative IMF  $B_z$ , and hence dayside reconnection, the tail reconnection rate then appears to have exceeded the dayside rate for the first time. Earthward flow continued on tail-like fields within the plasma sheet for  $\sim 15$  min during this interval in the first substorm, with corresponding ‘return’ flows being observed in the nightside ionosphere by SuperDARN. However, ‘dipolarisation’ of the plasma sheet (declining  $B_x$  and increasing  $B_z$ ) at  $\sim 20\text{--}40 R_E$  distances then followed, simultaneous reduction in the plasma sheet and ionospheric ‘return’ flow, inferred tailward retreat of the reconnection region, and simultaneous poleward motion of the nightside ground-based disturbance. Just after the end of the second substorm the spacecraft also made a brief transit through the magnetopause into the magnetosheath, which we suggest was directly related to the recovery-phase deflation of the tail diameter. After the spacecraft re-entered the tail, after a interval of  $\sim 10$  min, the field strength remained relatively steady with a significant positive  $B_z$ , suggesting that open flux destruction had by then ceased.

## 7. Summary

The principal observations and conclusions reached from our study of the data acquired during the outbound Cassini traversal of the tail are as follows.

(a) Cassini and geostationary spacecraft data show that tail-like fields associated with a thin equatorial current sheet extend inwards close to the Earth during the growth phase. Cassini was first immersed in a relatively steady dominant sunward-directed field at a down-tail distance of  $\sim 9.3 R_E$ , at a position which was only  $\sim 0.7 R_E$  above the GSM equatorial plane.

(b) Features observed during the growth phase of two substorms are entirely consistent with a system driven principally by the production of open flux at the magnetopause and its transport into the tail. Typical growth phase features were observed by Cassini in the dawn sector of the tail, namely enhancement of the tail field strength, and rapid plasma sheet thinning over  $\sim 10$  min prior to expansion phase onset in the pre-midnight sector. The thinning appears to have been arrested and reversed in the dawn sector promptly after expansion phase onset.

(c) Although Cassini was located eastward of the ‘active’ sector of the plasma sheet at expansion phase onset in both substorms, rapid responses in field and plasma were nevertheless observed. In the first substorm, when the spacecraft was located within the plasma sheet at  $\sim 15 R_E$  down-tail, the growth phase decline in particle fluxes was first halted and then reversed, while the magnetic pressure dropped rapidly by a factor of  $\sim 2$ . In the second substorm, when the spacecraft at  $\sim 34 R_E$  down-tail had just emerged from the plasma sheet into the tail lobe at the end of the growth phase, the plasma sheet promptly expanded across it once more, though without evidence of plasma heating. We suggest that these effects resulted from the onset of rapid reconnection in the adjacent dusk sector of the tail, which deflated the tail lobe pressure, and caused an expansion of the flanking plasma sheet. Related short-term ( $\sim 10$  min) flow reduction effects were observed in the nightside dawn flow cell in the near-conjugate ionosphere.

(d) An intensification which carried the substorm-disturbed region eastward into the local time sector of Cassini during the first substorm resulted in the simultaneous appearance of earthward-flowing plasma and a disturbed magnetic field at  $\sim 18 R_E$ . We infer this to have been due to the eastward expansion of the tail reconnection region into the dawn sector, tailward of the spacecraft. The field at the spacecraft remained ‘tail like’ during this interval, however, with a footprint that

was located just poleward of the bright UV auroras. We infer that this flow powered the bright auroral emission and dipolarisation phenomena that occurred closer to the Earth, in the near-geostationary environment. A similar intensification during the second substorm did not reach the local time of the Cassini footprint in the dawn sector, and no related effects were observed locally in the plasma sheet.

(e) Ionospheric flows within the substorm auroral bulge became semi-stagnant throughout the expansion phase. We infer that this was due to the high electrical conductivity of the bulge ionosphere compared with the surrounding region. The surrounding flow generally remained vigorous, however, and deflected around the semi-stagnant region (with the exception of the effect noted under (c) above). We infer that the latter flow was driven principally by flux closure in the tail, and was observed to occur essentially independently of concurrent IMF conditions. When IMF  $B_z$  was southward, strong flows in the dawn cell were observed both in the early morning sector (outside the bulge) and near noon, with a minimum between, near dawn. This suggests the presence of two separately-driven parts to the flow cell, one associated with tail reconnection during the substorm the other with magnetopause reconnection associated with the direction of the IMF.

(f) IMF  $B_z$  was strongly negative for  $\sim 30$  min during the expansion phases of both substorms, such that substantial driving was taking place from the solar wind during these intervals. The Cassini observations suggest that a quasi-equilibrium was formed during this period between open flux production at the magnetopause and transfer to the tail, and open flux closure through near-Earth tail reconnection. In particular, in the first substorm, earthward flow was observed in the dawn plasma sheet following the above intensification for  $\sim 40$  min without producing local dipolarisation of the field. In the second substorm, the lobe field strength after  $\sim 30$  min of expansion phase was observed to be essentially unchanged compared with that observed at the end of the growth phase.

(g) The recovery phase of both substorms began  $\sim 10$  min after a northward turning of the IMF to an extended interval of near-zero IMF  $B_z$  values. Taken together with (f) above, these observations thus emphasise the importance to the progress of substorm disturbances of the IMF behaviour which happens to follow expansion phase onset. In the present case of continuous solar wind driving during expansion, the principal interval of net closure of open flux occurred during ‘recovery’, after the IMF had turned to become nearer zero. The tail reconnection rate then appears to have exceeded the dayside rate, leading to magnetospheric and ionospheric flows which were driven principally by open flux closure in the tail. In the first substorm these flows continued for

~15 min before ‘dipolarisation’ occurred in the near-Earth ( $\sim 25 R_E$ ) tail. This was associated with a simultaneous reduction in the earthward plasma sheet flow, and that in the near-conjugate ionosphere, inferred tailward retreat of the reconnection region, and the contraction of the ground-based magnetic disturbance to high latitudes. In the second substorm, Cassini was located in the tail lobe during recovery rather than in the plasma sheet, and observed a monotonic decline in the field strength, culminating in a brief exit from the deflated tail lobe into the magnetosheath at the end of the substorm.

**Acknowledgements.** We would like to thank those many people from the various instrument teams that provided data to the Cassini ESB data base for their help in ensuring the availability of data during the interval. In particular, we would like to thank the PIs of the SuperDARN radars for ensuring the radars were operating in Common Mode during the Cassini ESB. The data presented in this paper were from radars funded by the research funding agencies of Canada, France, the UK, and USA. We also appreciate the co-operation of members of other Cassini instrument teams for allowing access to their results prior to publication. In particular, we would like to thank Gary Abel, Andreas Lagg, Abigail Rymer, and Michelle Thomsen for their help and comments. Research at The University of Iowa was supported by NASA through contract 961152 through the Jet Propulsion Laboratory. The AKR observations were made using the Cassini RPWS high frequency receiver developed at the Observatoire de Paris, Meudon, France. During the course of this study Drs Hina Khan and Elena Kolesnikova were supported by PPARC grant PPA/G/O/1999/00181.

## References

- Abel, G.A., A.J. Coates, A.M. Rymer, D.R. Linder, M.F. Thomsen, D.T. Young, and M.K. Dougherty, Cassini observations of bi-directional lobe electrons during the Earth fly-by, 18<sup>th</sup> August 1999, *J. Geophys. Res.*, this issue, 2001.
- Baker, D.N., T.I. Pulkkinen, V. Angelopoulos, W. Baumjohann, and R.L. McPherron, Neutral line model of substorms: Past results and present view, *J. Geophys. Res.*, *101*, 12975, 1996.
- Birn, J., and M. Hesse, Details of current disruption and diversion in simulations of magnetotail dynamics, *J. Geophys. Res.*, *101*, 15345, 1996.
- Birn, J., M. Hesse, G. Haerendel, W. Baumjohann, and K. Shiokawa, Flow braking and the substorm current wedge, *J. Geophys. Res.*, *104*, 19895, 1999.
- Bristow, W.A., J.M. Ruohoniemi, and R.A. Greenwald, Super Dual Auroral Radar Network observations of convection during a period of small-magnitude northward IMF, *J. Geophys. Res.*, *103*, 4051, 1998.
- Cogger, L.L., and R.D. Elphinstone, The Viking auroral substorm, in *Internat. Conf. On Substorms-1*, ESA SP-335, Noordwijk, The Netherlands, p. 77, 1992.
- Cowley, S.W.H., Plasma populations in a simple open model magnetosphere, *Space Sci. Rev.*, *26*, 217, 1980.
- Cowley, S.W.H., and M. Lockwood, Excitation and decay of solar wind-driven flows in the magnetosphere-ionosphere system, *Ann. Geophysicae*, *10*, 103, 1992.
- Cowley, S.W.H., H. Khan, and A. Stockton-Chalk, Plasma flow in the coupled magnetosphere-ionosphere system and its relationship to the substorm cycle, in *Substorms-4* edited by S. Kokobun and Y. Kamide, Terra Sci. Publ. Co., Tokyo, p. 623, 1998.
- Dougherty, M.K., S. Kellock, D.J. Southwood, A. Balogh, M. Barlow, T. Beek, M.W. Dunlop, R. White, E.J. Smith, L. Wigglesworth, M. Fong, R. Marquedant, B.T. Tsurutani, B. Gerlach, G. Musmann, K.-H. Glassmeier, H. Hartje, M. Rahm, I. Richter, C.T. Russell, D. Huddelston,

R.C. Snare, G. Erdos, S. Szalai, F.M. Neubauer, S.W.H. Cowley, and G.L. Siscoe, The Cassini magnetic field investigation, *Space Sci. Rev.*, submitted, 2001.

Engebretson, M.J., W.J. Hughes, J.L. Alford, E. Zesta, L.J. Cahill Jr., R.L. Arnoldy, and G.D. Reeves, Magnetometer array for cusp and cleft studies observations of the spatial extent of broadband ULF magnetic pulsations at cusp/cleft latitude, *J. Geophys. Res.*, *100*, 19371, 1995.

Glassmeier, K.-H., F.M. Neubauer, G. Brach, H. Marschall, M.H. Acuña, L.F. Burlaga, F. Mariani, G. Musmann, N.F. Ness, M.K. Wallis, E. Ungstrup, and H.U. Schmidt, Giotto's mission to planet Earth, *Geophys. Res. Lett.*, *18*, 1663, 1991.

Greenwald, R.A., K.B. Baker, J.R. Dudeney, M. Pinnock, T.B. Jones, E.C. Thomas, J.-P. Villain, J.-C. Cerisier, C. Senior, C. Hanuise, R.D. Hunsucker, G. Sofko, J. Koehler, E. Neilsen, R. Pellinen, A.D.M. Walker, N. Sato and H. Yamagishi, DARN/SuperDARN: A global view of the dynamics of high-latitude convection, *Space Sci. Rev.*, *71*, 761, 1995.

Gurnett, D.A., The Earth as a radio source: Terrestrial kilometric radiation, *J. Geophys. Res.*, *79*, 4227, 1974.

Gurnett, D.A., W.S. Kurth, D.L. Kirchner, G.B. Hospodarsky, T.F. Averkamp, P. Zarka, A. Lecacheux, R. Manning, A. Roux, P. Canu, N. Cornilleau-Wehrin, P. Galopeau, A. Meyer, R. Bostrom, G. Gustafsson, J.-E. Whalund, L. Aahlen, H.O. Rucker, H.P. Ladreiter, W. Macher, L.J.C. Woolliscroft, H. Alleyne, M.L. Kaiser, M.D. Desch, W.M. Farrell, C.C. Harvey, P. Louarn, P.J. Kellogg, K. Goetz, and A. Pedersen, The Cassini radio and plasma wave science investigation, *Space Sci. Rev.*, submitted, 2001.

Hones, E.W., Jr., Transient phenomena in the magnetotail and their relation to substorms, *Space Sci. Rev.*, *23*, 393, 1979.

Khan, H., and S.W.H. Cowley, Observations of the response time of high-latitude ionospheric convection to variations in the interplanetary magnetic field using EISCAT and IMP-8 data, *Ann. Geophysicae*, *17*, 1306, 1999.

- Kirkwood, S., H.J. Opgenoorth, and J.S. Murphree, Ionospheric conductivities, electric fields and currents associated with auroral substorms measured by the EISCAT radar, *Planet. Space Sci.*, *36*, 1359, 1988.
- Kivelson, M.G., C.F. Kennel, R.L. McPherron, C.T. Russell, D.J. Southwood, R.J. Walker, K.K. Khurana, P.J. Coleman, C.M. Hammond, V. Angelopoulos, A.J. Lazarus, R.P. Lepping, and T.J. Hughes, The Galileo Earth encounter: Magnetometer and allied measurements, *J. Geophys. Res.*, *98*, 11299, 1993.
- Kurth, W.S., and D.A. Gurnett, Auroral kilometric radiation integrated power flux as a proxy for  $A_E$ , *Adv. Space Res.*, *22*, (1)73, 1998.
- Kurth, W.S., T. Murata, G. Lu, D.A. Gurnett, and H. Matsumoto, Auroral kilometric radiation and the auroral electrojet index for the January 1997 magnetic cloud event, *Geophys. Res. Lett.*, *25*, 3027, 1998.
- Kurth, W.S., G.B. Hospodarsky, D.A. Gurnett, M.L. Kaiser, J.-E. Whalund, A. Roux, P. Canu, P. Zarka, and Y. Tokarev, An overview of observations by the Cassini Radio and Plasma Wave Investigation at Earth, *J. Geophys. Res.*, this issue, 2001.
- Lagg, A., N. Krupp, S. Livi, J. Woch, S.M. Krimigis, and M.K. Dougherty, Energetic particle measurements during the Earth swing-by of the Cassini spacecraft in August 1999, *J. Geophys. Res.*, this issue, 2001.
- Lepping, R.P., M.H. Acuna, L.F. Burlaga, W.M. Farrell, J.A. Slavin, K.H. Schatten, F. Mariani, N.F. Ness, F.M. Neubauer, Y.C. Whang, J.B. Barnes, R.S. Kennon, P.V. Panetta, J. Scheifele, and E.M. Worley, The WIND magnetic field investigation, *Space Sci. Rev.*, *71*, 207, 1995.
- Lühr, H., The IMAGE magnetometer network, *STEP Int. Newsl.*, *4*, (10), 4, 1994.
- Lui, A.T.Y., A synthesis of magnetospheric substorm models, *J. Geophys. Res.*, *96*, 1849, 1991.
- Lui, A.T.Y., Current disruption in the Earth's magnetosphere: observations and models, *J. Geophys. Res.*, *101*, 13067, 1996.

- Machida, S., Y. Miyashita, A. Ieda, A. Nishida, T. Mukai, Y. Saito, and S. Kokubun, Geotail observations of flow velocity and north-south magnetic field variations in the near and mid-distant tail associated with substorm onsets, *Geophys. Res. Lett.*, *26*, 635, 1999.
- McComas, D.J., S.J. Bame, P. Barker, W.C. Feldman, J.L. Phillips, P. Riley, and J.W. Griffee, Solar Wind Electron Proton Alpha Monitor (SWEPAM) for the Advanced Composition Explorer, *Space Sci. Rev.*, *86*, 561, 1998.
- Morelli, J.P., R.J. Bunting, S.W.H. Cowley, C.J. Farrugia, M.P. Freeman, E. Friis-Christensen, G.O.L. Jones, M. Lester, R.V. Lewis, H. Lühr, D. Orr, M. Pinnock, G.D. Reeves, P.J.S. Williams, and T.K. Yeoman, Radar observations of auroral zone flows during a multiple-onset substorm, *Ann. Geophysicae*, *13*, 1144, 1995.
- Murata, T., H. Matsumoto, H. Kojima, and T. Iyemori, Correlations of AKR index with  $K_p$  and  $D_{st}$  indices, in *Proc. NIPR Symp. Upper Atmos. Physics*, *10*, 64, 1997.
- Nagai, T., and S. Machida, Magnetic reconnection in the near-earth magnetotail, in *New Perspectives on the Earth's Magnetotail* edited by A. Nishida, D.N. Baker and S.W.H. Cowley, Geophys. Mono. 105, AGU, Washington, DC, p. 211, 1998.
- Nagai, T., M. Fujimoto, Y. Saito, S. Machida, T. Teresawa, R. Nakamura, T. Yamamoto, T. Mukai, A. Nishida, and S. Kokubun, Structure and dynamics of magnetic reconnection for substorm onsets with Geotail observations, *J. Geophys. Res.*, *103*, 13067, 1998.
- Opgenoorth, H.J., and R.J. Pellinen, The reaction of the global convection electrojets to the onset and expansion of the substorm current wedge, in *Substorms-4* edited by S. Kokubun and Y. Kamide, Terra Sci. Publ. Co., Tokyo, p. 663, 1998.
- Opgenoorth, H.J., R.J. Pellinen, W. Baumjohann, E. Nielsen, G. Marklund, and L. Eliasson, Three-dimensional current flow and particle precipitation in a westward travelling surge, *J. Geophys. Res.*, *88*, 3138, 1983.
- Petrukovich, A.A., V.A. Sergeev, L.M. Zleneyi, T. Mukai, T. Yamamoto, S. Kokubun, K. Shiokawa, C.S. Deehr, E.Y. Budnick, J. Büchner, A.O. Fedorov, V.P. Grigorieva,

- T.J. Hughes, N.F. Pissarenko, S.A. Romanov, and I. Sandahl, Two spacecraft observations of a reconnection pulse during an auroral breakup, *J. Geophys. Res.*, *103*, 47, 1998.
- Peredo, M., J.A. Slavin, E. Mazur, and S.A. Curtis, Three dimensional position and shape of the bow shock and their variation with the Alfvénic, sonic and magnetosonic Mach numbers and interplanetary magnetic field orientation, *J. Geophys. Res.*, *100*, 7907, 1995.
- Reeves, G.D., R.D. Belian, T.A. Fritz, M.G. Kivelson, R.W. McEntire, E.C. Roelof, B. Wilken, and D.J. Williams, Structured plasma sheet thinning observed by Galileo and 1984-129, *J. Geophys. Res.*, *98*, 21323, 1993.
- Roelof, E.C., and D.G. Sibeck, Magnetopause shape as a bivariate function of interplanetary magnetic field  $B_z$  and solar wind dynamic pressure, *J. Geophys. Res.*, *98*, 21421, 1993.
- Rostoker, G., J.C. Samson, F. Creutzberg, T.J. Hughs, D.R. McDiarmid, A.G. McNamara, A. Vallance Jones, D.D. Wallis, and L.L. Cogger, CANOPUS – A ground based array for remote sensing the high latitude ionosphere during the ISTP/GGS program, *Space Sci. Rev.*, *71*, 743, 1995.
- Ruohoniemi, J.M., and K.B. Baker, Large-scale imaging of high-latitude convection with Super Dual Auroral Radar Network HF radar observations, *J. Geophys. Res.*, *103*, 20797, 1998.
- Rymer, A.M., A.J. Coates, G.A. Abel, D.R. Linder, K.R. Svenes, B. Narheim, M.F. Thomsen, and D.T. Young, Cassini CAPS Electron Spectrometer measurements during the Earth swingby on 18 August 1999, *J. Geophys. Res.*, this issue, 2001.
- Shiokawa, K., W. Baumjohann, and G. Haerendel, Braking of high-speed flows in the near-Earth tail, *Geophys. Res. Lett.*, *24*, 1179, 1997.
- Shiokawa, K., W. Baumjohann, G. Haerendel, G. Paschmann, J.F. Fennel, E. Friis-Christensen, H. Lühr, G.D. Reeves, C.T. Russell, P.R. Sutcliffe, and K. Takahashi, High-speed ion flow, substorm current wedge, and multiple Pi 2 pulsations, *J. Geophys. Res.*, *103*, 4491, 1998.
- Siscoe, G.L., and T.S. Huang, Polar cap inflation and deflation, *J. Geophys. Res.*, *90*, 543, 1985.

- Smith, C.W., M.H. Acuña, L.F. Burlaga, J. L'Heureux, N.F. Ness, and J. Scheifele, The ACE Magnetic Fields Experiment, *Space Science Reviews*, 86, 611, 1998.
- Stone, E.C., A.M. Frandsen, R.A. Mewaldt, E.R. Christian, D. Marglies, J.F. Ormes, and F. Snow, The Advanced Composition Explorer, *Space Sci. Rev.*, 86, 1, 1998.
- Torr, M.R., D.G. Torr, M. Zukic, R.B. Johnson, J. Ajello, P. Banks, K. Clark, K. Cole, C. Keffer, G. Parks, B. Tsurutani, and J. Spann, A far ultraviolet imager for the international solar terrestrial physics mission, *Space Sci. Rev.*, 71, 329, 1995.
- Tsyganenko, N.A., A magnetospheric magnetic field model with a warped tail current sheet, *Planet. Space Sci.*, 37, 5, 1989.
- Voots, G., D.A. Gurnett, and S.-I. Akasofu, Auroral kilometric radiation as an indicator of auroral magnetic disturbances, *J. Geophys. Res.*, 82, 2259, 1977.
- Wilhelm, J., and E. Friis-Christensen, Electric fields and high latitude zonal currents induced by merging of field lines, *Geophys. Pap.*, R-31, Danish Meteorological Institute, Charlottenlund, Denmark, 1976.
- Yeoman, T.K., D.K. Milling, and D. Orr, Pi2 pulsation polarization patterns on the UK Sub-auroral Magnetometer Network (SAMNET), *Planet. Space Sci.*, 38, 589, 1990.
- Yeoman, T.K., R.V. Lewis, H. Khan, S.W.H. Cowley, and J.M. Ruohoniemi, Interhemispheric observations of nightside ionospheric electric fields in response to IMF  $B_z$  and  $B_y$  changes and substorm pseudobreakup, *Ann. Geophysicae*, 18, 897, 2000.
- Yumoto, K., and the 210° MM magnetic observation group, The 210° magnetic meridian network project, *J. Geomagn. Geoelectr.*, 48, 1297, 1996.

## Figure Captions

Figure 1. Trajectories of spacecraft whose data are employed in this study, namely Cassini, Wind, and GOES-10. The trajectories of geostationary spacecraft 1989-046 and GOES-8 are not shown, but are essentially similar to GOES-10. The open circles show hour markers in UT along the trajectories on 18 August 1999, at one hour intervals for Cassini, and two hour intervals for Wind and GOES-10. The upper panel shows the trajectories projected into the GSM  $X$ - $Y$  equatorial plane, while the lower panel shows them projected onto the GSM  $X$ - $Z$  noon-midnight meridian plane. Model bow shock and magnetopause positions are also shown, tailored to typical conditions during the Cassini ESB, as described in the text.

Figure 2. Map in magnetic coordinates showing the locations of the ground-based magnetometer stations whose data have been employed in this study. The magnetic grid has noon at the top and dusk to the left, and shows circles of magnetic latitude at  $10^\circ$  intervals down to  $50^\circ$ . Stations shown are from the CANOPUS network, the Geological Survey of Canada, MACCS, and the Greenland west chain. The maps show the locations of the stations at two key times, (a) 0511 UT (upper plot), and (b) 0733 UT (lower plot), corresponding to the expansion phase onsets of the two substorms studied here. Cassini, Wind, and GOES-10 spacecraft trajectories are also shown (only the post-perigee trajectory for Cassini), mapped to the ionosphere using the T89 model with  $Kp = 5$  (upper plot) and  $Kp = 4$  (lower plot). One-hour markers are shown by the open circles along each track, specifically for GOES-10 at geostationary orbit. The solid triangles show the positions of these spacecraft at the actual times corresponding to the plots, where the positions of all three geostationary spacecraft are now shown (1989-046, GOES-10, and GOES-8 from left to right).

Figure 3. Map in magnetic coordinates showing the overlapping fields-of-view of the six northern hemisphere SuperDARN radars whose data are employed in this study. The locations of the radar sites are shown by the solid circles with crosses. As in Figure 2, the magnetic grid has noon at the top and dusk to the left, and shows circles of magnetic latitude at  $10^\circ$  intervals down to  $50^\circ$ . We again show the radar locations at two specific times, (a) 0511 UT (upper plot) and (b) 0733 UT (lower plot), together with the mapped spacecraft trajectories in the same format as Figure 2.

Figure 4. Solar wind and IMF data obtained by the ACE spacecraft for the interval corresponding to the first substorm, 0345-0645 UT, but where the data have been shifted in time by

47.5 min to account for the solar wind propagation delay from the spacecraft to the subsolar magnetopause. From top to bottom the panels of the figure show the three GSM components of the IMF together with the field strength, and the density, velocity, and dynamic pressure of the solar wind. The dashed vertical lines show the time of the expansion phase onset of the first substorm (S1), together with the times of the substorm intensification (I1), the beginning of the recovery phase (R1), and the end of the substorm disturbance (E1). The data at the bottom of the figure give the spacecraft position in GSM coordinates.

Figure 5a. Ground-based magnetograms for the interval 0345-0645 UT for a latitude chain of stations spanning the range of magnetic latitudes from  $62.3^\circ$  to  $77.5^\circ$ , as indicated on the right hand side of the plot (see also Figure 2). The local time of the chain is approximately given by  $MLT \sim UT+15.6$  h. The left hand panel shows the geographic northward X component of the field, the centre panel shows the geographic eastward Y component, while the right hand panel shows the vertically downward Z component. The baselines are the averaged values over the interval shown. The vertical dashed lines are as in Figure 4.

Figure 5b. The upper panel shows a logarithmic plot of the power flux in the AKR band (integrated between 50 and 800 kHz) in the interval 0345-0645 UT, observed by the RPWS instrument on the Cassini spacecraft. One-minute values are shown, inverse-square normalised to the power that would be observed at a constant geocentric distance of  $9 R_E$ . Below we show for purposes of comparison the X-component magnetogram from station MCM, which was essentially co-located with the substorm expansion phase onset disturbance. The vertical dashed lines are as in Figure 4.

Figure 6. Ground-based magnetograms for the interval 0345-0645 UT for a longitude chain of stations at a magnetic latitude of  $\sim 67^\circ$  (see also Figure 2). The chain spans the range of longitudes from  $\sim 2$  h MLT earlier than that of the latitude chain shown in Figure 5a (station DAW) to  $\sim 7$  h later (station NAQ). Otherwise as for Figure 5a.

Figure 7. Ground-based magnetograms for the interval 0345-0645 UT for a longitude chain of stations at a magnetic latitude of  $\sim 74^\circ$  (see also Figure 2). The chain spans a range of longitudes from that of the latitude chain shown in Figure 5a (station CON) to  $\sim 7$  h later (station ATU). Otherwise as for Figure 5a.

Figure 8. Magnetic field and energetic particle data from geostationary spacecraft GOES–8, GOES–10, and 1989–046, for the interval 0345-0645 UT. From top to bottom, the top five panels of the figure show the three GSM field components, the total field strength, and the field latitude angle measured by GOES–8 (heavier line) and GOES–10 (lighter line). The heavy and lighter dashed lines show the corresponding model fields of the T89  $Kp = 5$  model. The lower two panels show energetic electron (upper) and proton (lower) fluxes measured in three channels by spacecraft 1989–046. The three electron channels span 105-150 keV (upper trace), 150-225 keV (middle), and 225-315 keV (lower). The three proton channels span 113-170 keV (upper trace), 170-250 keV (middle), and 250-400 keV (lower). The vertical dashed lines are as in Figure 4.

Figure 9. Composite ‘snapshots’ at selected times during the interval 0345-0645 UT of the UV auroral emission obtained by the UVI instrument on the Polar spacecraft, and the simultaneous ionospheric flow determined from SuperDARN radar data using the ‘map potential’ technique as described in the text. The data are shown on a magnetic grid, where noon is at the top and dusk to the left, and the concentric circles are shown at  $10^\circ$  intervals of latitude down to  $50^\circ$ , as in Figures 2 and 3. The trajectories of the Cassini, Wind, and geostationary spacecraft (specifically GOES–10) are also magnetically projected into the plane, using the T89  $Kp = 5$  field model. The open circles on the Cassini and Wind trajectories indicate hour markers (as in Figure 2), while the solid triangles indicate the instantaneous locations of the spacecraft (including all three geostationary spacecraft employed here; from left to right in the figure these show the footprints of spacecraft 1989–046, GOES–10, and GOES–8). The UVI data are 36 s exposures, while the SuperDARN data are 2-min integrations, with the following start times: (a) 0454:12 UT (for UVI) and 0454 UT (for SuperDARN); (b) 0518:07 UT and 0518 UT; (c) 0537:45 UT and 0538 UT; (d) 0554:19 UT and 0554 UT; and (e) 0608:25 UT and 0608 UT. In the top left corner of each plot we give the total transpolar voltage associated with the ‘map potential’ flow pattern shown. The equipotentials of the flow (the streamlines) are shown as solid lines for negative voltages (as marked), and as dashed lines for positive voltages. The voltage between the equipotentials is 6 kV.

Figure 10a. Cassini magnetic field data for the interval 0345-0645 UT. From top to bottom we show the three components of the field in GSM coordinates, the field strength, and the latitude and longitude angles of the field. The latter is measured from noon, positive anticlockwise towards dusk. The dashed curves show the values determined from the T89  $Kp = 5$  magnetic model. The dashed vertical lines are as in Figure 4. The data at the bottom of the figure give the spacecraft position in GSM coordinates.

Figure 10b. Cassini magnetic field vectors are shown projected onto the GSM X-Z plane for the interval 0400-0700 UT, encompassing the first substorm. Spot values are shown at 2 min intervals. Open circles show hour markers in UT along the trajectory. The length of a vector which corresponds to a 10 nT field is shown in the top right corner. The spacecraft locations corresponding to the principal times of the first substorm are indicated by the vertical arrows marked S1, I1, etc. The dashed lines show the noon-midnight meridian field lines of the T89  $Kp = 5$  magnetic model, specifically for 0500 UT.

Figure 11. Wind magnetic field data for the interval 0345-0645 UT, in the same format as Figure 10.

Figure 12. Solar wind and IMF data obtained by the ACE spacecraft as in Figure 4, but for the interval corresponding to the second substorm, 0645-0945 UT. The data have again been shifted in time by 47.5 min to account for the solar wind propagation delay.

Figure 13a. Ground-based magnetograms for the interval 0645-0945 UT for a latitude chain of stations spanning the range of magnetic latitudes from  $62.3^\circ$  to  $77.5^\circ$ , as in Figure 5a.

Figure 13b. Cassini RPWS integrated AKR power flux for the interval 0645-0945 UT, together with X component magnetometer data from station MCM, as in Figure 5b.

Figure 14. Ground-based magnetograms for the interval 0645-0945 UT for a longitude chain of stations at a magnetic latitude of  $\sim 67^\circ$ , as in Figure 6.

Figure 15. Ground-based magnetograms for the interval 0645-0945 UT for a longitude chain of stations at a magnetic latitude of  $\sim 74^\circ$ , as in Figure 7.

Figure 16. Magnetic field and energetic particle data from geostationary spacecraft GOES-8, GOES-10, and 1989-046, for the interval 0645-0945 UT, as in Figure 8, except that the dashed lines now correspond to the T89  $Kp = 4$  magnetic model.

Figure 17. Composite ‘snapshots’ at selected times during the interval 0645-0945 UT of the UV auroral emission obtained by the UVI instrument on the Polar spacecraft, and the simultaneous ionospheric flow determined from SuperDARN radar data using the ‘map potential’ technique, as in Figure 9 (except that the spacecraft mapping to the ionosphere has been calculated using the T89

$Kp = 4$  magnetic model). The start times of the data integration intervals are as follows: (a) 0740:25 UT (for UVI) and 0740 UT (for SuperDARN); and (b) 0854:01 UT and 0854 UT.

Figure 18. Cassini magnetic field data for the interval 0645-0945 UT, as in Figure 10 except that the dashed lines correspond to the T89  $Kp = 4$  magnetic model.

Figure 19. Wind magnetic field data for the interval 0645-0945 UT, as in Figure 11 except that the dashed lines correspond to the T89  $Kp = 4$  magnetic model.

Figure 20. Sketch of a cross-section through the tail at down-tail distances of  $\sim 20-40 R_E$ , showing the flow of tail lobe flux towards the dusk-side reconnection region after the onset of the expansion phase. Also shown is the outward expansion of the 'inactive' flank plasma sheet which is induced by the drop in tail lobe pressure.

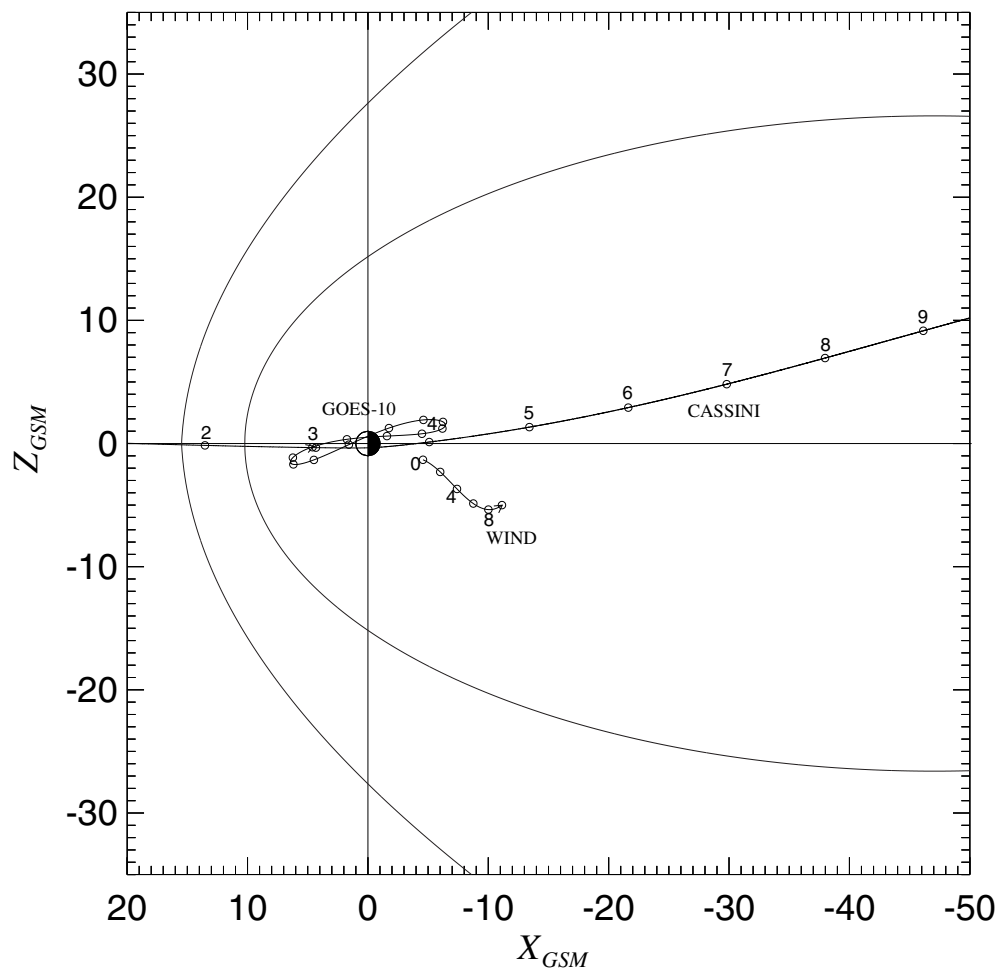
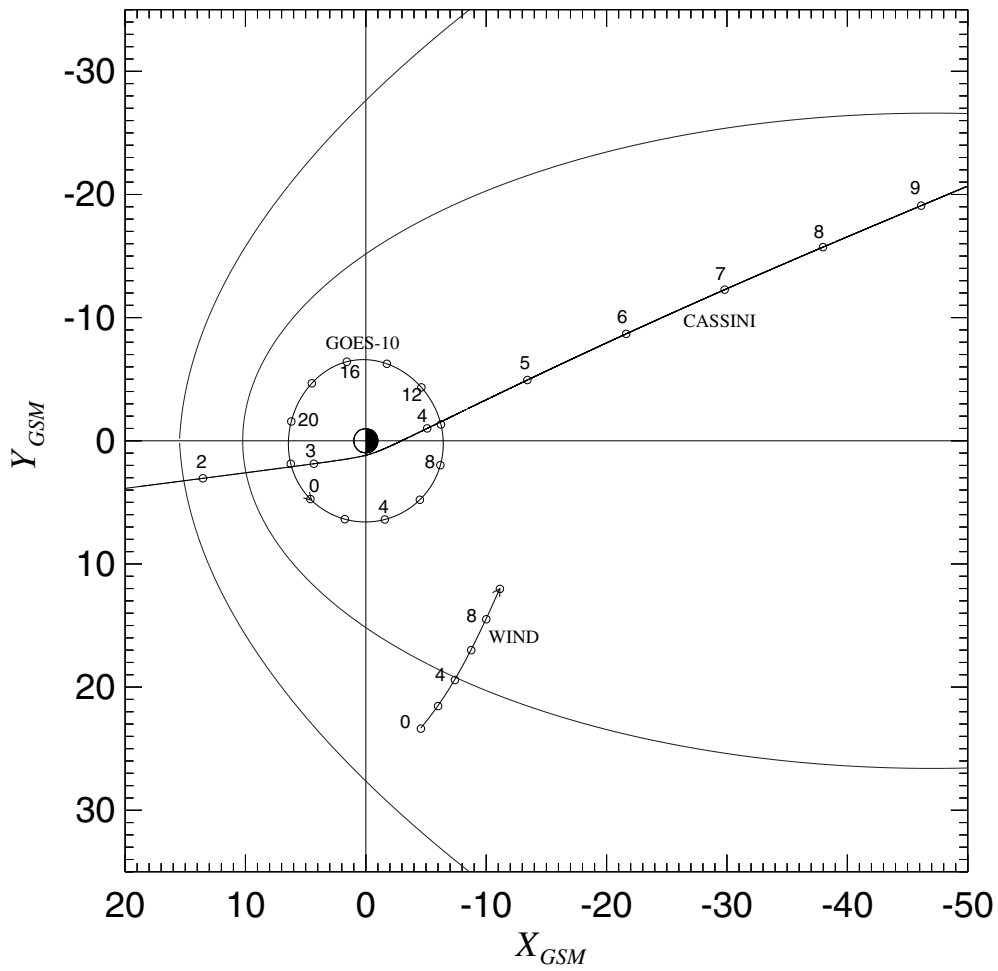
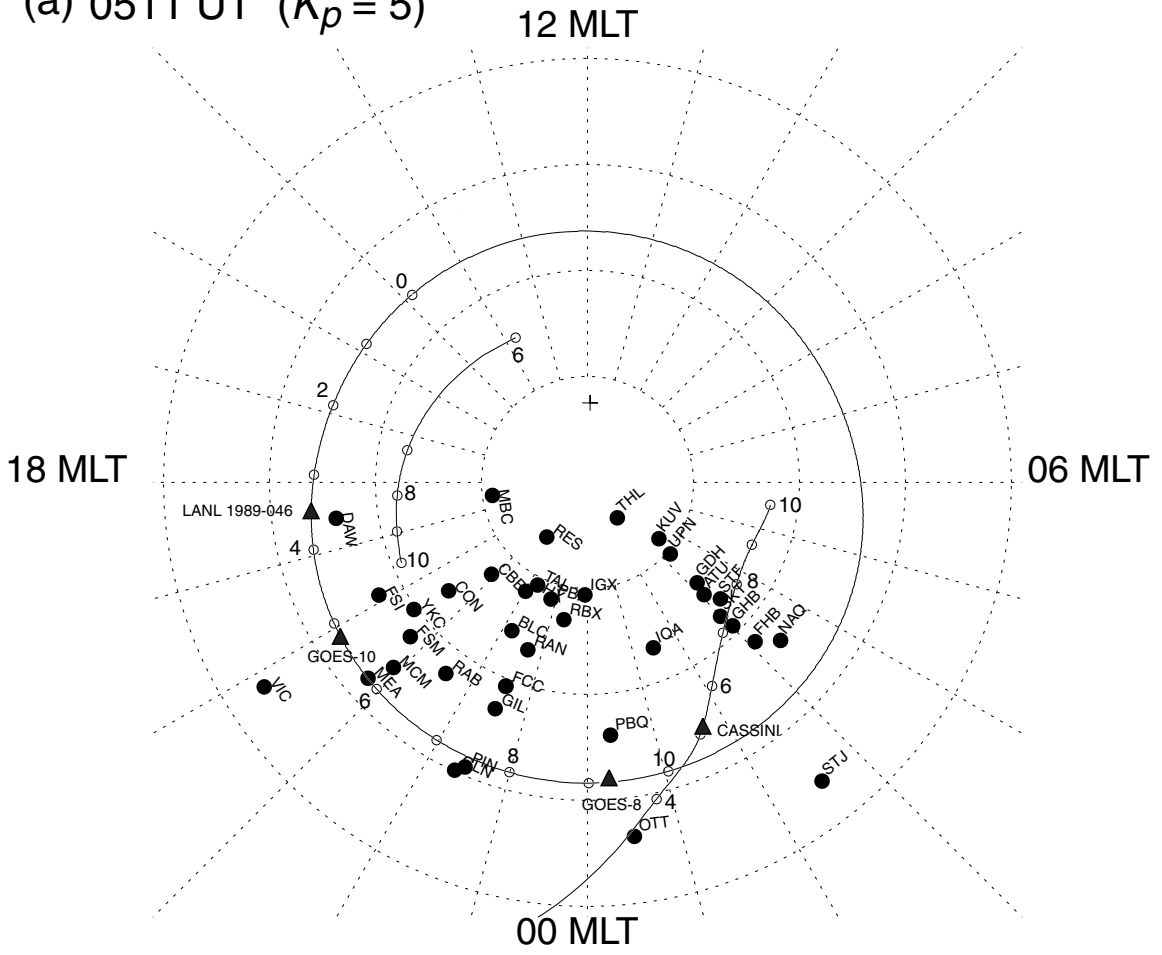


Fig. 1

(a) 0511 UT ( $K_p = 5$ )



(b) 0733 UT ( $K_p = 4$ )

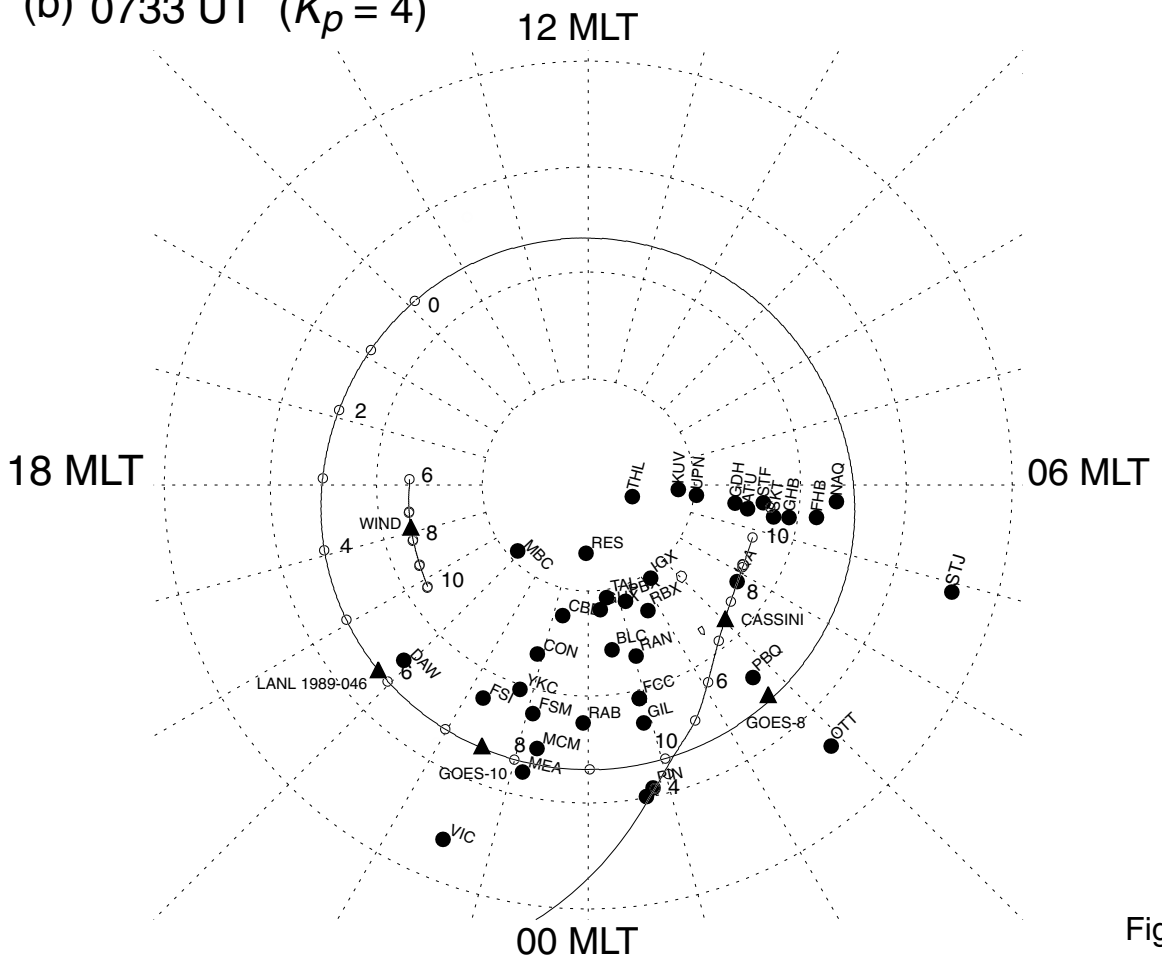
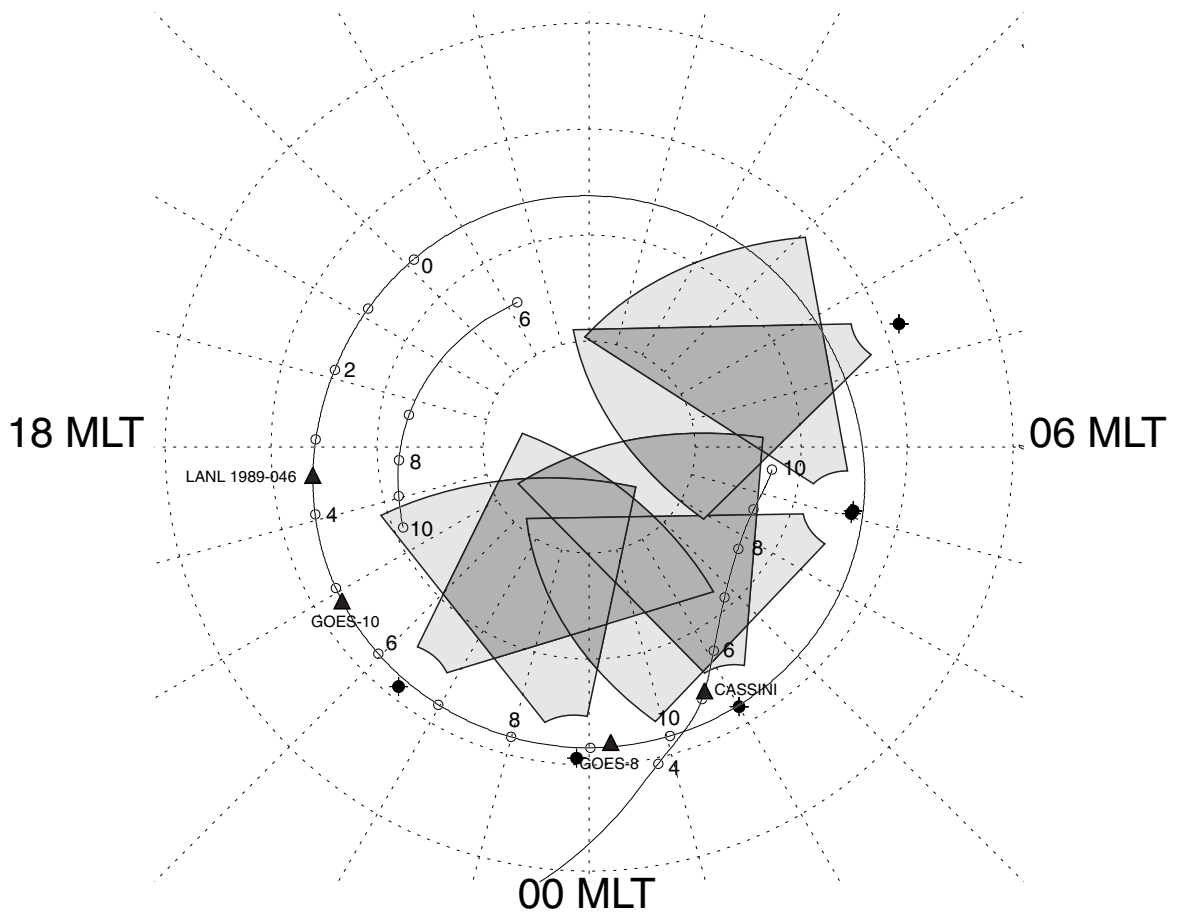


Fig. 2

(a) 0511 UT ( $K_p = 5$ )



(b) 0733 UT ( $K_p = 4$ )

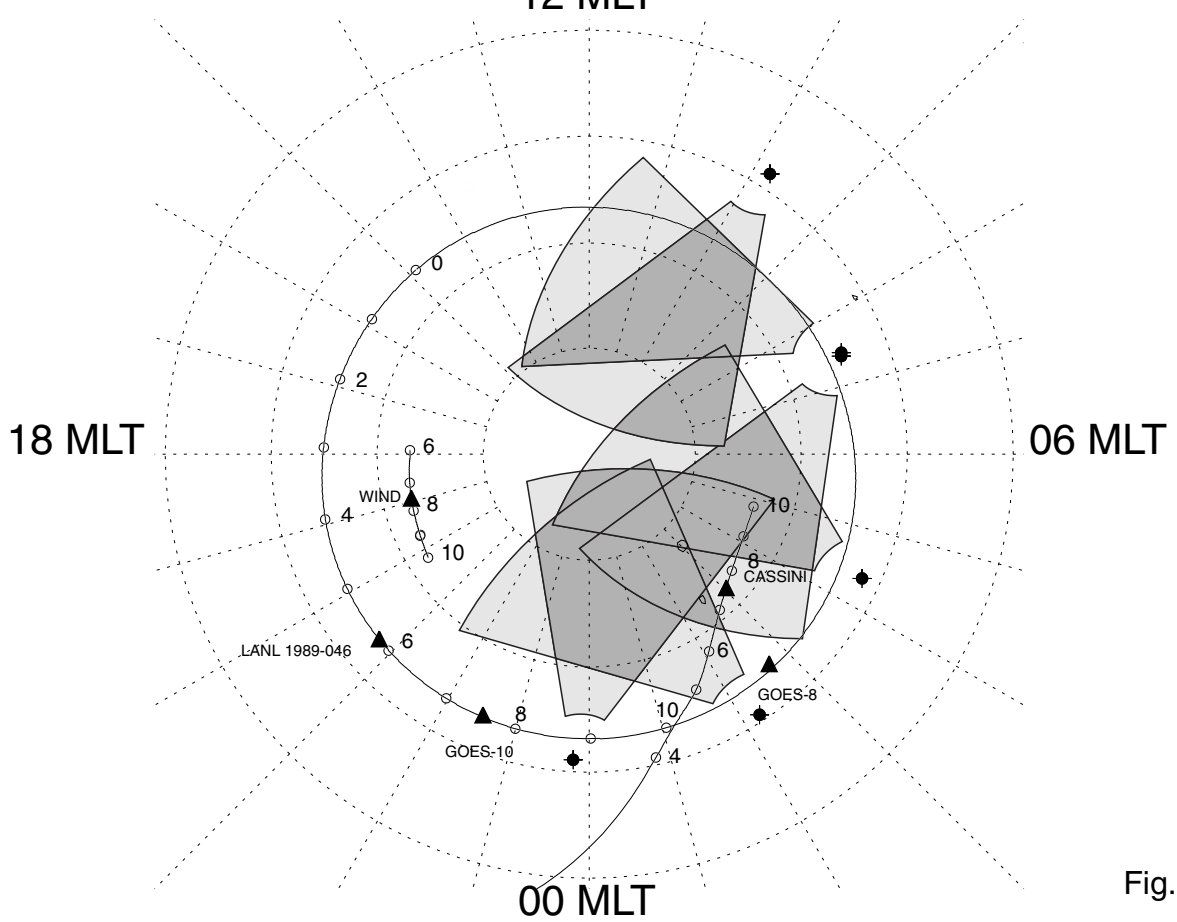
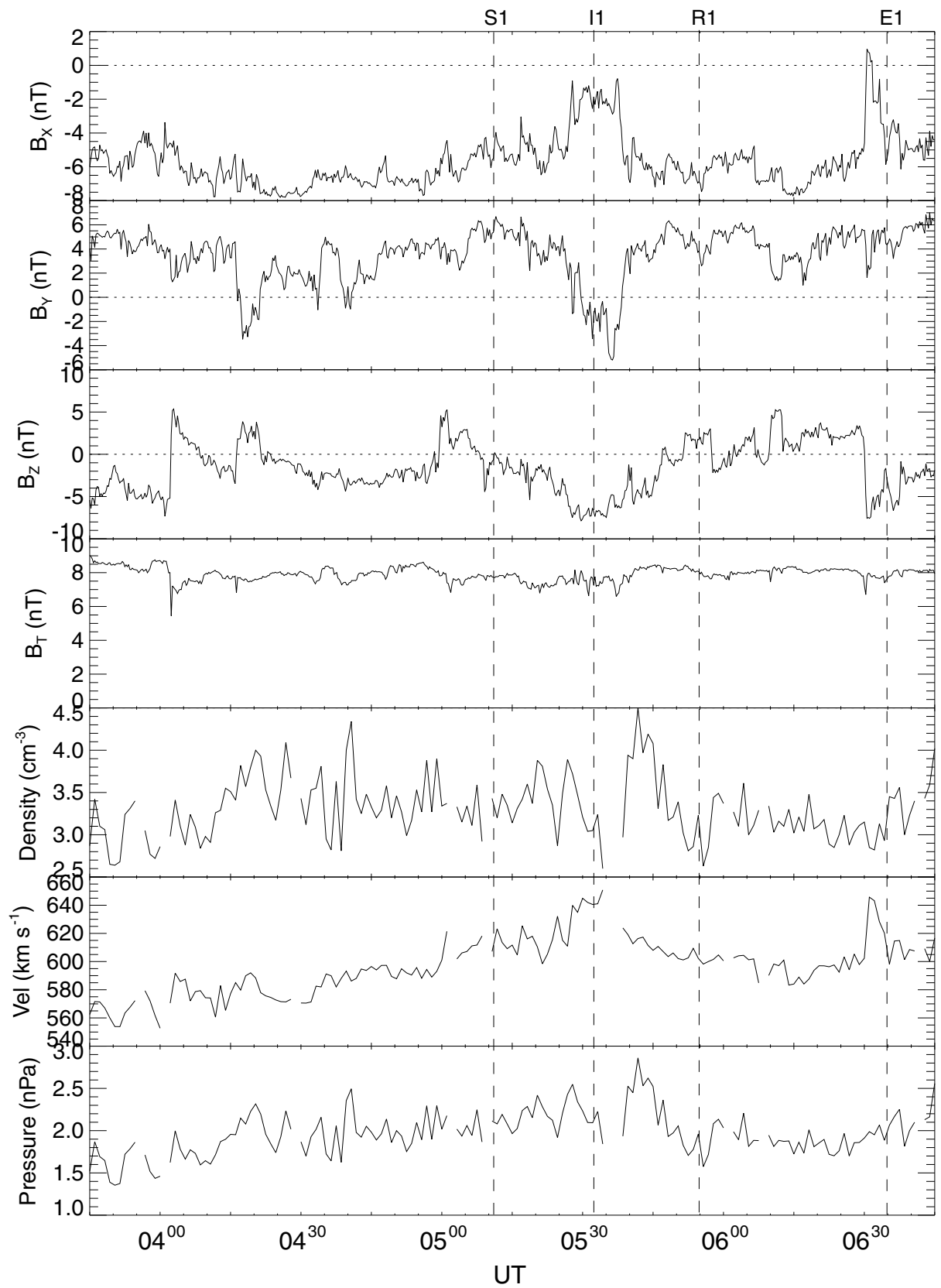


Fig. 3



X, R <sub>E</sub>	248.3	248.3	248.3
Y, R <sub>E</sub>	6.2	6.2	6.3
Z, R <sub>E</sub>	23.9	23.9	23.9

Fig. 4

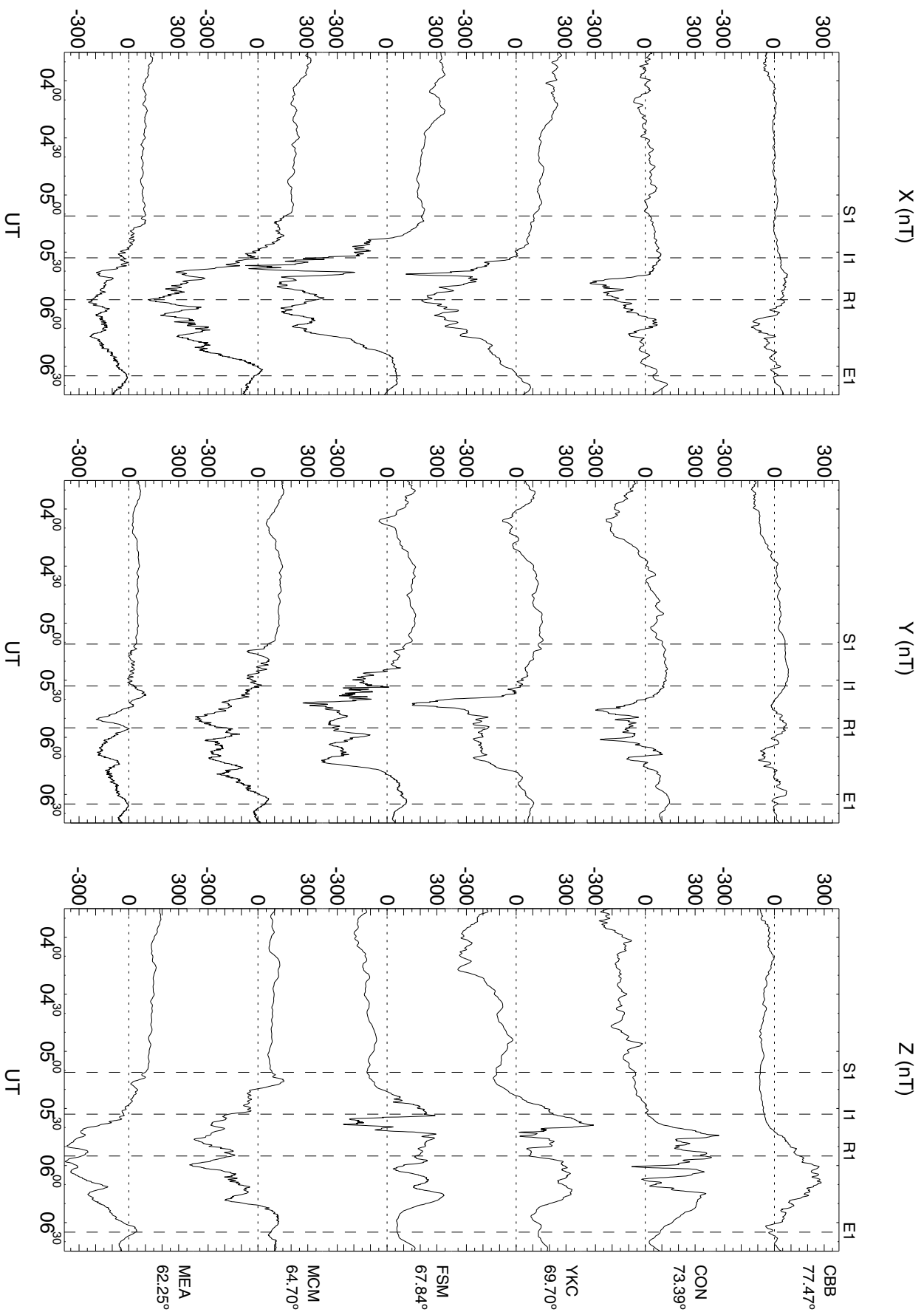


Fig. 5a

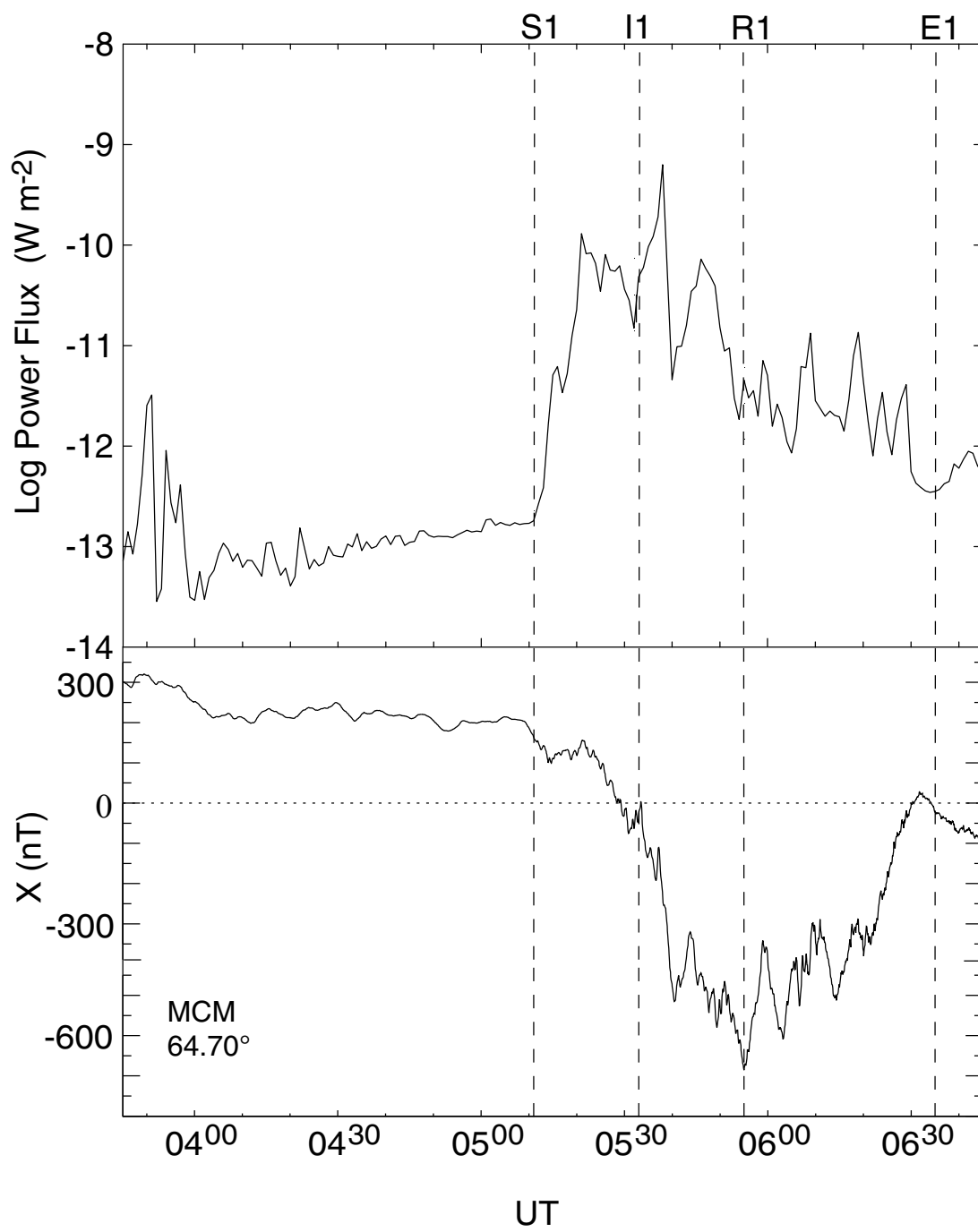


Fig. 5b

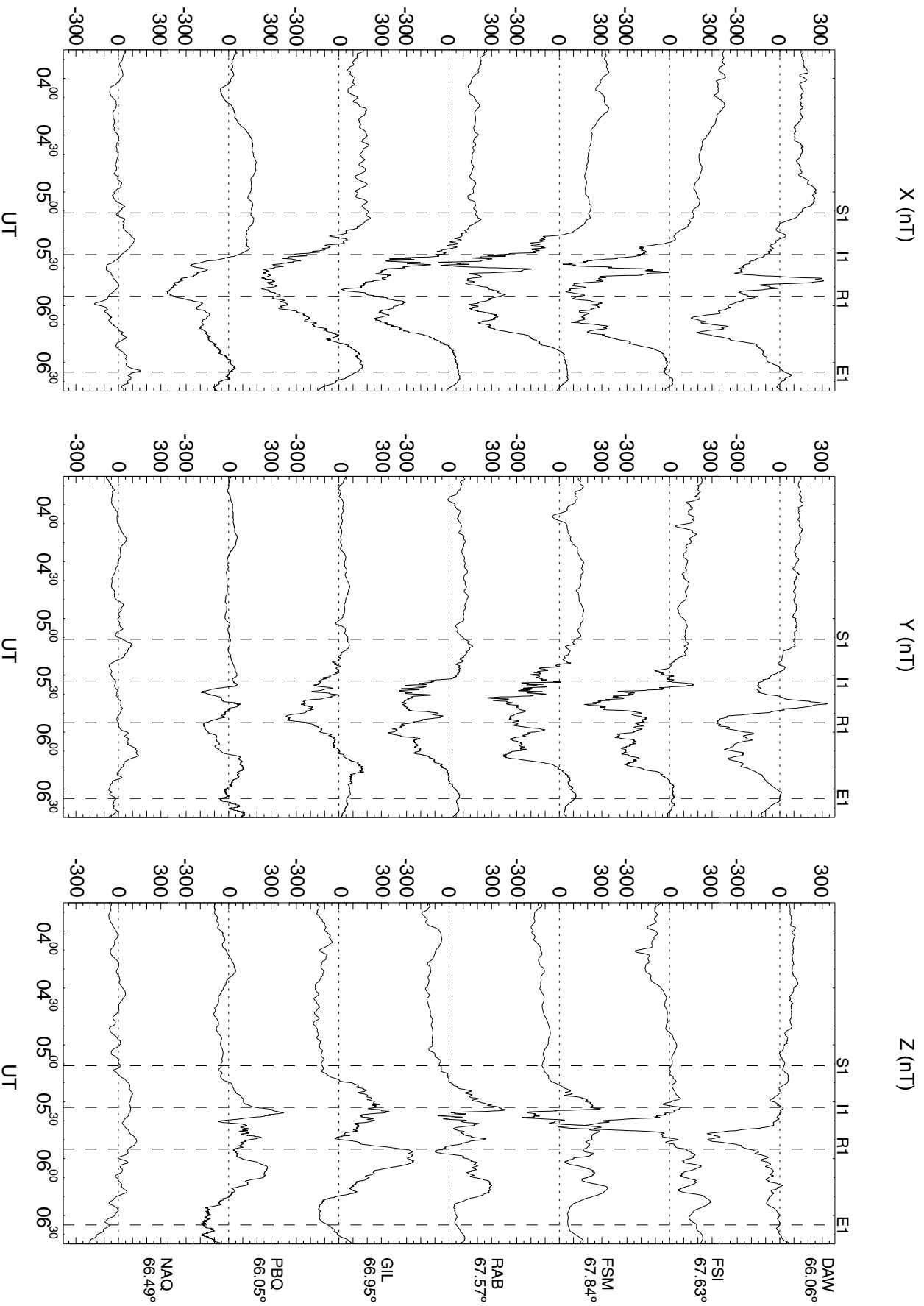


Fig. 6

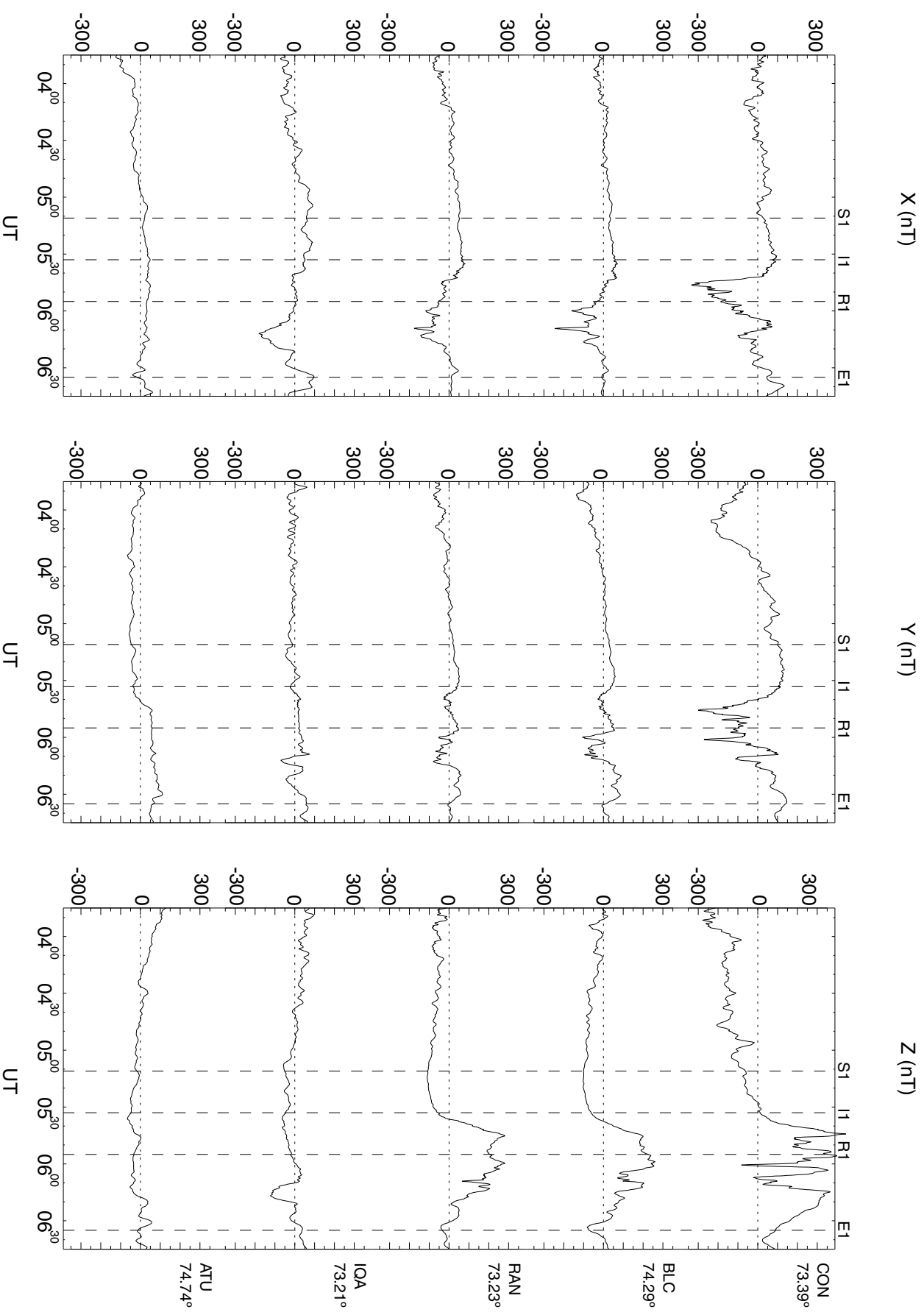


Fig. 7

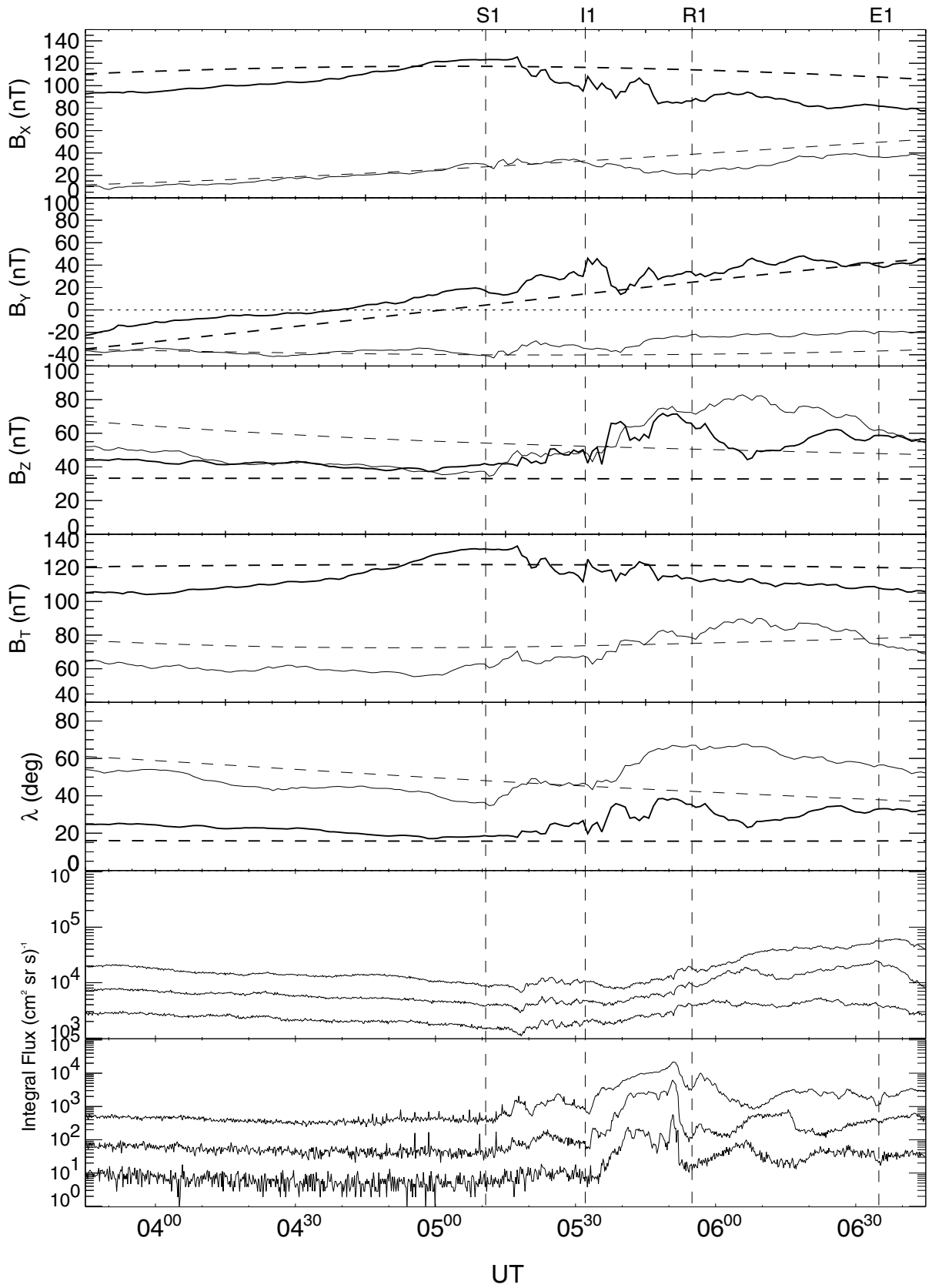


Fig. 8

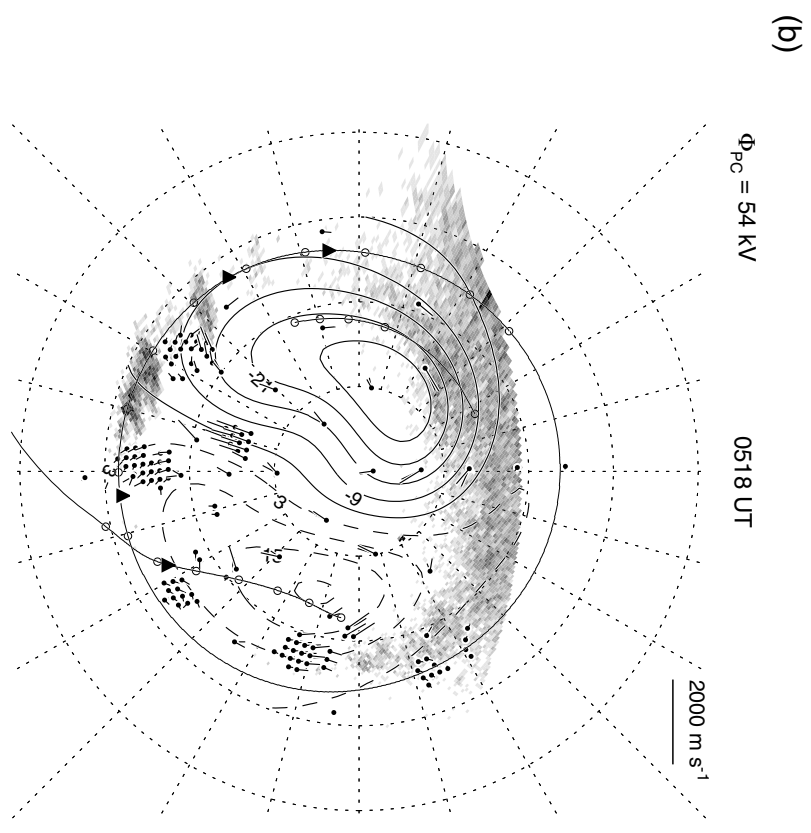
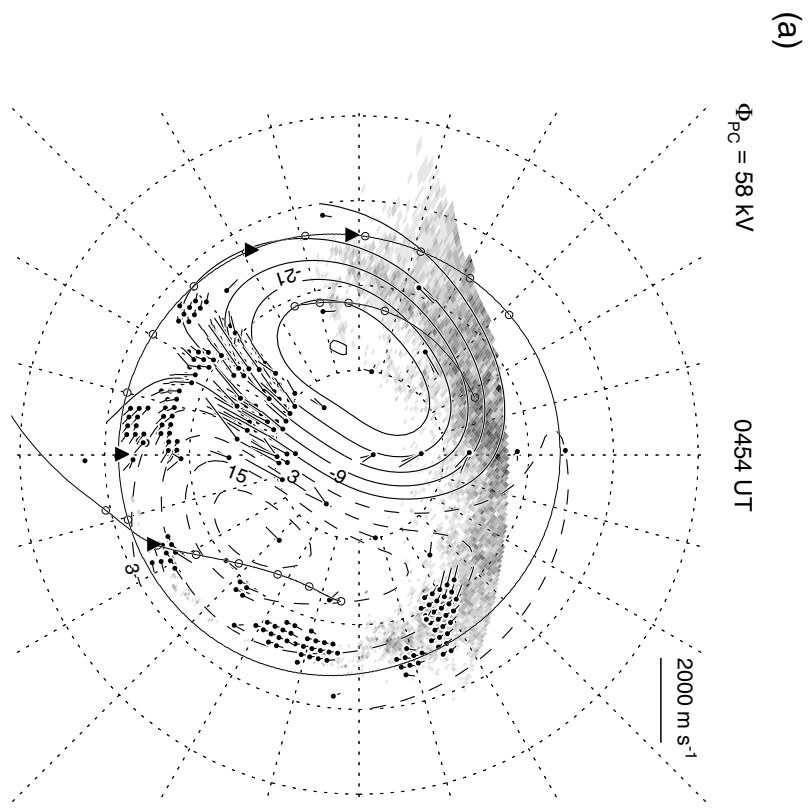


Fig. 9

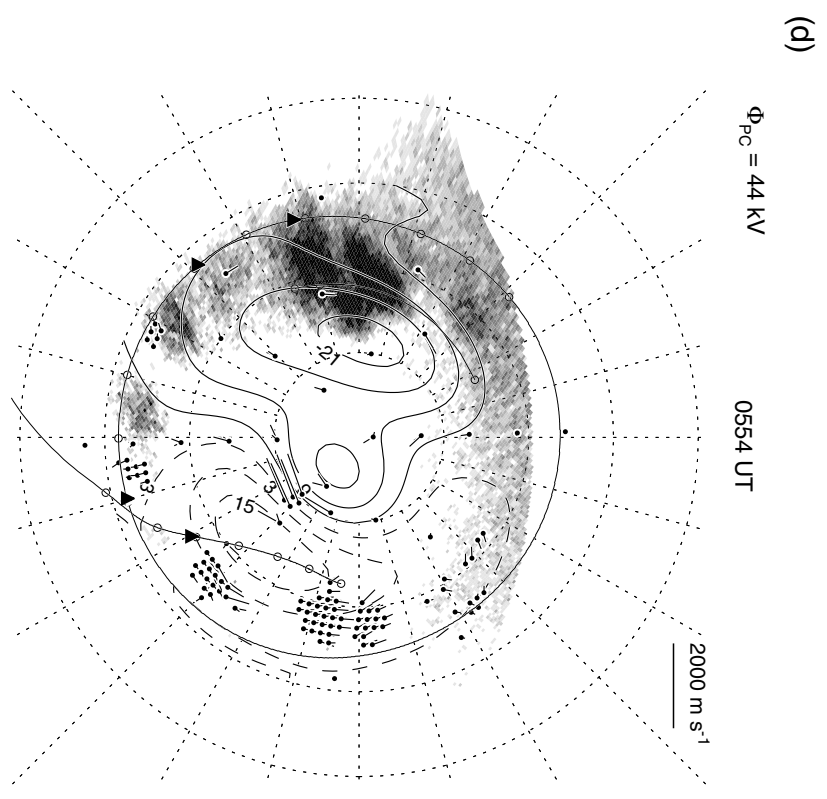
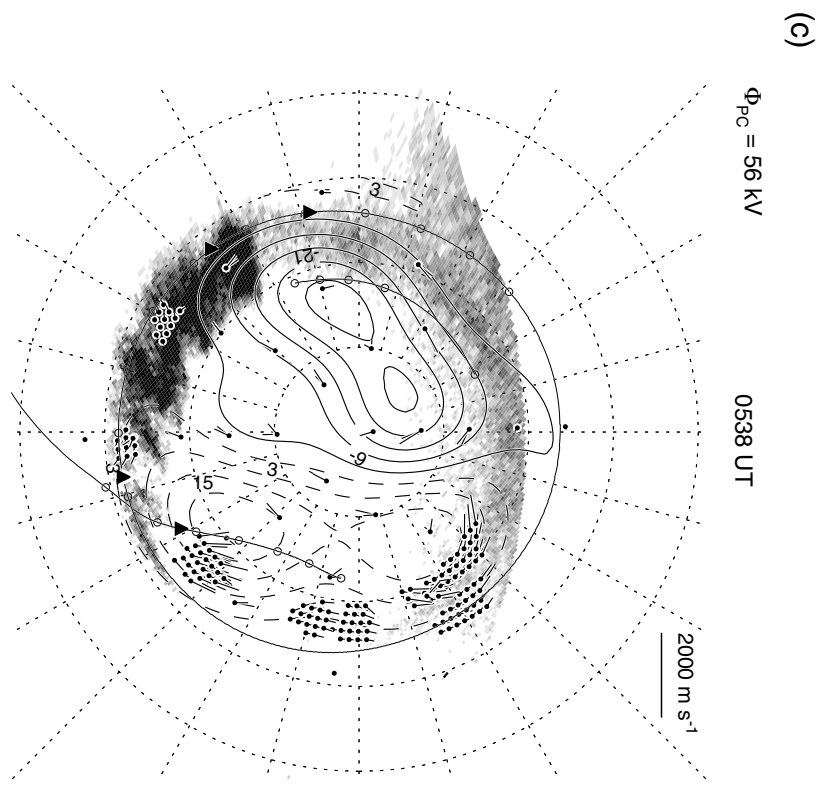


Fig. 9

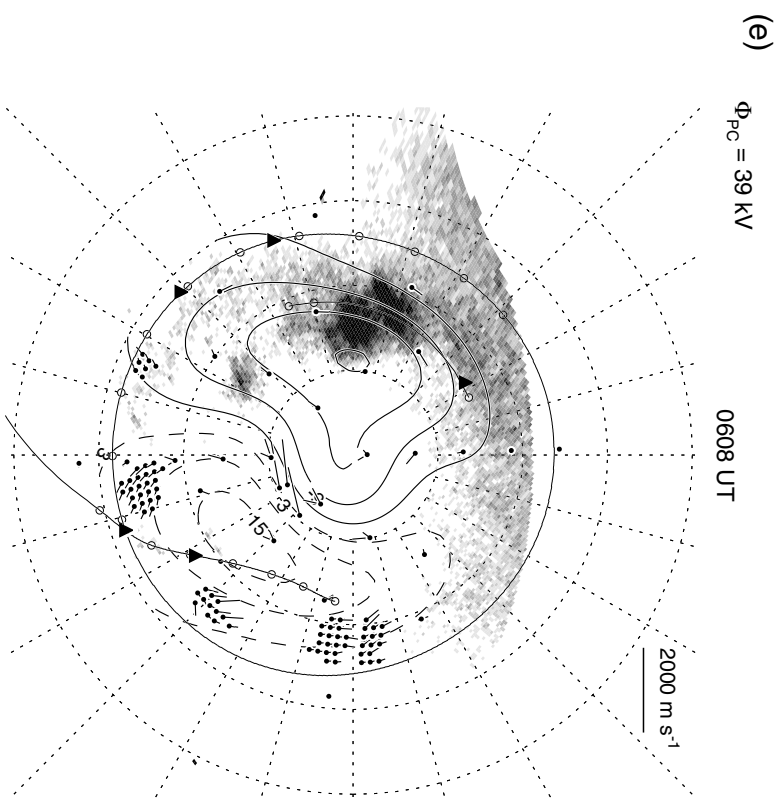
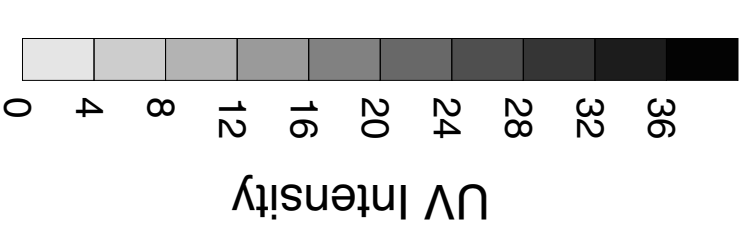


Fig. 9

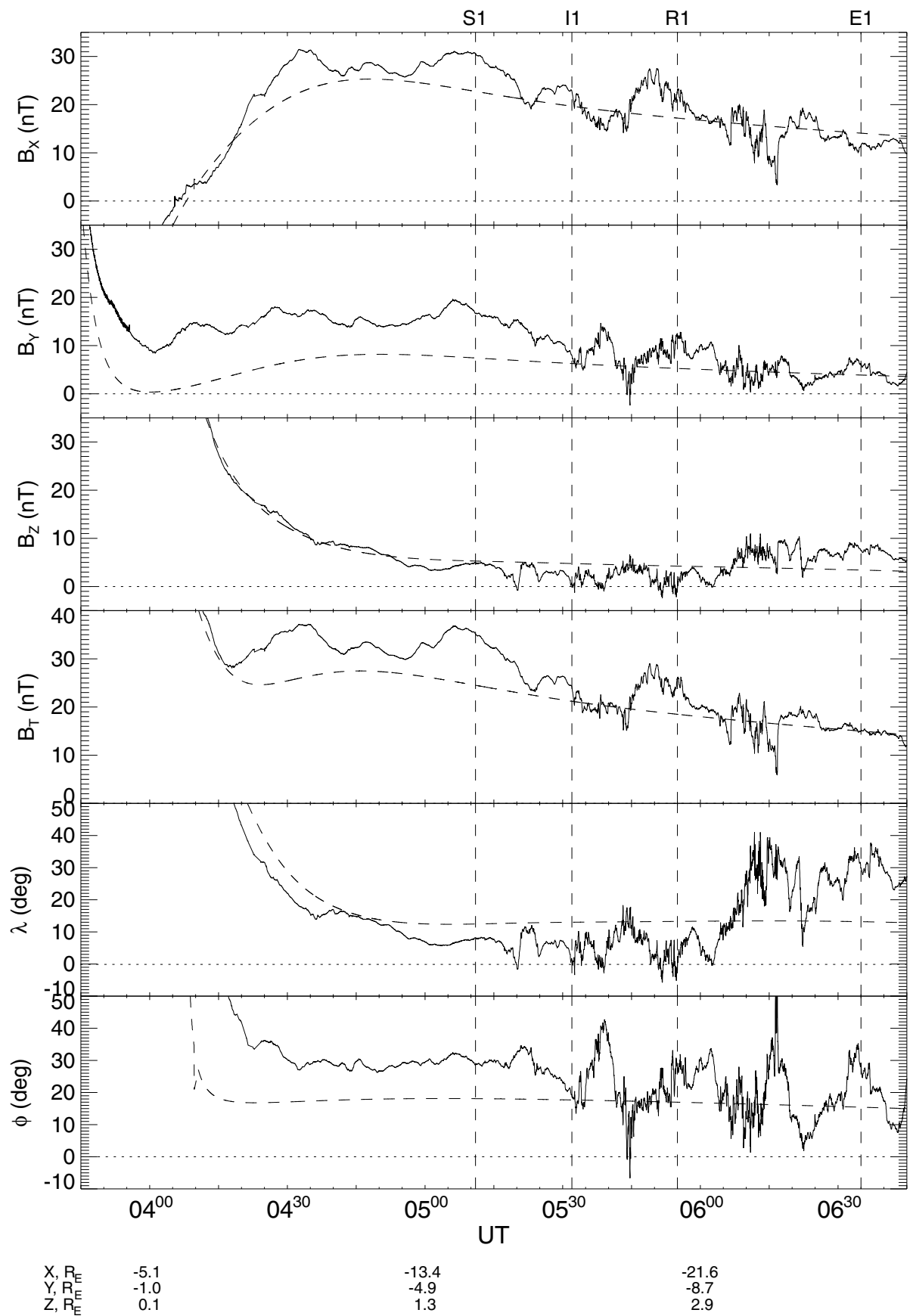


Fig. 10a

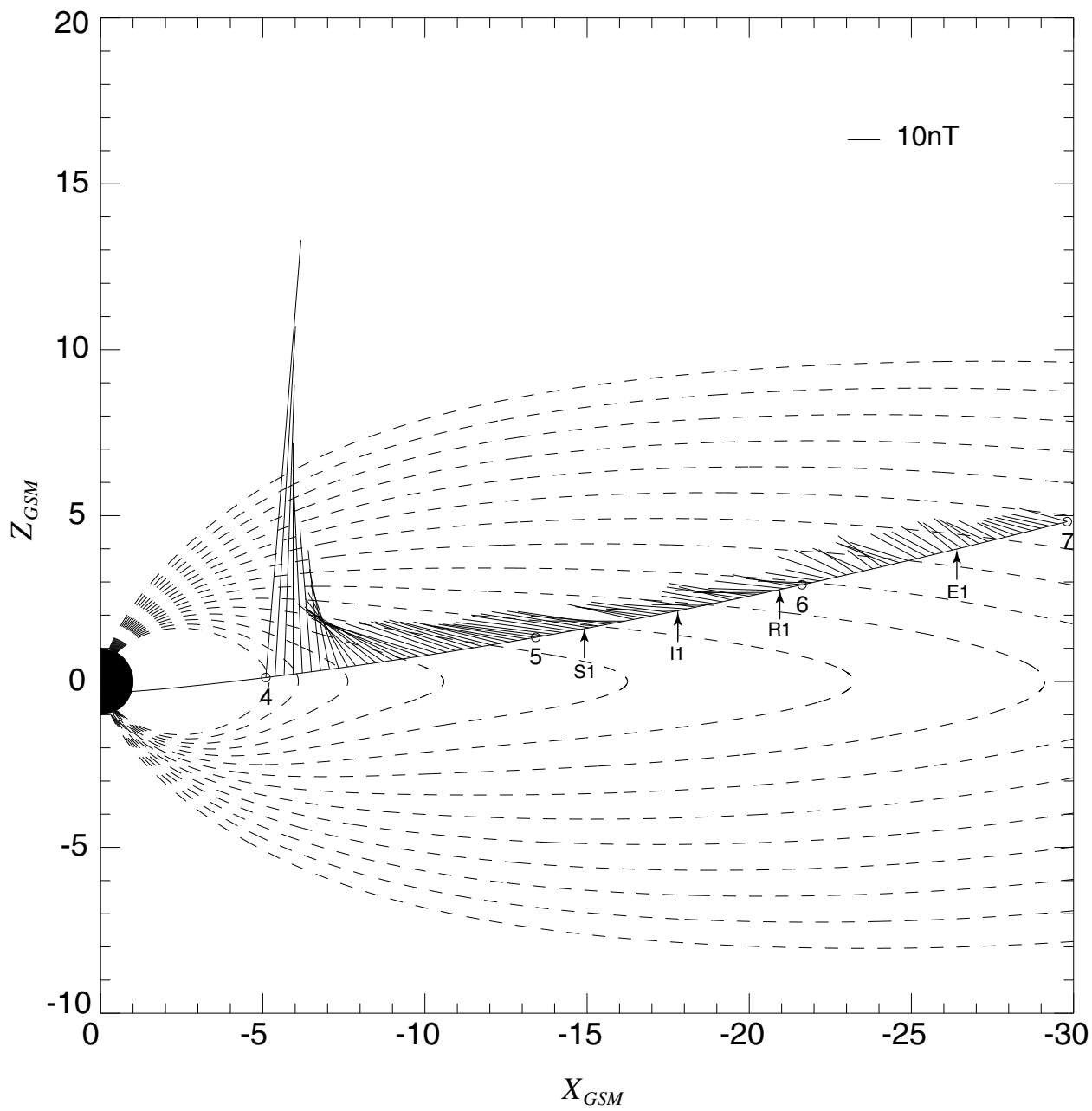


Fig. 10b

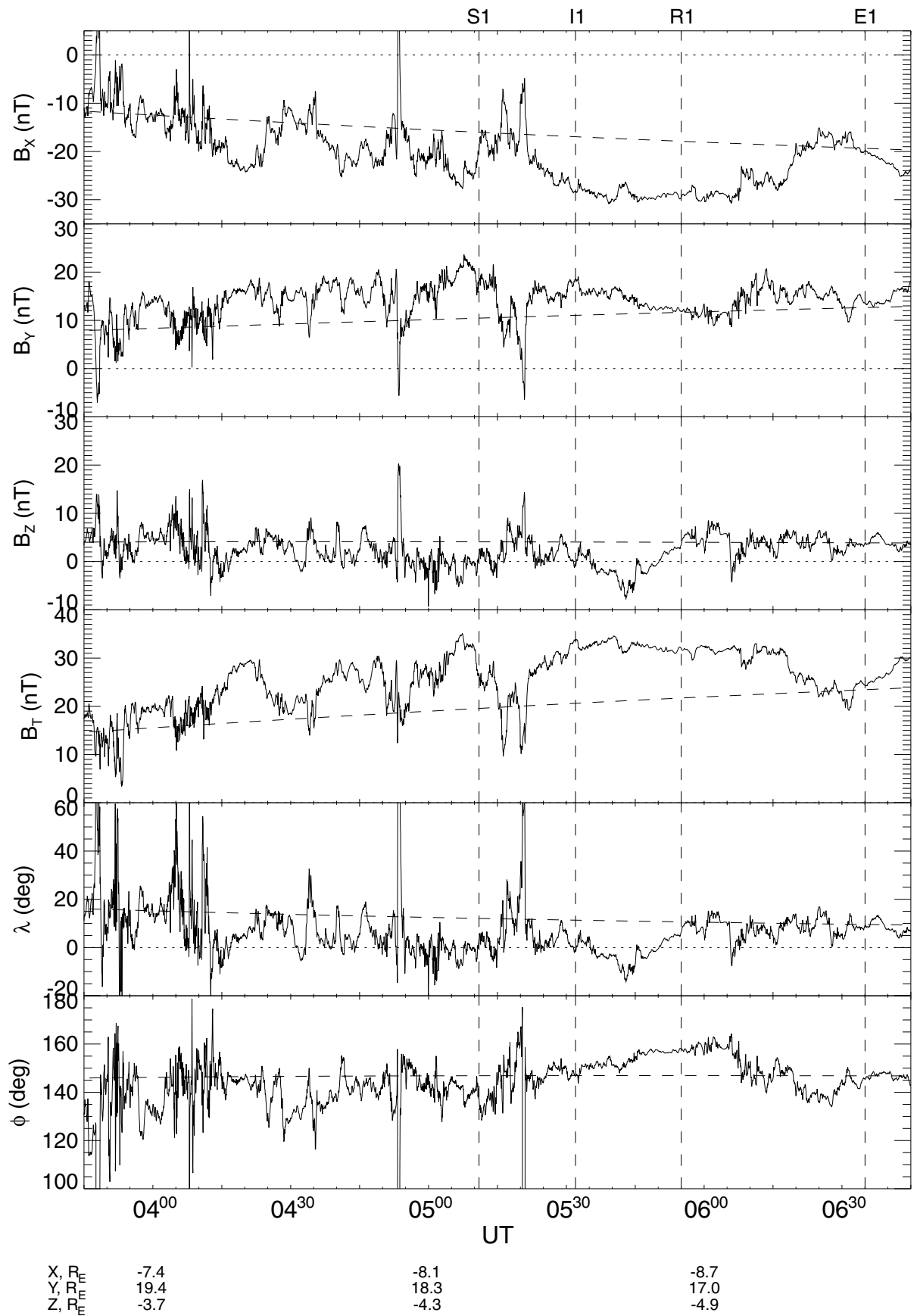
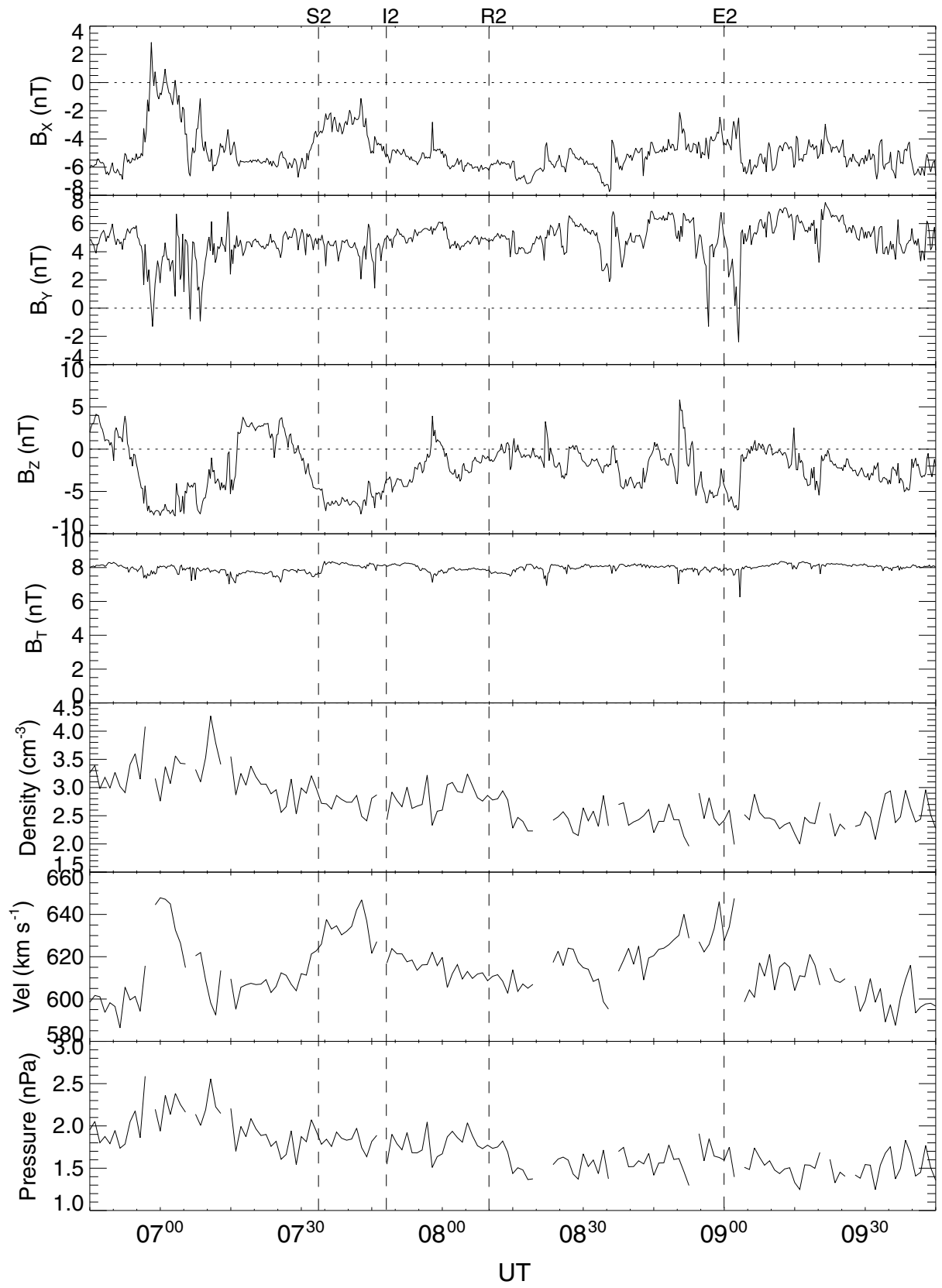


Fig. 11



X, $R_E$	248.3	248.3	248.3
Y, $R_E$	6.3	6.3	6.3
Z, $R_E$	23.9	24.0	24.0

Fig. 12

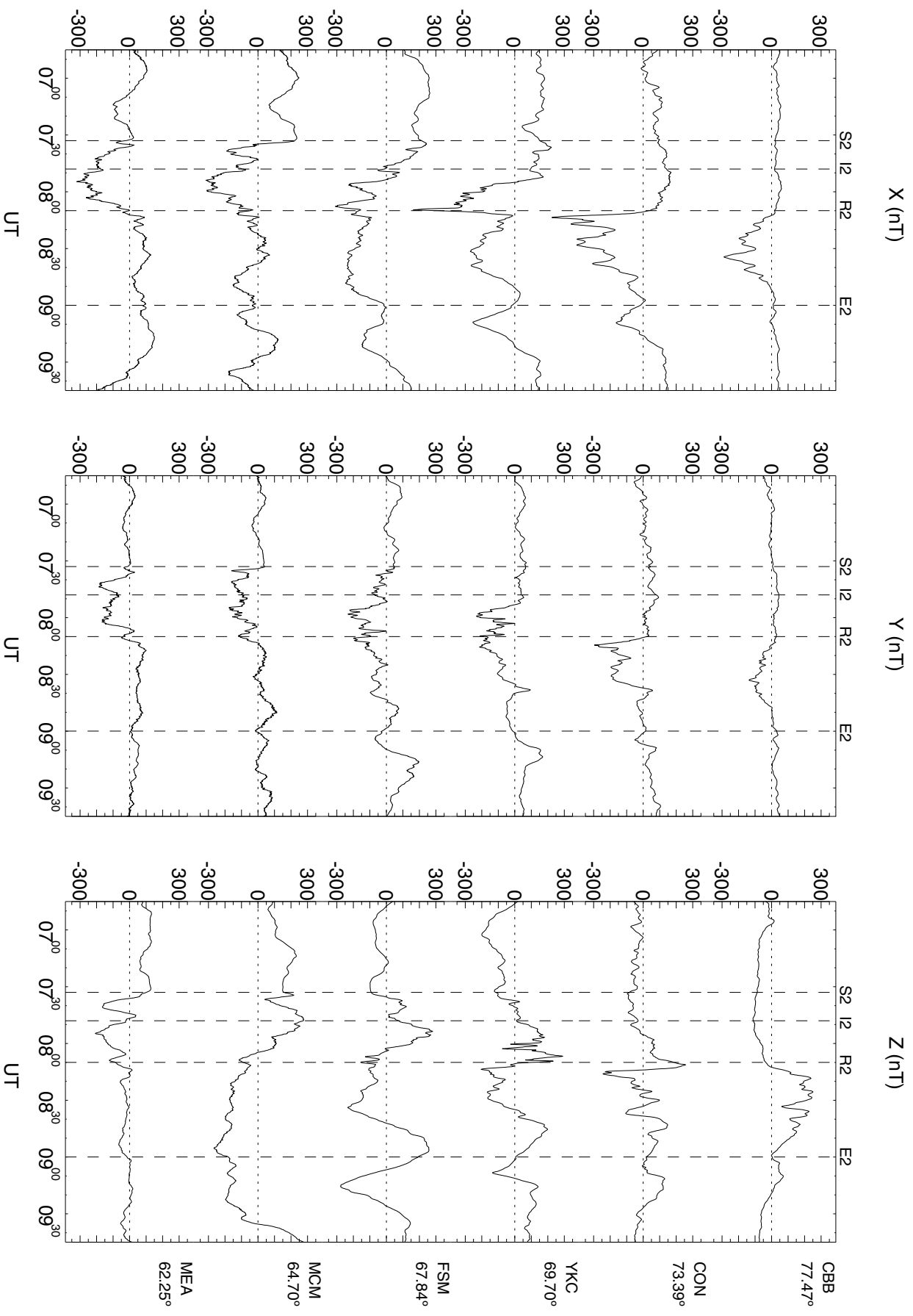


Fig. 13a

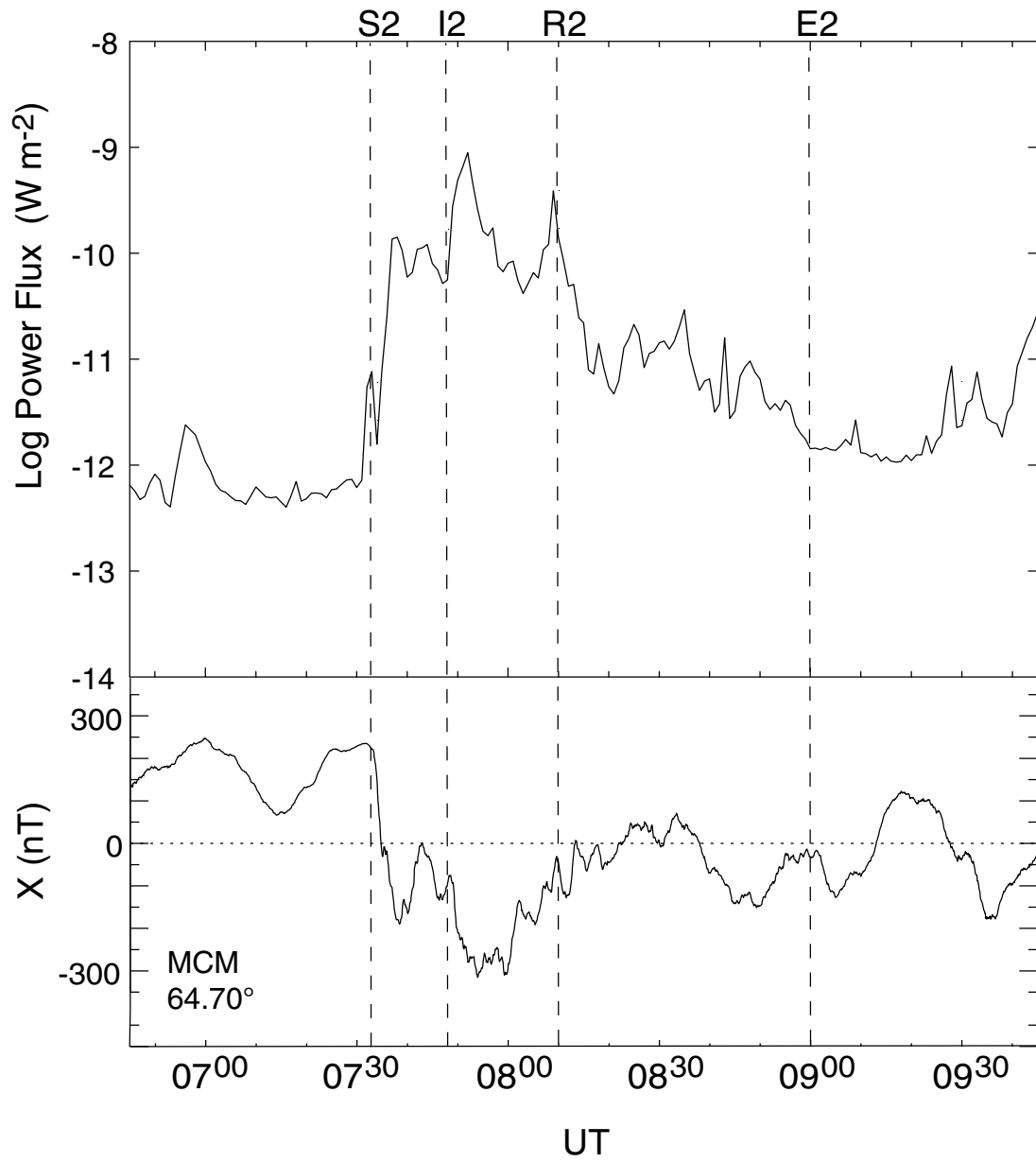


Fig 13b

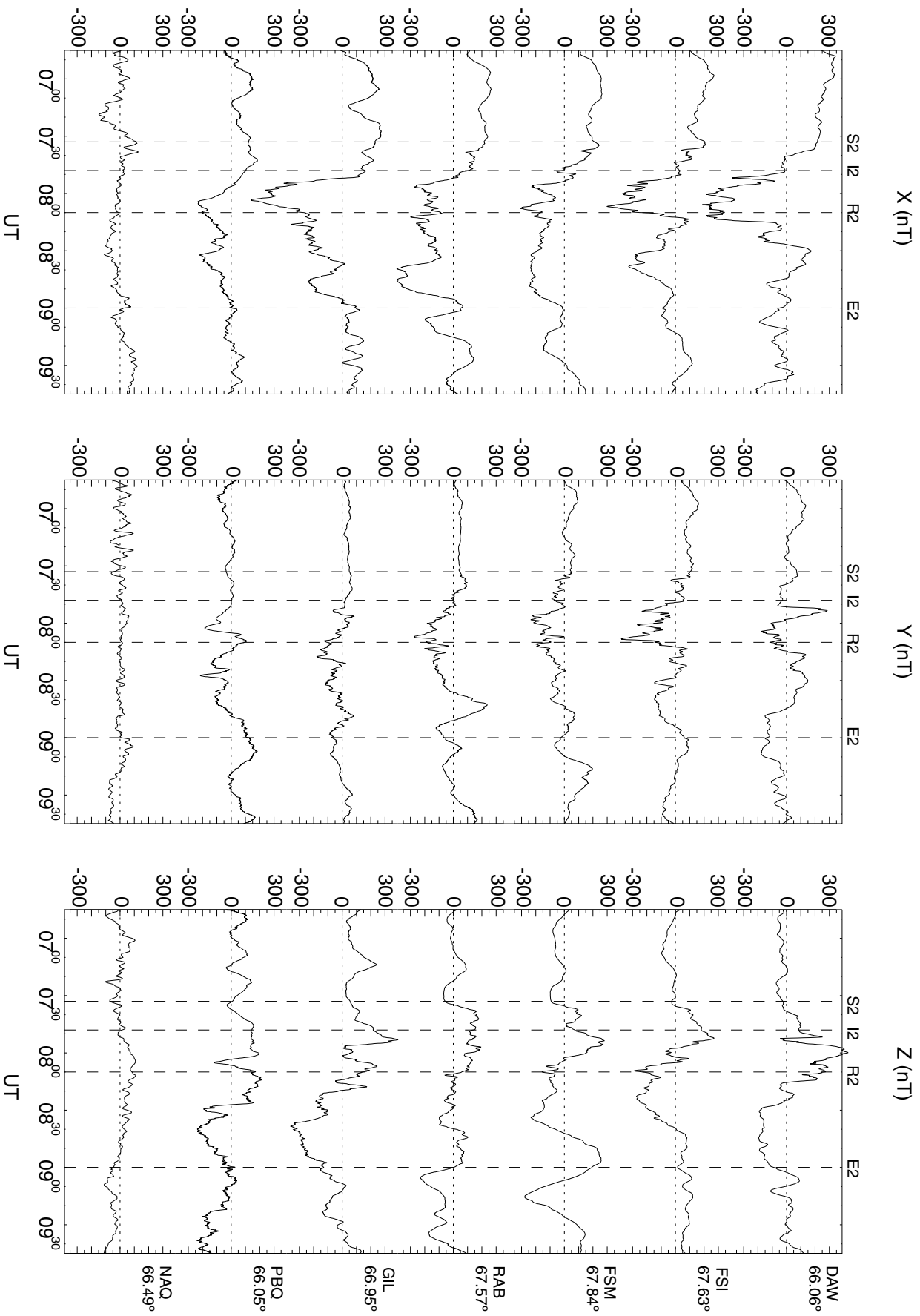


Fig. 14

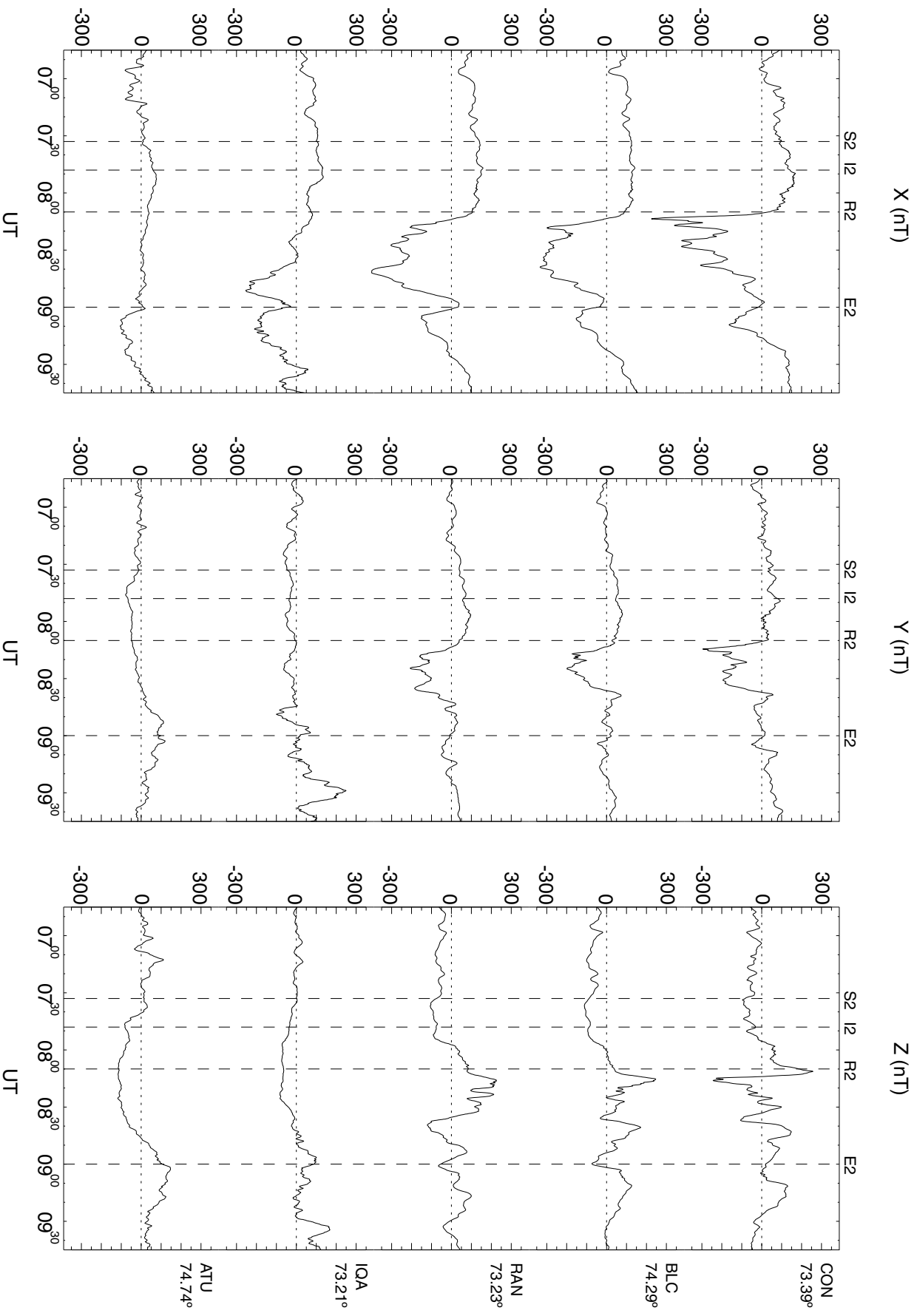


Fig. 15

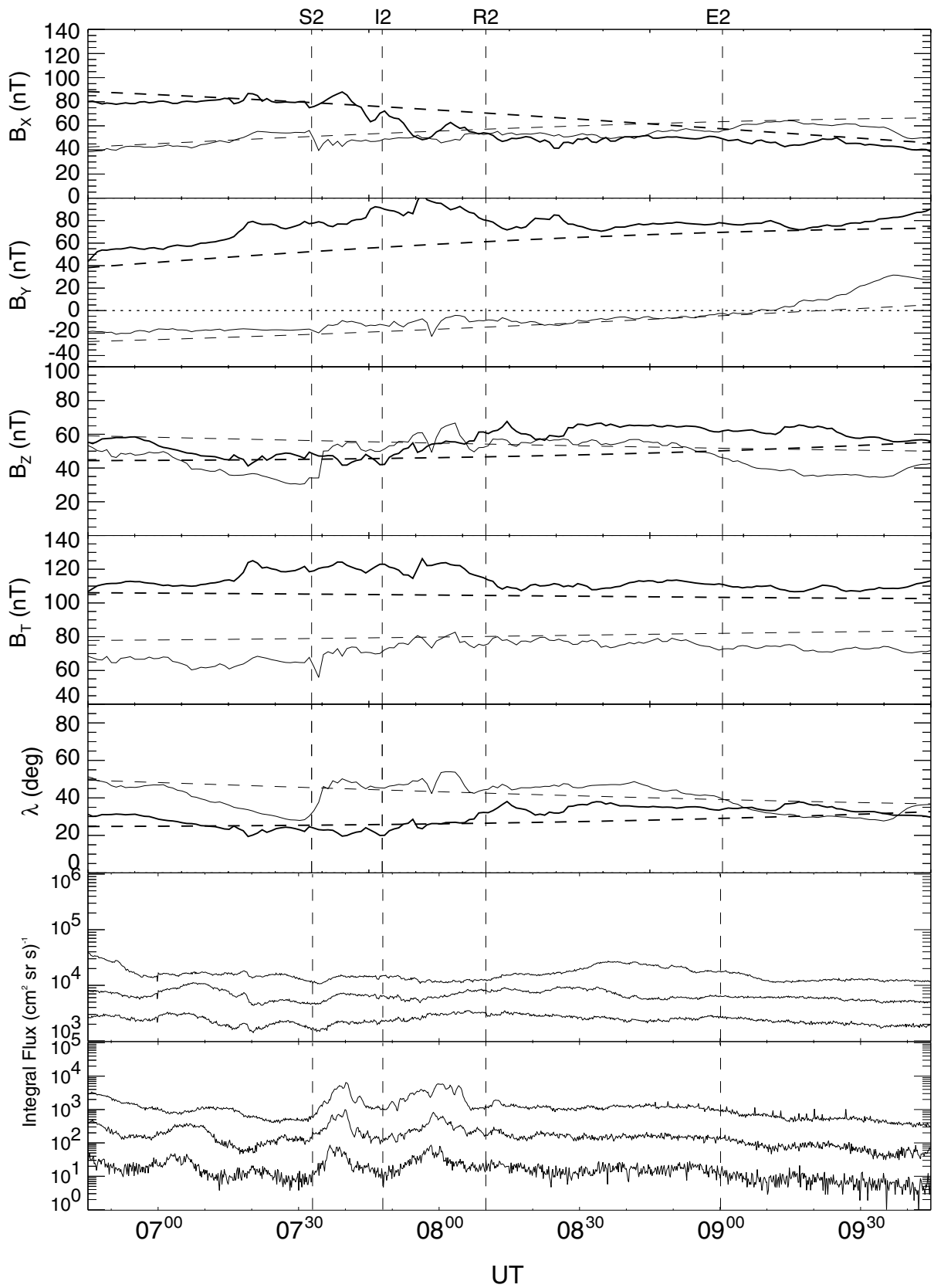


Fig. 16

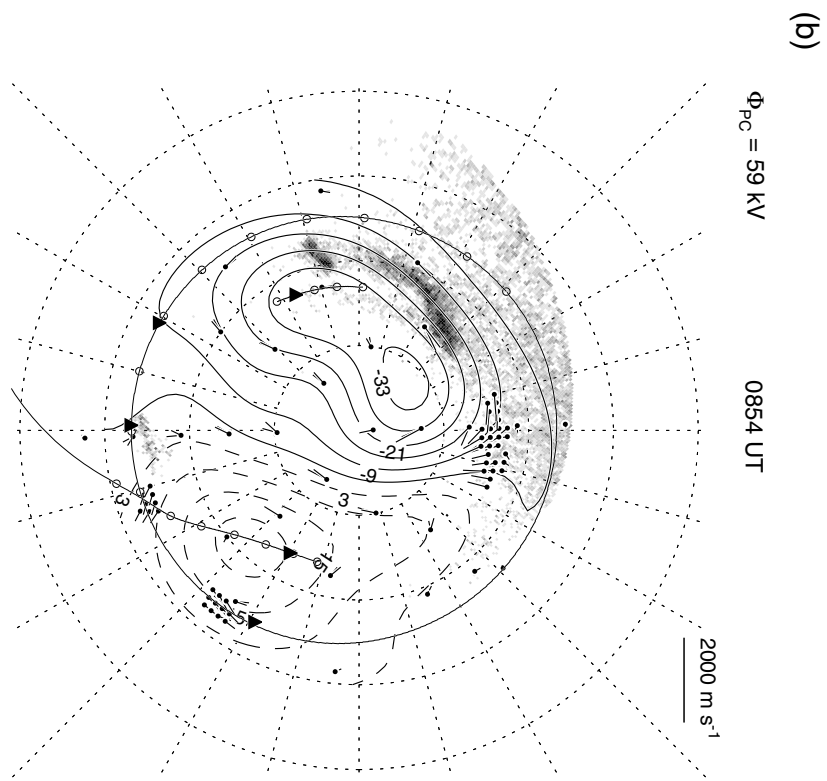
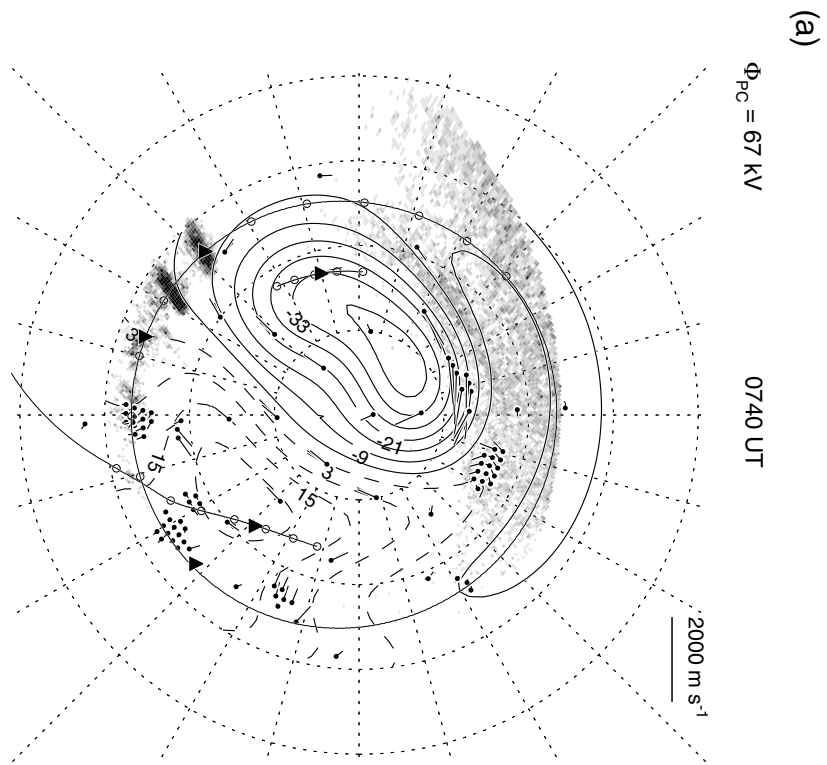


Fig. 17

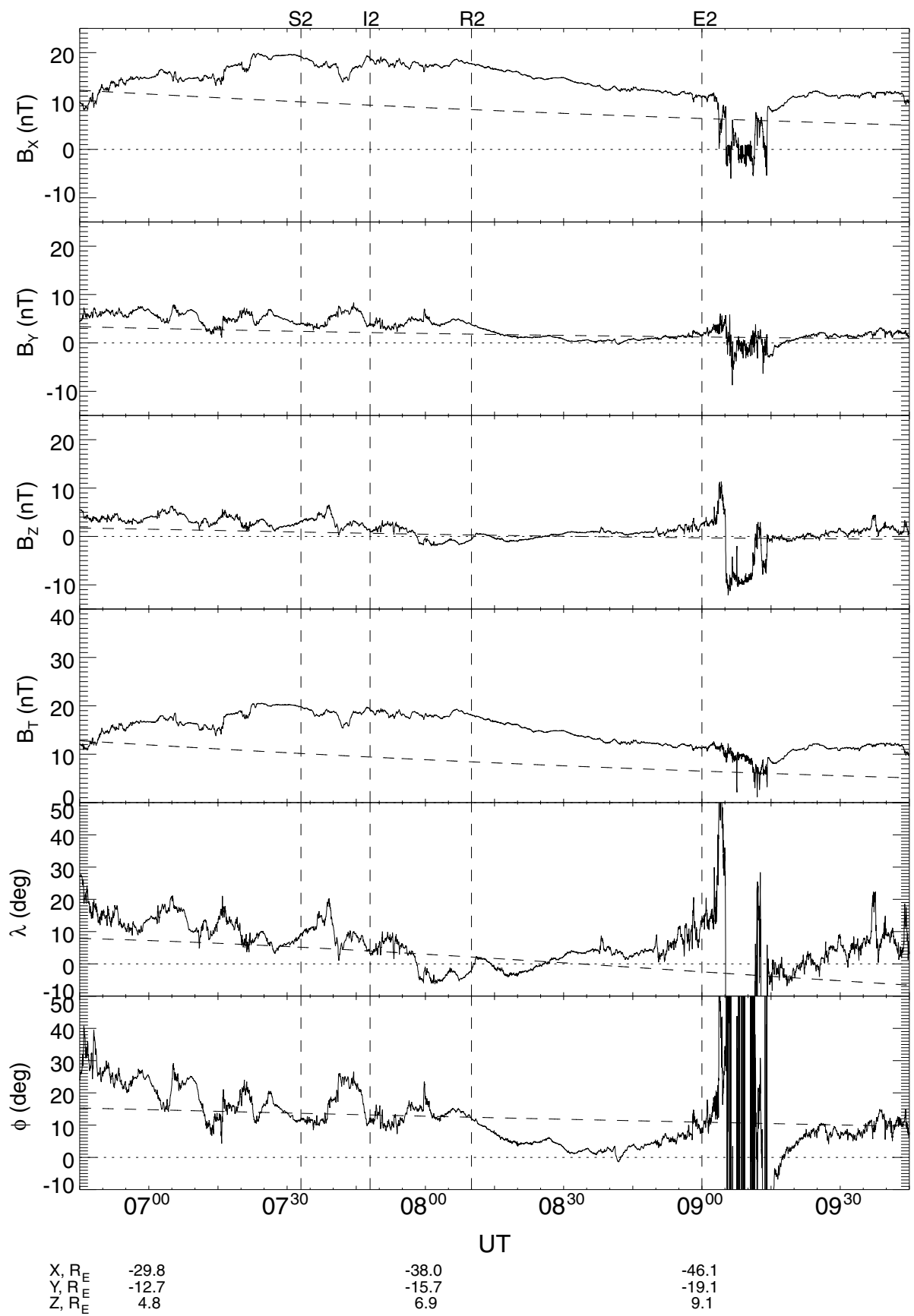
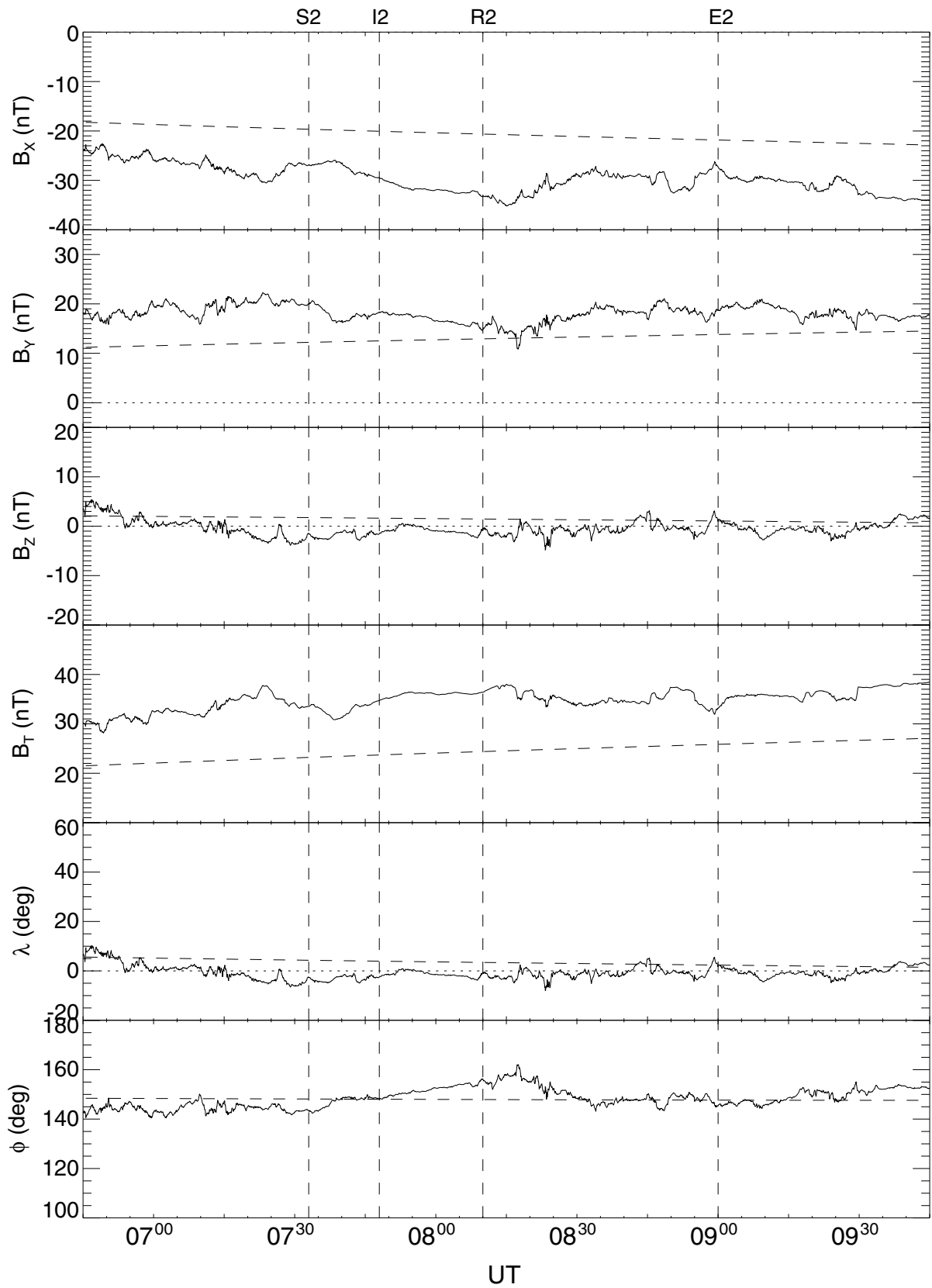


Fig. 18



	S2	I2	R2	E2
X, $R_E$	-9.4	-10.0	-10.6	
Y, $R_E$	15.8	14.5	13.2	
Z, $R_E$	-5.2	-5.4	-5.3	

Fig. 19

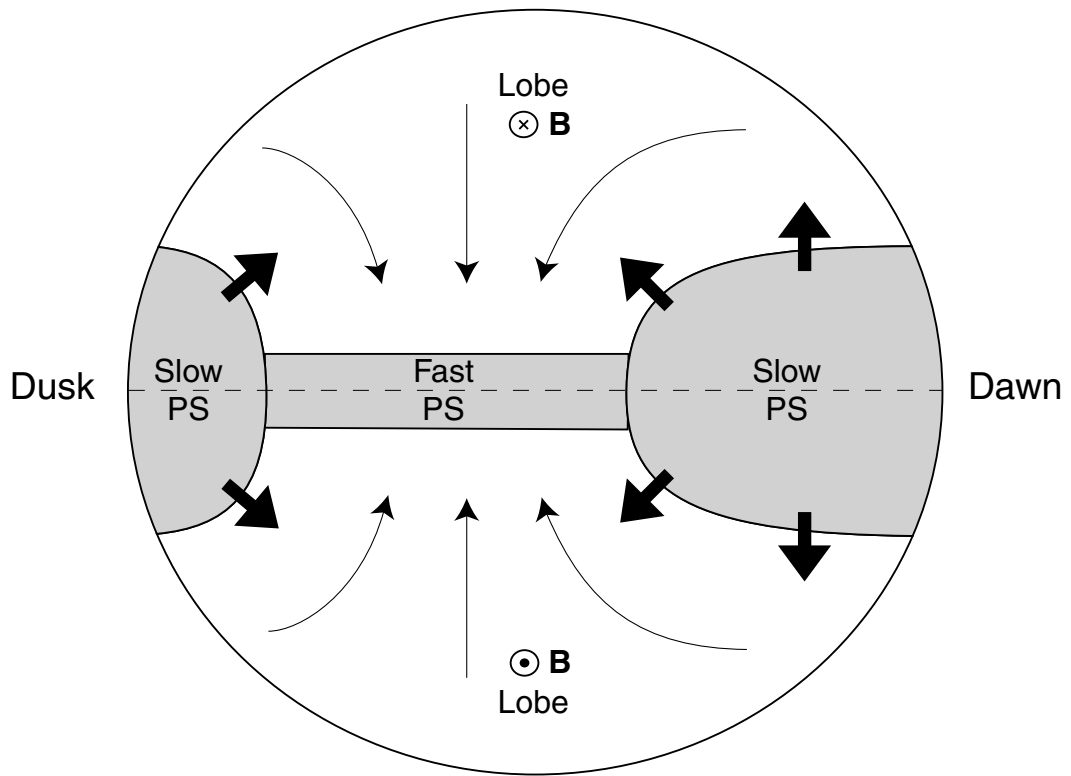


Fig. 20